Titre: Title:	Texture Analysis of Late Gadolinium Enhanced Cardiac Magnetic Resonance Images for Characterizing Myocardial Fibrosis and Infarction
Auteur: Author:	Pascale Béliveau
Date:	2017
Type:	Mémoire ou thèse / Dissertation or Thesis
Référence: Citation:	Béliveau, P. (2017). Texture Analysis of Late Gadolinium Enhanced Cardiac Magnetic Resonance Images for Characterizing Myocardial Fibrosis and Infarction [Ph.D. thesis, École Polytechnique de Montréal]. PolyPublie. https://publications.polymtl.ca/2483/

UNIVERSITÉ DE MONTRÉAL

TEXTURE ANALYSIS OF LATE GADOLINIUM ENHANCED CARDIAC MAGNETIC RESONANCE IMAGES FOR CHARACTERIZING MYOCARDIAL FIBROSIS AND INFARCTION

PASCALE BÉLIVEAU

INSTITUT DE GÉNIE BIOMÉDICAL

ÉCOLE POLYTECHNIQUE DE MONTRÉAL

THÈSE PRÉSENTÉE EN VUE DE L'OBTENTION

DU DIPLÔME DE PHILOSOPHIAE DOCTOR

(GÉNIE BIOMÉDICAL)

FÉVRIER 2017

UNIVERSITÉ DE MONTRÉAL

ÉCOLE POLYTECHNIQUE DE MONTRÉAL

Cette thèse intitulée :

TEXTURE ANALYSIS OF LATE GADOLINIUM ENHANCED CARDIAC MAGNETIC RESONANCE IMAGES FOR CHARACTERIZING MYOCARDIAL FIBROSIS AND INFARCTION

présentée par : BÉLIVEAU Pascale

en vue de l'obtention du diplôme de : Philosophiae Doctor

a été dûment acceptée par le jury d'examen constitué de :

M. VINET Alain, Ph. D., président

Mme CHERIET Farida, Ph. D., membre et directrice de recherche

M. HSU Li-Yueh, Ph. D., membre et codirecteur de recherche

M. ARAI Andrew, MD, membre et codirecteur de recherche

M. DESCHÊNES Sylvain, Ph. D., membre

M. KRZYZAK Adam, Ph. D., membre externe

DEDICATION

To my husband Samuel for his support,

my kids Alessia and David who put sunshine and joy in my studies,

my father Jacques and Mamie Solange, forever with me.

ACKNOWLEDGEMENTS

I would like to first thank my director, Prof. Farida Cheriet and my co-directors, Li-Yueh Hsu and Dr. Andrew Arai, for their support, guidance and knowledge. I have learned a lot under their supervision and am grateful for the opportunities that were provided to me. Their advice, all along my PhD studies, has made me work hard to achieve my goals. They have always been supportive of my work and understanding in the personal challenges I encountered during my studies.

Thank you to everyone at the lab at the NHLBI that welcomed me and shared their knowledge with me. It was a pleasure to be part of their team and I am grateful for having had the opportunity of being part of such a dynamic and knowledgeable group. Thank you as well to the Graduate Partnership Program, to its members who were very supportive and understanding. Their availability and the resources that they provide added value to my experience at NIH.

Thank you to the members of the LIV4D lab at École Polytechnique of Montreal. Although I was sporadically present, I always felt part of the group. Thank you to Philippe Debanné for his support and availability.

A special and fond thank you to my parents, Jacques and Solange, who no doubt loved me and gave me opportunities to succeed. Papa, although you have left me too soon, I always kept your memory with me, following you to your lab when school was out. Maman, this Ph.D. is for you. You have inspired me in so many ways, with your own studies and quest for knowledge. You have guided and assisted me in pursuing my Ph.D. and you became an incredible grandmother while doing it. You were at my side, always supportive and I am eternally grateful for all you have done for me.

I would like to thank my in-laws, Dominique and Morris, along with Martin and Melissa. I couldn’t ask for a better family. They have been at my side, always supportive. A special thank you to my daughter Alessia and my son David, although you added challenge to my studies, you also added sunshine to my days by making me smile.

And finally but not least, thank you to my husband Samuel, who was by my side throughout this long journey, who never let me back down and pushed me to succeed. He was supportive as we shared life changing events during my Ph.D.

RÉSUMÉ

Le tiers de la population aux États-Unis est affecté par des cardiomyopathies. Lorsque le muscle du cœur, le myocarde, est altéré par la maladie, la santé du patient est détériorée et peut même entrainer la mort. Les maladies ischémiques sont le résultat d'artères coronariennes bloquées (sténose), limitant l'apport sanguin vers le myocarde. Les cardiomyopathies non-ischémiques sont les maladies dues à d'autres causes que des sténoses. Les fibres de collagène (fibrose) s'infiltrent dans le muscle cardiaque dans le but de maintenir la forme et les fonctions cardiaques lorsque la structure du myocarde est affectée par des cardiomyopathies. Ce principe, nécessaire au fonctionnement du cœur en présence de maladies, devient mal adapté et mène à des altérations du myocarde aux conséquences négatives, par exemple l'augmentation de la rigidité du myocarde. Une partie du diagnostic clinique lors de cardiomyopathies consiste à évaluer la fibrose dans le cœur avec différentes modalités d'imagerie. Les fibres de collagène s'infiltrent et s'accumulent dans la zone extracellulaire du myocarde ou peuvent remplacer progressivement les cardiomyocytes compromises. L'infiltration de fibrose dans le myocarde peut possiblement être réversible, ce qui rend sa détection particulièrement importante pour le clinicien.

Différents tests diagnostiques existent pour aider le clinicien à établir l'état du patient en présence de cardiomyopathies. L'imagerie par résonance magnétique (IRM) est une modalité d'imagerie qui offre une haute résolution pour la visualisation du myocarde. Parmi les séquences disponibles avec cette modalité, l'imagerie par rehaussement tardif (RT) augmente le contraste du signal existant entre les tissus sains et les tissues malades du myocarde. Il s'agit d'images en pondération T_1 avec administration d'agent de contraste qui se propage dans la matrice extracellulaire et résulte en un rehaussement du signal à cet endroit. Les images IRM RT permettent d'évaluer la présence et l'étendue des dommages au myocarde. Le clinicien peut évaluer la sévérité des cardiomyopathies et poser un pronostique à l'aide de ces images. La détection de fibrose diffuse dans ces images peut informer le clinicien sur l'état du patient et est un important marqueur de cardiomyopathies.

Il est important d'établir l'occurrence de l'infarctus en présence de maladies ischémiques. En effet, l'approche interventionnelle varie selon que le clinicien fait face à une ischémie aigue ou chronique. Lors du diagnostic, Il serait donc bénéfique de différencier les infarctus du myocarde aigu de ceux chronique. Ceci s'est avéré difficile à l'aide des images IRM RT où l'intensité du signal ou la taille des régions sont similaires dans les deux types d'ischémie.

Le but de la présente thèse est donc d'appliquer les méthodes d'analyse de texture à des images IRM RT afin de détecter la présence de fibrose diffuse dans le myocarde et de plus de déterminer l'âge de l'infarctus du myocarde. La première étude portait sur la détection de fibrose diffuse dans le myocarde à l'aide de l'analyse de texture appliquée à des images IRM RT afin d'établir si un lien existe entre la variation du signal d'intensité et la structure sous-jacente du myocarde. La présence de collagène dans le myocarde augmente avec l'âge et nous avons utilisé un modèle animal de rats jeunes et âgés. Nous avons fait une étude ex-vivo afin d'obtenir des images IRM RT de haute résolution avec absence de mouvement et ainsi permettre une comparaison des images avec des coupes histologiques des cœurs imagés. Des images IRM RT ont été acquises sur vingt-quatre animaux. Les coupes histologiques ont été traitées avec la méthode utilisant un marqueur 'picrosirius red' qui donne une teinte rouge au collagène. La quantification de la fibrose obtenue avec les images IRM RT a été comparée à la quantification obtenue sur les coupes histologiques. Ces quantifications ont de plus été comparées à l'analyse de texture appliquée aux images IRM RT. La méthode de texture a été appliquée en créant des cartes de texture basées sur la valeur de *Contraste*, cette mesure étant obtenue par des calculs statistiques sur la matrice de cooccurrence. Les régions montrant une plus grande complexité de signal d'intensité sur les images IRM RT ont été rehaussées avec les cartes de textures. Un calcul de régression linéaire a permis d'étudier le lien entre les différentes méthodes de quantification. Nous avons trouvés que la quantification de fibrose dans le myocarde à l'aide de l'analyse de texture appliquée sur des images IRM RT concordait avec le niveau de collagène identifié avec les images IRM et avec les coupes histologiques. De plus, nous avons trouvés que l'analyse de texture rehausse la présence de fibrose diffuse dans le myocarde.

La seconde étude a pour but de discriminer les infarctus aigus du myocarde de ceux qui sont chroniques sur des images IRM RT de patients souffrant de cardiomyopathies ischémiques. Vingt-deux patients ont subi l'imagerie IRM (12 avec infarctus aigu du myocarde et 12 avec infarctus chronique). Une segmentation des images a permis d'isoler les différentes zones du myocarde, soit la zone d'infarctus, la zone grise au rebord de l'infarctus et la zone du myocarde sain, dans les deux groupes de patients. L'analyse de texture s'est faite dans ces régions en comparant les valeurs obtenues dans les deux groupes. Nous avons obtenu plus de valeurs de texture discriminantes dans la zone grise, en comparaison avec la région du myocarde sain, où aucune valeur de texture n'était significativement différente, et à la zone d'infarctus, où seule la valeur de texture statistique

Moyenne était différentes dans les deux groupes. La zone grise a déjà fait l'objet d'études ayant établis cette région comme composée de cardiomyocytes sains entremêlés avec des fibres de collagène. Notre étude montre que cette région peut exhiber des différences structurelles entre les infarctus aigus du myocarde et ceux qui sont chroniques et que l'analyse de texture a réussi à les détecter.

L'étude de la présence de collagène dans le myocarde est importante pour le clinicien afin qu'il puisse faire un diagnostic adéquat du patient et pour qu'il puisse faire un choix de traitement approprié. Nous avons montrés que l'analyse de texture sur des images IRM RT de patients peut différencier et même permettre la classification des ischémies aigues des ischémies chroniques, ce qui n'était pas possible avec uniquement ce type d'images. Nous avons de plus démontrés que l'analyse de texture d'images IRM RT permettait d'évaluer le contenu de fibrose diffuse dans un modèle animal de haute résolution avec validation histologique. Une telle relation entre les résultats d'analyse de texture d'images IRM RT et la structure sous-jacente du myocarde n'avait pas été étudiée dans la littérature.

Notre méthode pourra être améliorée en effectuant d'autres calculs statistiques sur la matrice de cooccurrence, en testant d'autres méthodes d'analyse de texture et en appliquant notre méthode à de nouvelles séquences d'acquisition IRM, tel les images en pondération T_1. D'autres améliorations possibles pourraient porter sur une évaluation de matrice de cooccurrence avec voisinage circulaire suivant la forme du myocarde sur les tranches d'images IRM RT. Plusieurs matrice de cooccurrence pourraient aussi être évaluées en fonction de la position dans l'espace du voisinage afin d'intégrer une composante directionnelle dans les calculs de texture. D'autres études sont nécessaires afin d'établir si une analyse de texture des images IRM RT pourrait différencier le stade de la fibrose pour un même patient lors d'une étude de suivi. De même, d'autres études sont nécessaires afin de valider l'utilisation de texture sur des scanners IRM différents. Établir l'âge de l'infarctus du myocarde permettra de planifier les interventions thérapeutiques et d'évaluer le pronostique pour le patient.

ABSTRACT

A third of the United States population is affected by cardiomyopathies. Impairment of the heart muscle, the myocardium, puts the patient's health at risk and could ultimately lead to death. Ischemic cardiomyopathies result from lack of blood (ischemia) reaching the myocardium from blocked coronary arteries. Non-ischemic cardiomyopathies are diseases from other etiology than ischemia. Often collagen fibers infiltrate the heart (fibrosis), as a means to maintain its shape and function in the presence of disease that affects the myocardial cellular structure. This necessary phenomenon ultimately becomes maladaptive and results in the heart's impairment. Part of the heart's involvement in disease can be assessed through the analysis of myocardial fibrosis. Cardiomyopathy diagnosis involves the investigation of the presence of myocardial fibrosis, either infiltrative, defined as the increased presence of collagen protein in the extracellular space, or replacement fibrosis, when collagen fibers progressively replace diseased cardiomyocytes. The infiltrative fibrosis is believed to be reversible in some instances and consequently, myocardial fibrosis analysis has decisional impact on the interventional procedure that would benefit the health of the patient. The heart contracts and relaxes as it pumps blood to the rest of the body, an action directly impaired by myocardial damage. Any myocardial involvement should be assessed by the clinician to identify the severity of the myocardial damage, establish a prognosis and plan therapeutic intervention.

Different diagnostic tests are required to image the myocardium and help the clinician in the diagnostic process. Cardiac magnetic resonance (CMR) imaging has emerged as a high resolution imaging modality that offers precise structural analysis of the heart. Among the different imaging sequences available with CMR, late gadolinium enhancement (LGE) shows the myocardium and enhances any impairments that may exist with the use of a contrast agent. It is a T_1-weighted image with extracellular contrast agent (CA) administration. Increased signal intensity in the infarct scar is created from the CA dynamics. LGE CMR imaging offers information on the scar size and its location. The clinician can estimate the severity of the disease and establish prognosis with LGE CMR images.

In ischemic cardiomyopathy, it is important to establish the occurrence of the infarction and know the age of the infarct to plan surgical intervention. Differentiation of acute from chronic MI is therefore important in the diagnostic process. In LGE CMR the level of signal intensity or the size

of infarction are both similar in acute or in chronic MI. It has therefore been challenging to distinguish acute MI from chronic MI scars with LGE CMR images alone.

The aim of this thesis was to investigate texture analysis of LGE CMR images to determine if acute MI could be distinguished from chronic MI and to detect increased presence of diffuse myocardial fibrosis in the myocardium. The first study was performed to investigate if texture analysis of LGE CMR images could detect variations in the presence of diffuse myocardial fibrosis and if the underlying myocardial structure could be related to the texture measures. Collagen content increased with aging and we used an animal model of young versus old rat. An ex-vivo animal model was necessary to allow for higher image resolution in LGE CMR images and to perform validation of our texture measures with histology images. Twenty four animals were scanned for LGE CMR images and texture analysis was applied to the heart images. Histology slices were stained with picrosirius red and collagen fibers were isolated based on their color content. LGE CMR quantification was compared to histological slices of the heart stained with the picrosirius red method. Texture analysis of LGE CMR images was also compared to the original LGE CMR image quantification and to histology. Texture analysis was done by creating contrast texture maps extracted from Haralick's gray level co-occurrence matrix (GLCM). Regions of complex signal intensity combination were enhanced in LGE CMR images and in contrast texture maps. Regression analysis was performed to assess the level of agreement between the different analysis methods. We found that LGE CMR images could assess the different levels of collagen content in the different aged animal model, and that moreover texture analysis enhanced those differences. The location of enhancement from texture analysis images corresponded to location of increased collagen content in the old compared to the young rat hearts. Histological validation was shown for texture analysis applied to LGE CMR images to assess myocardial fibrosis.

Our second study aimed at discriminating acute versus chronic MI from LGE CMR patient images alone through the use of texture analysis. Twenty two patients who had LGE CMR images were included in our study (12 acute and 12 chronic MI). Regional segmentation was performed and texture features were compared in those regions between both groups of patient. Texture analysis resulted in significantly different values between the two groups. More specifically the peri-infarct zone had the most number of discriminative features compared to the remote myocardium which had none and to the infarct core where only the *mean* features was significantly different. The border zone has been shown to be composed of healthy cardiomyocytes intermingled with the

scar's collagen fibers. Our study indicates this region might exhibit structural differences in the myocardium in acute from chronic MI patients that texture analysis of LGE CMR images can detect.

Characterization of myocardial collagen content is important while clinicians analyze the state of the patient since it influences the course of action required to treat cardiomyopathies. LGE CMR images have been thoroughly used and validated to characterize focal myocardial scar, however it was limited in characterizing the age of infarction or quantifying diffuse collagen content. We have shown texture analysis of LGE CMR images alone can differentiate and even classify, acute from chronic MI patients, which was not previously possible. Characterization of myocardial infarction according to age will prove important in planning therapeutic interventions in clinical practice. Moreover, we have established texture analysis as a means to characterize the myocardium and detect variation in fibrosis content from high resolution LGE CMR images with histology validation. To our knowledge, such a relation between texture analysis of LGE CMR images and the underlying myocardial structure had not been done previously.

Improvements could be done to our method, as we can increase the number of texture features that were analyzed from the GLCM, include other texture analysis methods such as the run-length matrix, and apply our method to other CMR imaging sequences such as T_1 mapping. Adapting the GLCM to the heart could also be investigated, such as considering circular GLCM computation to consider the round shape of the myocardium in the short axis LGE CMR image slices. Directional GLCM could also be computed individually and analyzed for any myocardial or collagen fiber orientation indication. Further analysis is also required to establish if texture analysis could differentiate the age of MI in the same individual through a follow-up study. The measures of texture analysis from LGE CMR images obtained through different CMR scanners remains to be investigated as well. Knowing the age of infarct and evaluating the presence of diffuse myocardial fibrosis will help the clinician plan therapeutic interventions and establish a prognosis for the patient.

TABLE OF CONTENTS

LIST OF TABLES

LIST OF FIGURES

LIST OF SYMBOLS AND ABBREVIATIONS

AUC	Area under the curve
ANN	Artificial neural network
CA	Contrast agent
CMR	Cardiac magnetic resonance
DCM	Dilated cardiomyopathy
DTI	Diffusion tensor imaging
DTPA	Diethylenetriamine pentaacetic acid
ECV	Extracellular volume
FACT	Feature analysis and combined thresholding
FWHM	Full width at half maximum
Gd	Gadolinium
GLCM	Gray level co-occurrence matrix
GRE	Gradient echo
HCM	Hypertrophic cardiomyopathy
HSV	Hue saturation value
ICM	Ischemic cardiomyopathy
IR	Inversion recovery
LBP	Local binary pattern
LDA	Linear discriminant analysis
LGE	Late gadolinium enhanced
LV	Left ventricle
MI	Myocardial infarction
NICM	Non-ischemic cardiomyopathy

NN	Nearest neighbor
NS	Not significant
PCA	Principal component analysis
PI	Peri-infarct
PIM	Percent infarct mapping
PSIR	Phase sensitive inversion recovery
RBF	Radial basis function
RF	Radio frequency
RGB	Red green blue
RLM	Run length matrix
ROI	Region of interest
RT	Rehaussement tardif
SD	Standard deviation
SI	Signal intensity
SNR	Signal to noise ratio
SVM	Support vector machine

CHAPTER 1 INTRODUCTION

Cardiovascular diseases affect more than 1 in 3 adults in the United States [1]. The heart is the main supplier of blood to the rest of the body and any impairment might have life-threatening consequences. Cardiovascular diseases claim more lives than any other diseases in the United States [1] and affect the heart by modifying the cellular structure or global shape of the myocardium (the muscle of the heart). The heart's function is negatively affected as the myocardium is progressively impaired. Ischemic cardiomyopathies are characterized by lack of blood reaching the myocardium (ischemia) and are caused by an obstruction in the coronary arteries. Other myocardial diseases originate from various etiologies other than ischemia, such as amyloidosis, hypertrophic or dilated cardiomyopathies. A diagnosis is needed to identify the different diseases by analyzing the state of the patient and of the heart in order to perform the appropriate therapeutic intervention.

A combination of investigative tests and image analysis will inform the clinician on a patients' state. The clinician uses diagnostic tests, such as the electrocardiogram or biomarkers such as Troponin for example, to identify specific symptoms associated to types of cardiomyopathies. However, it is with ultrasound or cardiac magnetic resonance (CMR) that the myocardium can be visualized. Ultrasound is less expensive and a rapid imaging modality however CMR offers a higher resolution. Magnetic resonance is therefore used to obtain information on the pathological transformation of the myocardium whenever the precise state of the myocardium has to be established. Late gadolinium enhanced (LGE) CMR is a high resolution imaging method with which the clinician can identify and characterize any damage due to cardiomyopathies. LGE CMR imaging has been thoroughly validated and is used to measure the size and evaluate the severity of myocardial scar in ischemic cardiomyopathy [2]. Such an analysis has prognostic impact for the patient and helps the clinician plan therapeutic interventions. Although LGE CMR offers a high resolution visualization of the myocardium, there are limitations.

LGE CMR images show the location and pattern of enhancement in the presence of non-ischemic cardiomyopathy [3-6]. However, diffuse myocardial fibrosis cannot be quantified with this modality. The enhancements that are seen in LGE CMR are concentrated in a limited but definite location in the myocardium and can easily be isolated from the rest of the myocardium. Diffuse myocardial fibrosis has been identified as a structural alteration to the myocardium in the presence of non-ischemic cardiomyopathies [5] and is widespread in the heart muscle. Although it is crucial

in maintaining the heart's shape and function in disease, collagen is also responsible for stiffening of the heart and ultimately impairing myocardial function. Quantifying diffuse fibrosis would be beneficial since it was suggested that the early stages of fibrosis can possibly be reversible [7]. LGE CMR images are however limited in diffuse fibrosis characterization in non-ischemic cardiomyopathies, due to the diffusive nature of the myocardial alteration. The standard signal intensity based methods, applying a threshold of a number of standard deviation above the mean signal intensity of the myocardium, are non-applicable since there is no remote myocardium that can be identified, and consequently no threshold value that can be determined [8-11]. It would be beneficial if LGE CMR images alone could allow quantifying diffuse myocardial fibrosis in non-ischemic cardiomyopathy. Research has shown that T_1 mapping and extracellular volume (ECV) CMR imaging methods could show diffuse fibrosis [8-16]. However, it would be beneficial to use an imaging method already used in clinical practice and that has been thoroughly validated such as LGE CMR images. The signal intensity pattern in non-ischemic cardiomyopathies from this modality has frequently been identified with descriptive terms, for example "patchy" or "foci, heterogeneous, multifocal, and non-specific" [17]. These descriptions indicate a complex signal intensity pattern present in LGE CMR images in the presence of diffuse fibrosis, well suited for texture analysis. Consequently, our first contribution consists in applying texture analysis methods to LGE CMR images to characterize diffuse myocardial fibrosis at a high image resolution and to perform a comparison with the ground truth from histology. To our knowledge there has not been any association of texture analysis from LGE CMR images to the presence of diffuse fibrosis in the heart, as assessed with histology images stained with a collagen specific dye.

In ischemic cardiomyopathies, it is not possible to differentiate acute from chronic MI with LGE CMR images alone [18-21]. As more effective interventions are performed following acute myocardial infarction (MI), there is an increased number of patients with chronic MI. Part of the population can live with unrecognized MI, notably for patients with diabetes [22]. Since the age of infarct will have an impact on the decision of the therapeutic intervention to use, it is important for the clinician to distinguish acute from chronic MI scars. The signal intensity based methods that are currently used to segment the infarct scar in LGE CMR images have been unable to characterize the infarct age. Other imaging sequences or modalities have been used for its assessment, exploiting the physiological aspects of the myocardium in pathology, for example by detecting the presence of edema that occurs only in acute MI [18]. However, there is a definite advantage to using a well-

established modality such as LGE CMR images alone during diagnosis and avoiding extra imaging acquisition time. The peri-infarct zone has been described with respect to its heterogeneity, a reference to its appearance in LGE CMR images and an indication of a complex pattern of signal intensity in that region [23-27]. Patterns of signal intensity in medical images have been quantified with texture analysis. Our second contribution consists in characterizing the myocardial infarct age from texture analysis of LGE CMR images for patient with acute or chronic MI. Automatic classification of patients with acute versus chronic myocardial infarction is also desirable. The LGE CMR images are currently useful in characterizing the state of the myocardium, can differentiate ischemic from non-ischemic cardiomyopathies and can be an indication of the type of non-ischemic cardiomyopathy [4]. Classification of LGE CMR images of patients according to the age of the myocardial infarction would be beneficial. Using LGE CMR images to assess the infarct age or quantify diffuse myocardial fibrosis would be beneficial during the diagnosis process to estimate the prognosis for the patient and help the clinician plan therapeutic interventions according to the characterization of fibrosis in the heart.

The research question that is addressed in this thesis consists in the following: *Is it possible, relying only on LGE CMR images, to characterize myocardial fibrosis and ischemic cardiomyopathies, notably differentiate between acute and chronic myocardial infarction?* The aim of this study is to apply quantitative pattern analysis methods to understand how LGE CMR images can objectively assess the state of the myocardium and thus help in the diagnostic process. Texture analysis has never been fully investigated to study the various types of cardiomyopathies as seen in LGE CMR images. This method could help distinguish the underlying microstructure of the heart in the presence of ischemic and non-ischemic heart diseases.

This thesis includes seven chapters and will focus on the exploration of texture analysis as an alternative method to the usual intensity-based methods applied to LGE CMR images. Chapter 2 presents the literature review, briefly explaining the anatomy of the heart and how cardiomyopathies affect the myocardium, then explaining different magnetic resonance imaging methods used in medicine and more specifically in cardiology. It also presents a review of texture analysis and classification methods. In chapter 3, we present our research hypotheses and objectives as well as the general methodology by presenting texture analysis of LGE CMR images to characterize ischemic cardiomyopathies and assess diffuse myocardial fibrosis. Our first published paper is in chapter 4 and presents our investigate work on texture analysis of high

resolution LGE CMR images as a means of identification of diffuse myocardial fibrosis with ground truth validation from histology images. This lays the ground work to use texture analysis of LGE CMR images in cardiac diseases from other etiologies. Chapter 5 contains the second submitted paper that consists in applying texture analysis to LGE CMR images in order to grade myocardial fibrosis as acute or chronic myocardial infarction in a patient population. This part of the project assesses the performance of texture analysis of LGE CMR images in lower resolution images to characterize the underlying structure of the myocardium in a patient population. Initial results for classification of acute versus chronic MI from LGE CMR patient images will be described in chapter 6. The methods, along with the limitations, will be discussed in chapter six. Further considerations that could improve the method and its application are presented in conclusion in chapter 7.

CHAPTER 2 LITTERATURE REVIEW

The background information necessary to understand the work done in this thesis is presented in this chapter. The pathophysiological responses of the myocardium when ischemic or non-ischemic cardiomyopathies occur, along with the imaging methods that are used to view the myocardium, are in the first part of this chapter. Texture analysis methods used in medical imaging are presented in the second part of this chapter. Finally the last section of this chapter presents texture analysis in cardiology, more specifically in ischemic cardiomyopathy or in the presence of diffuse fibrosis in non-ischemic cardiomyopathies.

1.1 Background

1.1.1 Physiology of the healthy heart

The heart is a muscle that is called the myocardium and which forms four chambers, two atria and two ventricles (Figure 0-1). Valves are located between the atria and ventricles to control blood flow. Blood originating from the lungs reaches the left atrium and is pushed to the left ventricle via the mitral valve. The left ventricle then contracts and ejects the oxygen-rich blood to the aorta which supplies it to the rest of the body. Once the blood flows through the organs it releases oxygen and returns to the right atria via the inferior and superior vena cava. Blood then travels to the right ventricle through the tricuspid valve. The right ventricle ejects the deoxygenated blood through the pulmonary artery. The myocardium is supplied oxygenated blood by the coronaries that depart from the aorta and surround and penetrate the heart tissue.

A contraction signal propagates through the heart. A signal is sent from the sinoatrial node for the atria to contract. The signal then propagates to the atrioventricular node where a slight delay allows finishing the filling process of the ventricles with blood. The signal then follows the bundle of His that goes through the myocardium from the basal area to the apex of the heart. The Purkinje fibers lead the signal into the right and the left ventricle. The signal is then propagated from the apex of the ventricles to the basal area.

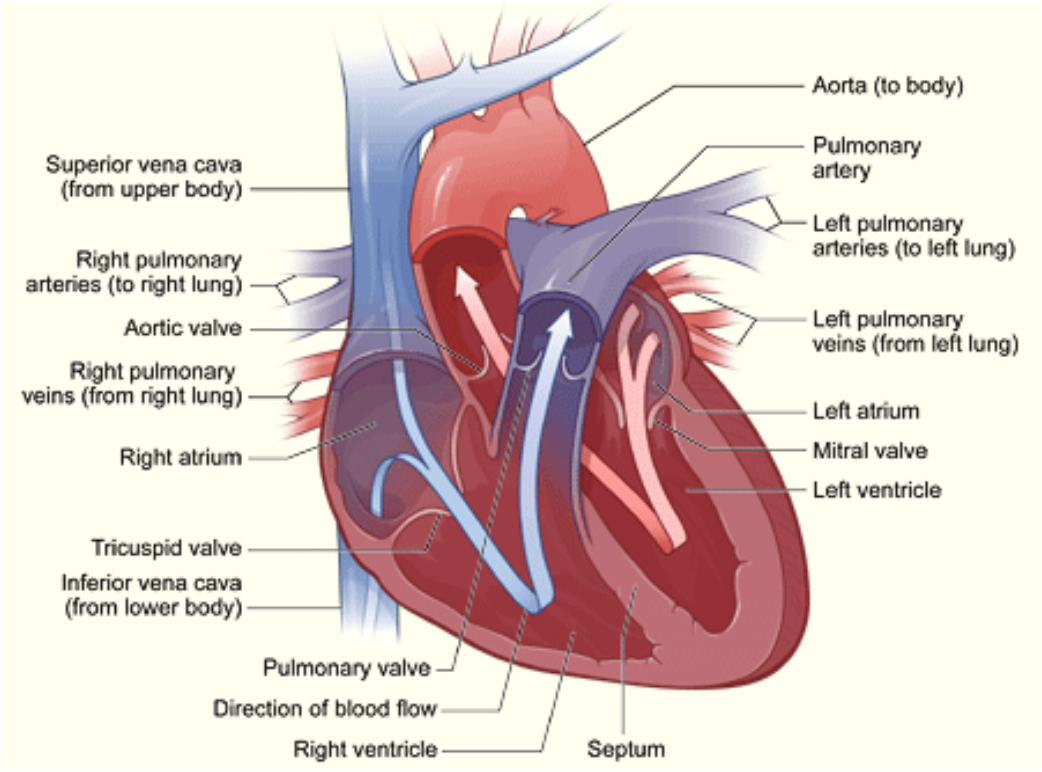

Figure 0-1 : The heart and its four chambers. The blood flows from one atria to its adjacent ventricle, which releases the blood to other anatomical parts of the body [28].

Collagen fibers are present in the healthy heart. These fibrous connective tissues act as scaffold by maintaining the macro- and micro- structure of the heart [29]. The different types of collagen in the heart are:

- Epimysium: is the epicardium (outer layer of the heart).
- Perimysium: creates groups of cardiomyocytes into bundles, and as well maintains connectivity between these bundles. The structural presence of the perimysium is believed to be related to the heart's function [30].
- Endomysium: is located around each cardiomyocytes and capillaries, maintaining the connectivity between these structures [31]. It is believed that it avoids cardiomyocytes to slip on each other, maintains their shape and maintains the vessels during muscle contraction [31].

1.1.2 Pathophysiological Changes from Cardiomyopathies

The increased infiltration of collagenous fibers in tissue alters the physiology and the function of organs that are affected, such as in the lung, the heart, the liver or the kidney. The increased presence of fibrosis in the heart is associated with adverse cardiac outcome, in the presence or absence of disease [29]. Myocardial fibrosis is characterized by the increased presence of collagen fibers in the heart [17]. In this section there will be reference to the two identified types of fibrosis: replacement and infiltrative. Replacement fibrosis consists of an increase of collagen fibers as a response to compromised cardiomyocytes during ischemia [17]. In this case, collagen fibers deposition acts as a scaffold to maintain the heart's shape and function in the areas normally occupied by cardiomyocytes. The scars composed of collagen fibers can form relatively large regions that are distinguished from healthy myocardium with imaging modality. LGE CMR images are routinely used in clinical practice in the presence of ischemic cardiomyopathy to determine scar characteristics, such as the location and the extent of damage to the myocardium [2]. Infiltrative fibrosis is the presence of collagen fibers in the interstitial space. Collagen fibers are present in the myocardium in response to pathophysiological transformations that occur with disease from various etiology [32]. It consists in increased presence of collagen fibers in the interstitial space, expanding the extracellular matrix [33].

1.1.2.1 Ischemic Cardiomyopathy

In ischemic cardiomyopathy, myocardial remodeling happens in response to ischemia and injury. However, this mechanism is believed to become maladaptive and harmful to the heart, leading eventually to heart failure. Different stages of the disease lead to various levels of damage and remodeling. In the early onset of the disease, or acute myocardial infarction, the cardiomyocytes lower their energy consumption in reaction to ischemia and therefore diminish their contraction to survive upon diminished supply of blood to the region. Without intervention to res-establish blood flow, cell death occurs from necrosis but apoptosis (programmed cell death) may also contribute to eventual cell death.

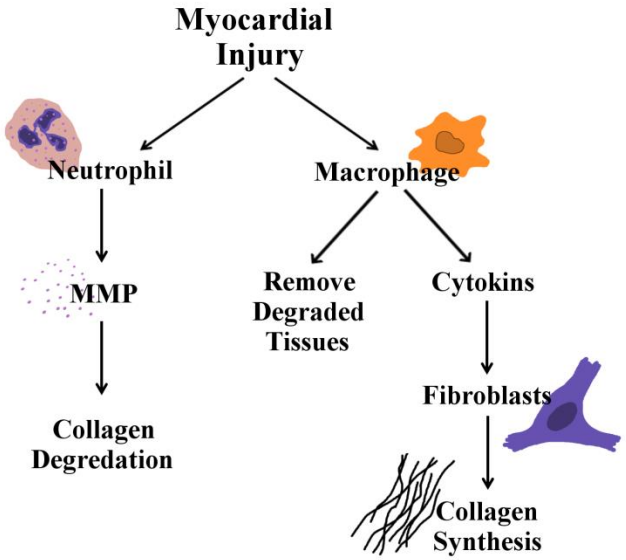

Figure 0-2 : The response to myocardial injury is an increase of inflammatory cells that include neutrophil and macrophages, amongst others. In acute myocardial infarction there is degradation of collagen fibers that is followed by increase of collagen synthesis to eventually form fibrosis.

When the myocardium is injured, the body responds by increasing the number of inflammatory cells (neutrophil, macrophage and others) in the region (see Figure 0-2) [34]. There is edema and swelling of the myocardium. Initially, increase of metalloproteinase cells, which originate from neutrophil cells, disintegrate collagen fibers. This results in higher risk of rupture of the heart wall. However, macrophages reduce the debris of necrosis and indirectly increase fibroblasts, one of the many mechanisms that results in synthesis of collagen in the heart [34]. Collagen is present in the healthy heart and acts as an element that maintains structure: it surrounds myocyte cells individually (endomysium) or in a bundle (perimysium). There is a slow turnover of collagen in the healthy myocardium that is disrupted in the presence of myocardial infarction. The long term result is excess collagen deposition (fibrosis). In chronic myocardial infarction there is thinning of the myocardium. The progress of damage to the myocardium typically starts in the subendocardial region (interior cavity of the left ventricle) and progressively spreads towards the epicardium (the outer surface of the heart).

1.1.2.2 Non-Ischemic Cardiomyopathy

Non-ischemic cardiomyopathies originate from different causes than coronary obstruction. In amyloidosis, amyloid proteins infiltrate the extracellular space over all the myocardium accompanied with wall thickening [35]. There might as well be presence of focal or diffuse fibrosis. Myocarditis is the inflammation of the heart muscle, most often due to infection, and that can lead to dilated cardiomyopathy (DCM) [36]. In DCM, the heart muscle is enlarged, with the possible presence of fibrosis [37]. In hypertrophic cardiomyopathy (HCM) the myocardium is thickened from cellular disarray [38].

1.1.3 LGE CMR Image Acquisition

During diagnosis, image acquisition parameters are chosen to obtain different information on cardiomyopathies. LGE CMR characterizes myocardial tissue in ways that are useful for diagnosis of many diseases including ischemic and non-ischemic cardiomyopathies. Magnetic resonance is an imaging procedure which exploits the energy released by proton excitation [39]. Randomly oriented protons are aligned in an applied magnetic field B_0. The net magnetization refers to the resulting magnetization of all protons. Following the application of selected radio frequency (RF) pulses, protons change orientation and there is a change of orientation of the magnetization. The return to equilibrium of the magnetization is what creates the signal that is imaged. In gradient echo (GRE) sequences, a gradient is applied after the RF pulse to generate a signal. LGE CMR images are T_1-weighted and use an MR acquisition sequence called inversion recovery (IR) [40, 41]. T_1 times are defined as the time when 60% of the signal has been recovered. All tissues return to equilibrium at a different pace, which results in different signal intensity levels in different tissues. IR is done by flipping the protons 180^o and letting magnetization recover. When magnetization is in the transverse plane, there is no signal intensity. Since all tissues will recover at their own pace, it is used to null the healthy myocardium while still seeing other diseased parts of the myocardium. An alternative method is now used that employs the phase sensitive inversion recovery (PSIR) technique and which allows more latitude in selecting the time to null the myocardium while maintaining contrast between healthy and diseased tissues. Shortening of the T_1 time in the infarct zone results in brighter signal intensity in that area and is done through the use of a contrast agent (CA).

LGE CMR images are obtained after administrating an intravenous CA that spreads in the heart cavity and later spreads in the myocardium with altered kinetics and volume distribution in the area of damage. The contrast agents are gadolinium (Gd) based. This metal interacts with protons and shortens the T_1 relaxation time of the myocardium or blood, enhancing the signal intensity of the region where the contrast is present [42-44]. However this metal is toxic and blocks calcium channels [43, 44]. It is therefore combined with a chelate to form a molecular structure that is stable in the body and is excreted by the kidney. Gadolinium combined with pentetic acid, Gd-DTPA, is one of five agents approved by the FDA for investigational use. The CA is extracellular. The result is relatively more enhancement of intensities where the myocardium is altered by the pathology. The signal intensity of the myocardium is nulled using an IR acquisition method [45] to provide high contrast ratio between the remote myocardium and the affected region. The cause of enhancement is different depending on the disease, ischemic or non-ischemic cardiomyopathies [46].

Alternative methods to LGE CMR images have emerged recently. T_1 maps are created either with pre- or post-contrast T_1-weighted images [7]. Magnetization recovery is changed with disease and can be analyzed with T_1 recovery times, pre- or post- contrast administration [7]. Extracellular volume (ECV) is obtained by measuring the hematocrit in the blood, extracting concentration of Gd in the heart and extrapolating the myocardial fibrosis content from an estimate of the extracellular space [7].

1.1.4 LGE CMR Imaging of Cardiomyopathies

1.1.4.1 Ischemic Cardiomyopathy

Hyperenhancement occurs in the presence of either acute or chronic myocardial infarction (MI) [47, 48]. In the presence of acute infarction, cell membranes may have ruptured, allowing the extracellular contrast agent to reach what had previously been the intracellular space. In chronic infarction, the myocardium has been replaced by collagen scar and the extracellular space is increased [49].

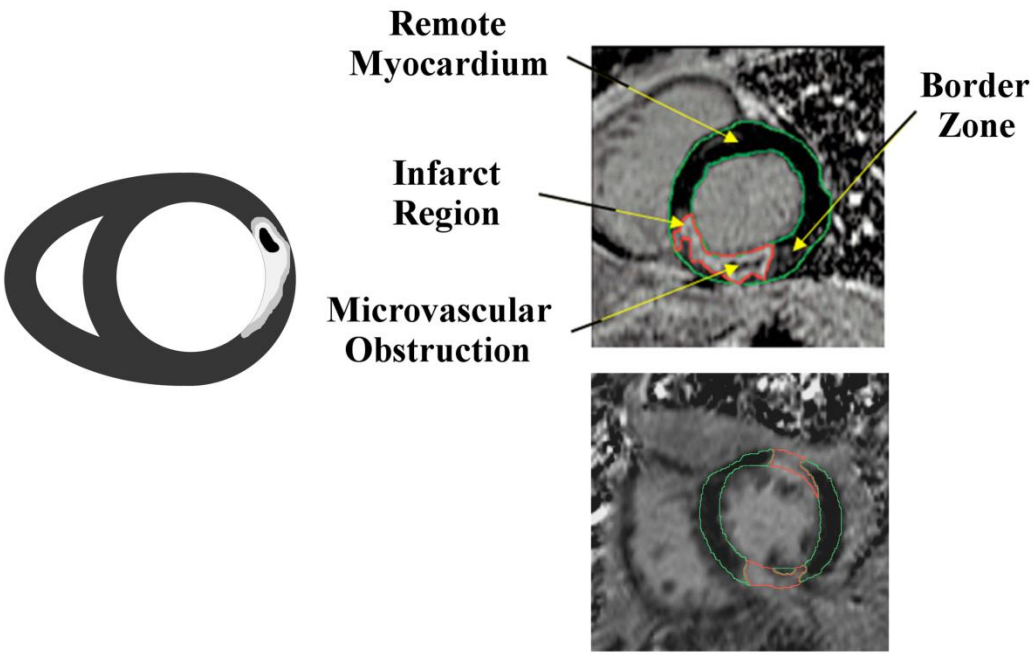

Figure 0-3 : Schematic representation of an LGE CMR image of a patient with acute MI (left). Example images to the right show an acute MI (top image) and a chronic MI (bottom image) LGE CMR patient image. The acute MI image shows macrovascular obstruction (MVO) as an island of dark signal intensity in the bright infarct region (red outline). The remote myocardium is nulled and outlined in green. The peri-infarct zone is seen as lighter shades of gray that surrounds the infarct region.

The severity and transmurality of the ischemic area can be established with LGE CMR images. This modality has the highest resolution method for imaging myocardial infarction and assessing myocardial viability [2, 50]. Four regions may be identified on LGE CMR images in the presence of myocardial infarction (Figure 0-3):

- The remote myocardium is a dark region in the myocardium. It is considered healthy, although there might be small regions of fibrosis present in the case of chronic infarctions.
- The infarction is the brightest region due to the use of the contrast agent and identifies the diseased region.

- The border zone is in tones of gray intensities that range between those of the remote myocardium and the infarct region. It is located around the infarct and is also called the gray zone.
- The microvascular obstructions (MVO) are the dark regions that can appear central to the infarcted area if the contrast agent cannot reach the center of the infarct.

The border zone is highly influenced by partial volume effects. The image resolution in the current clinical setting does not permit the analysis of the underlying fibers. This region is believed to be one of two states: a clear delineation between infarct and healthy cardiomyocytes, or the result of intermingling of infarct and healthy cells [51].

It has been shown that gadolinium based contrast agent spreads in the myocardium and enhances infarct at a near cellular level [51]. Acute and chronic infarctions exhibit different enhancement patterns on high resolution LGE CMR images. In acute myocardial infarction, lesions show some dark patches of microvascular obstruction (MVO) that are seen inside the bright region of infarct. There are also regions with less severe enhancement around the edge of the infarct. Chronic infarction is characterized by fibrosis and the myocardial wall may have thinned. The infarct then appears to be more fibrous than the remote myocardium. The MRI appearance of chronic infarction tends to be more binary with a bright region for the infarct and a dark remote myocardium.

Ischemic cardiomyopathies are amongst the most common cause of death in developed countries. However, as more acute ischemic cardiomyopathies are treated with success in the population (with interventions such as bypass surgery) more people now suffer from chronic myocardial infarction. In the clinical context, this requires doctors to distinguish an area of acute infarction in the myocardium from an underlying chronic infarction. MRI can also detect silent or unrecognized myocardial infarction in certain patients, notably those suffering from diabetes [22]. It is likely that recent unrecognized MI may be prognostically important. Since the age of myocardial infarction gives insight to the possible outcome following a cardiovascular intervention [19], it would be useful to distinguish acute from chronic myocardial infarction during diagnosis for example for a patient presenting acute symptoms with underlying chronic myocardial infarction [52]. During the diagnosis, since the standard analysis of images relies on the detection of bright regions, discrimination of the age of infarction is limited. Since the structure of the myocardium is altered

in different ways in the presence of acute or chronic myocardial infarction, exploiting these differences while analyzing LGE CMR images might help to distinguish them.

1.1.4.2 Non-ischemic cardiomyopathy

Non-ischemic cardiomyopathies result from damage to the myocardium that originates from causes other than ischemia. Enhancement of the diseased areas in LGE CMR images depends on the disease. It is believed that bright regions in LGE CMR images indicate damage to the myocardium and this modality is used as a diagnostic tool to detect non-ischemic cardiomyopathies [53]. In the presence of disease, fibrosis or other structural changes to the myocardium may lead to a signal enhancement in LGE CMR images.

Unlike ischemic cardiomyopathies that originate in the endocardium (the interior cavity of the left ventricle) [54], enhanced signal intensities with non-ischemic cardiomyopathies can originate from any location in the myocardium (Figure 0-4). Some patterns of enhancement have been observed for various diseases. In amyloidosis, the extracellular space is expanded due to amyloid deposition along with the possible presence of diffuse or focal fibrosis. Cardiac involvement in amyloidosis has been studied with LGE CMR images, where enhancement is observed in all the myocardium and with possible focal locations of enhancement [55]. LGE CMR images can help determine to what extent the heart is involved for patients with amyloidosis. Hypertrophic cardiomyopathy (HCM) is the enlargement and disarray of the heart muscle cells which leads to abnormal thickness of the left ventricular walls [56, 57]. Studies found most of the patients with HCM exhibit enhancement in the anterior or the anteroseptal segments of the left ventricle [3, 57]; however a focal pattern was also present in some HCM patients. Jiji et al. [57] report a “focal or patchy enhancement in the mid-myocardium” region. One case study presented a clear difference between enhancements caused by MI and by HCM [58]. Various cardiomyopathies affect the heart in different ways and result in different structural changes.

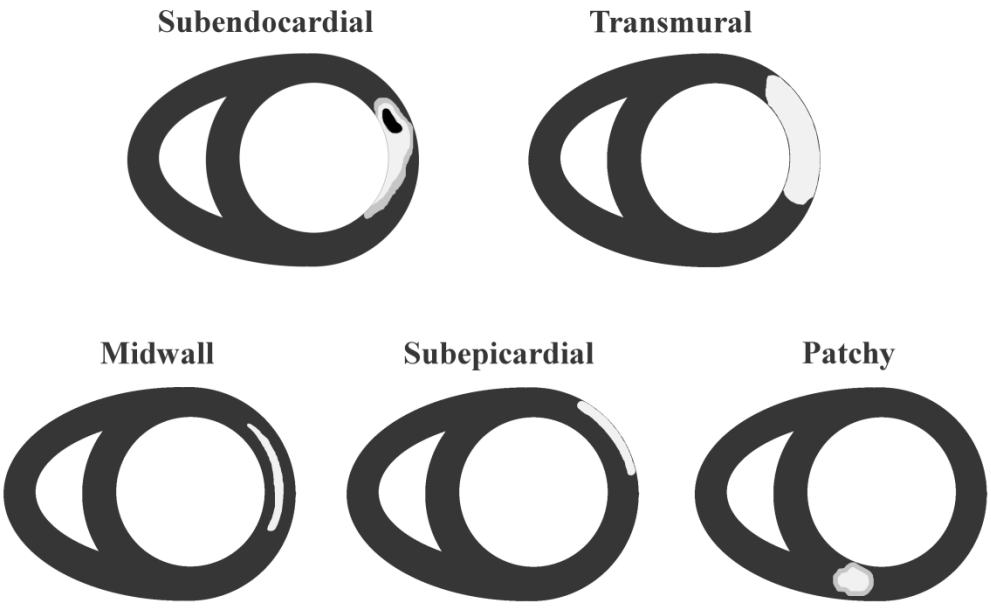

Figure 0-4 : Schematic representation of typical enhancement in LGE CMR images. The subendocardial and transmural locations of enhancement are seen in ischemic cardiomyopathies. The midwall, subepicardial and patchy enhancements are seen in non-ischemic cardiomyopathies.

Diffuse myocardial fibrosis

The increased presence of collagen fibers that can naturally occur in the myocardial muscle (diffuse myocardial fibrosis) may be attributed to aging [8, 59-63]. In the aging heart, the presence of additional interstitial collagen fibers can alter the myocardial morphology and function, adversely impacting cardiac outcome. In contrast to ischemic cardiomyopathies which exhibit focal scars near the ischemic region, myocardial fibrosis due to aging is diffusely spread across the heart muscle. Diffuse myocardial fibrosis appears intermingled with healthy cardiomyocytes in histological images. Therefore in LGE CMR images, there is little remote myocardial region that can be nulled to obtain contrast between the fibrosis and the healthy regions of the myocardium [9, 10]. Diffuse myocardial fibrosis is also present in other diseases where LGE CMR images' limitation has prevented its identification. Clinicians are now increasingly relying on other methods, such as T_1 or ECV mapping [9, 10, 12-14, 16, 64, 65].

Locations of diffuse myocardial fibrosis were identified with T_1 mapping for patients with rheumatoid arthritis [66], dilated [67] and hypertrophic [68] cardiomyopathy. T_1 mapping could identify diffuse myocardial fibrosis but could also estimate its progression in disease [69].

Extracellular volume fraction identified regions of diffuse fibrosis in dilated cardiomyopathy, even in the absence of identified enhancement from LGE CMR images [70], and in muscular dystrophy [71]. Using native T_1 values is a method which avoids administration of contrast agent to the patient and could offer diffuse fibrosis quantification [72]. However, native T_1 values have also been investigated on a 3T scanner and were not found to identify diffuse myocardial fibrosis [73]. This quantification method therefore needs more validation.

1.2 Texture Analysis in Medical Imaging

In medicine, analysis of diseases based on their underlying physiological structure has been fruitful with texture analysis. Texture features have been successfully used in magnetic resonance images to distinguish benign from malignant lesions in prostate [74, 75], breast [76-78] and liver [79] cancer as well as to study brain tissues [80]. This method seems promising, since the various cardiomyopathies affect the heart differently and result in structural differences. Acute and chronic myocardial infarctions alter the heart structure in different ways. In acute infarctions, damage is recent and there might be swelling in response to injury and signal homogeneity due to microvascular obstruction. In the presence of chronic infarctions, the heart has walls that are thinner than normal, and there is presence of fibrosis in the myocardium. These structural alterations are possible candidates for differentiation of acute and chronic infarctions and may be suitable targets for texture analysis methods. Analysis of the various underlying structural patterns of the myocardium in non-ischemic cardiac diseases could help in the diagnosis process [3]. Quantitative analysis of signal intensity or locality patterns in the myocardium in LGE CMR images could characterize aspects of cardiac diseases [3].

Texture analysis relates to the exhibited appearance of a material. Merriam Webster [81] dictionary defines texture as “the disposition or manner of union of the particles of a body or substance” or “the visual or tactile surface characteristics and appearance of something.” Texture can be more easily understood when thinking about textiles. Silk is most commonly known as a textile composed of delicate fibers. It is soft and smooth to the touch, whereas tweed is a rougher textile made of interwoven strands of wool. Silk appears more delicate and intricate whereas tweed looks rougher and bulkier. Texture, as the perceived appearance of objects, can be transposed to other fields. In imaging, texture refers to the local variation of intensities that creates the visual

appearance of objects. Satellite imagery is one application where texture analysis has been successfully applied. In this field, coarse texture can characterize a surface that exhibits many changes for example in elevation, as opposed to a smooth surface whose elevation would be more constant. In medical imaging, texture analysis is applied to describe the displayed appearance of organs as seen on images from various modalities. It can be used to delineate organs and diseased regions which are physiologically altered or to grade diseases that progressively modify the appearance of an organ in the images.

The detection and description of texture in images has been enhanced through computational processing. The limitation of the human eye to precisely distinguish different texture features in images is overcome with mathematical analysis and description of image composition. The visual perception of pattern was studied by Julesz, who described textons, or texture units [82]. Different methods have emerged that analyze characteristics of the image. Texture analysis methods have been classified into four main groups: "structural, model, statistical or transform" based [83, 84]. Methods were also described for three dimensional analysis of images [85].

1.2.1 Structural Methods

Structural methods rely on a textural entity described as the assembly of its structural parts. It involves the definition of primitives or individual components that once assembled create a texture pattern. Texels, for texture elements, were defined as primitive components [84, 86]. A lexicon of geometric patterns and the rules regarding their spatial arrangement was described by Carlucci [87] to define texture. In a similar way, Vilnrotter et al. [88] identified edge components as primitives and studied their spatial arrangement to form various textures. These methods seem to recall the receptive field in the human visual cortex that contains cells sensitive to specific edges and orientations. Structural texture analysis methods were found to be effective when the pattern analyzed was composed of an orderly pattern [89].

1.2.2 Model based Methods

Model based methods describe textures as mathematical models. Fractal geometry has been shown to represent the structural composition of many objects in nature [90]. Fractal analysis of patterns has been used to evaluate texture features in images [91, 92] and in medical imaging [93, 94]. Another model based approach uses the markov random fields for texture analysis [95]. Kashyap

et al. [96] presented a model based approach that was rotation invariant. The application of fractals in cardiology was mostly to study the physical presentation of the heart anatomy. For example, fractals have been used to study structural components such as the coronary tree in coronary angiography [97] and intravascular ultrasound [98]. Captur et al. [99] presented fractals to analyze the left ventricle anatomy from CMR images. It was suggested that heart rate variability over time could be analyzed with fractals and could be a predictor of future cardiovascular events after acute myocardial infarction [100]. This method was also applied to analyze an aging population without the presence of cardiovascular diseases [101]. However, heart rate variability is in need of more clinical validation [102]. Fractals have also been suggested to study the electrocardiogram [103].

1.2.3 Statistical Methods

Texture can be characterized by the occurrence of signal intensities found in an image or in a region of interest. Quantification of first order statistics is obtained through histogram analysis and the measures include the minimum, the maximum, the mean, the standard deviation and the kurtosis. These measures describe the range and characteristics of the signal intensity that composes the image. However, they do not provide information on the spatial distribution of the signal. A common example is given that compares a chess board pattern to a half white and half black image. Histogram analysis is incapable of differentiating the two patterns. Only methods that would consider the spatial distribution of the intensities can discern this type of difference. Spatial information is therefore important in texture analysis since repetitive patterns will contain high occurrences of signal intensities at given intervals in the image.

The limitation of histogram analysis has been addressed in methods that include the spatial information of signal intensity. In these methods, signal intensity is analyzed in constrained neighborhoods. The position and orientation of neighbor pixels with regards to a central position is used in the grey level co-occurrence matrix (GLCM). This method was described by Haralick et al. in 1973 [104]. A matrix is built that records the number of occurrences of signal intensity pairs that are formed by considering a constrained neighborhood. The matrix size is as big as the signal intensity range. Each entry of the matrix at position (i, j) corresponds to the number of times the combination of intensities (i, j) occurs in the image. The neighborhood is determined with a distance d between position of intensity i and that of intensity j. The background should not interfere with the neighborhood calculation. Once the count of occurrences of pairs of intensities

is done, the matrix should be added to its transpose to make it symmetric and remove the directional dependence of the result. In the horizontal direction, moving east or west should not impact the result and as an example, the set (2,5) and (5,2) should both count in the matrix. In order to have a probability matrix, all the entries are divided by the sum of the entries of the GLCM. Features are mathematically extracted from this GLCM, resulting in a quantification of the pattern seen in the image. The three dimensional GLCM was also computed in image volumes for medical imaging [85]. Lam et al. [105] modified the GLCM to include gradient information of neighbor pixels. One disadvantage of the GLCM method was the computational time. This was improved with optimization algorithms, variation on the matrix calculation with linked lists [106], or hardware acceleration [107]. Multi-scale calculation of the GLCM was also considered [108, 109] or distance consideration were also used to modify the algorithm [110].

Others texture analysis methods are based on the spatial distribution of signal intensity. Galloway et al. [111] described the run-length matrix (RLM), which is built by calculating the sequential occurrence of a grey level observed in the space that surrounds a specified pixel, and in various directions. Texture features are estimated from this matrix by mathematical computation similar to that of the GLCM features. Additional texture features from the RLM were proposed to increase the identification of texture in images [112]. Ojala et al. [113] compared different approaches to texture analysis and concluded the co-occurrence matrix was the most performant in discriminating texture patterns in images and simple to comprehend.

Laws features are the result of windowed analysis of signal intensity distribution [114]. An energy component is evaluated following a convolution operation over regions of the image.

The signal intensity distribution surrounding a local pixel was used to define texture by Wang and He [115]. They define *texture units* as a dictionary that defines the surrounding signal intensity values relative to a central position. *Texture units* are determined by the signal intensity of the neighbor pixels to the central position. Each neighbor is given one of three values to identify their relative signal intensity with regards to the signal intensity of the central pixel, depending if they are lower, equal or higher to the central pixel's signal intensity. The statistical analysis of the modeled local pattern gives information on the broader observed texture. Wang and He define the *texture spectrum* as the occurrences of the *texture units* and use this modeling to discriminate texture [115]. They later defined descriptive features from the statistical evaluation of their texture

spectrum [116]. The texture spectrum defined by He and Wang was promising but required heavy computational load from the high number of possible neighbor combination when assessing the neighbor signal intensities in the texture units. Reduction of the computational load from the calculation of the *texture spectrum* was done by Ojala et al. [117]. They referenced their method as local binary patterns (LBP). LBP also evaluates the binary pattern present around a central pixel [113, 117]. To do so the central signal intensity is used as a threshold and binary values are assigned to neighbor pixels that have higher or lower intensities. A binary sequence is created that characterizes the textural pattern seen in the image. The binary sequence occurrences are recorded as histograms [118]. LBP have been a successful texture analysis method, for example in medical imaging [119], and have prompted the development of improved algorithms. Hafiane et al. [120, 121] replaced the central pixel value that was used for thresholding by the median value of the designated area around the pixel. Kaya et al. [122] included the distance and the orientation information between the central pixel and its neighbors in the LBP calculations. Zhu et al. [123] improved the LBP's robustness to noise by introducing intensity normalization in the LBP calculation and furthermore considering the joint probabilities of intensities in a local region of interest with the image intensity information. Another study attempting to reduce the noise influence on texture evaluation introduced fuzzy logic in LBP evaluation [124].

1.2.4 Transform Methods

The transform methods are the analysis of texture in another domain. It was initially used to analyze texture with structural methods, such as to analyze the occurrence of primitives in the frequency domain with a Fourier transform [125]. Images are transformed into the Fourier domain where repetitive patterns in the image are described in the frequency domain.

Analysis of texture in a multi-scale approach is performed with the Wavelet or Gabor methods [126]. Wavelets were used to incorporate spatial information into texture analysis [127]. Chang et al. [126] used a tree structure in wavelet analysis to improve the identification of texture by analyzing the frequency domain only in the area of highest information content, and not only in the low frequencies as was previously done. The frequency response of images was also analyzed with a Gabor filter to locate "dominant spatial frequencies" associated to different texture pattern and allowing textural discrimination [128].

1.3 Texture Analysis in Cardiology

Late gadolinium enhanced cardiac magnetic resonance imaging is routinely used in clinical practice upon onset of cardiomyopathy diseases. In ischemic cardiomyopathies, an intensity-based approach allows identification of the location and of the extent of damage to the myocardium with LGE CMR images. However this method is limited when fibrosis is present across the myocardium, from the absence of reference signal intensity in remote and unaffected myocardium.

1.3.1 Ischemic cardiomyopathy Imaging

In ischemic cardiomyopathy, the location or transmurality and as well the extent of myocardium affected can be assessed with LGE CMR images [2]. The variation of brightness in the myocardium on LGE CMR images is obtained from the combination of different wash-in and wash-out rate by the diseased or affected cardiomyocytes and as well by a higher accumulation of the agent in the increased extracellular space. Increased intensity is associated to the presence of disease in the heart. The importance of LGE CMR images in the diagnosis of ischemic cardiomyopathies has been established and thoroughly validated and reproduced [129]. However, the enhancement in LGE CMR is similar for acute and for chronic myocardial infarction. This prevents the clinicians to assess the age of infarct. Other methods were developed to grade MI.

1.3.1.1 Signal Intensity Methods

Many image analysis methods are employed to delineate infarct in LGE images, all relying purely on signal intensity (SI) based schemes since it is generally accepted that bright areas indicate regions of myocardial infarction (Figure 0-5). One method uses a multiple standard deviations (SD) brighter than the signal intensity found in the remote myocardium as a threshold value to delineate infarct region in LGE images [130]. The threshold can range from 2 to 6SD, but is usually set to 2SD. This thresholding method is currently used in clinical practice and as well in research [19, 20, 23, 131-133]. However, it is prone to overestimation of infarct size [134, 135].

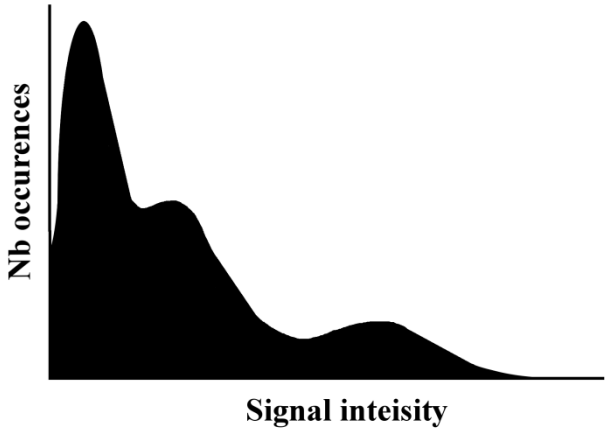

Figure 0-5 : Schematic signal intensity distribution in the myocardium from an LGE CMR image. The leftmost and highest signal distribution in the histogram corresponds to the background of the segmented image. The central distribution represents signal intensities in the myocardium and the trail of signal intensity distribution to the right would correspond to signal intensity in the myocardial infarcted region.

The full width at half maximum (FWHM) method [136, 137] evaluates the size of infarct by assigning a pixel to the infarct region if its intensity is more than 50% that of the maximal intensity found in the myocardium. However, manual delineation of the infarct region in patients with chronic MI has given better results than the FWHM method [138]. FWHM overestimated canine and human MI [137, 138].

Signal intensity based analysis of the peri-infarct zone has also been of interest since it was found to be a predictor of adverse cardiac events [24]. Signal intensity ranging from 2 to 3SD above the mean signal found in the myocardium was defined as PI zone and this size was normalized by the total myocardial infarct area [24]. These signal intensity based methods, for MI or peri-infarct zone characterization, cannot discriminate acute from chronic myocardial infarction.

1.3.1.2 Percent Infarct Mapping

In the percent infarct mapping (PIM) method a percentage (based on the proportion of infarct that a pixel might contain) is assigned to each pixel in the MR image [139]. This method was based on R_1 (the inverse of T_1) and required a new gadolinium derived contrast agent since the peak enhancement of the currently used contrast agent, Gd-DTPA, was too early following intravenous administration to estimate R_1. A subsequent method was developed to use PIM in a clinical context,

overcoming the need for a new contrast agent [140]. Another method developed to overcome partial volume effects weighted the amount of infarcted tissue that a pixel might contain [141]. This method requires the user to select a threshold to differentiate normal from abnormal tissues. That threshold problem becomes equivalent to the SI threshold.

1.3.1.3 Image Processing Method

The feature analysis and combined thresholding algorithm (FACT) [142, 143] is composed of a series of image processing steps. The SD thresholding method is first applied to the image, followed by feature analysis to remove sparse artifact areas detected by the SD thresholding step. The region is further processed by the FWHM method to have the area of infarct determined by a final feature analysis. The FACT method includes volumetric considerations, automatic threshold determinations, and steps that account for both partial volume errors and the random isolated bright pixels that are expected to exceed a simple 2 standard deviation threshold. The FACT method was validated in animals where it was compared to histology and with human subjects, yielding better results than manual planimetry, the SD method, or the FWHM method. Again, this method does not discriminate the age of infarct.

1.3.1.4 Infarct Age Discrimination

Classification of MI according to age is important however difficult to accomplish automatically with methods based on average signal intensity since pixel enhancement is said to be similar for acute and chronic infarcts [18-21]. The myocardium remodels during the recovery period after myocardial infarction [144]. Cellular structures appear disorganized in acute MI and microvascular obstruction (MVO) can be present. MVO appear as hypo-enhanced regions inside the bright area that is infarct in MRI images. This is explained by the lack of blood that reaches this region due to obstruction of microvascular vessels. This low signal intensity is therefore an exception to the general rule that associates bright regions in MRI to dead tissue. In chronic MI, there is thinning of the myocardial wall [145] and cells appear more elongated and the cardiomyocytes are replaced by a fibrous scar. This variation in structure is seen in histology [19] and since gadolinium enhancement closely corresponds to fibrosis at a near cellular level [51], the complex structure of the acutely and chronically infarcted myocardium could be distinguishable in LGE images. The physiological changes that arise from acute to chronic could be characterized with pattern analysis methods and thus may provide insight into the age of the infarct.

1.3.1.5 Acquisition Based Methods

Other methods rely on MRI sequence acquisition to delineate areas of infarction, such as T_1 mapping. The T_1 mapping technique is promising to assess diseased myocardium without the need for contrast agent [146-148]. Extracellular volume fraction is a more precise measure of the expansion of extracellular space in disease, but does need contrast agent and hematocrit measures [15, 147, 149]. Those methods are promising, however they were unable to assess the age of infarct [150].

1.3.2 Fibrosis Imaging in Non-Ischemic Cardiomyopathy

1.3.2.1 Limitation of Myocardial Fibrosis Analysis

The presence of myocardial fibrosis has been associated with increased stiffening of the heart, altering the heart's function and ultimately leading to sudden death. CMR imaging has proven a reliable indicator of the presence of fibrosis in non-ischemic cardiomyopathies which have been associated with adverse cardiac outcome [151-158]. While the myocardial scar characteristics from LGE CMR images have been thoroughly validated clinically, the detection of diffuse myocardial fibrosis has proven challenging with conventional signal intensity based methods applied to LGE CMR images. In the thresholding method, a value above the mean signal intensity of the remote myocardium is chosen. The remote myocardium is identified as the area where signal intensity isn't enhanced by the contrast agent. Collagen fibers are present across the myocardium and there are therefore no areas clear of fibrosis in LGE CMR images that can serve as a reference signal intensity from which enhancement could be determined. This limits the precise identification of the location of fibrosis in non-ischemic cardiomyopathies. First order statistics from LGE CMR images are therefore limited in the presence of non-typical pattern of enhancement in the myocardium.

1.3.2.2 Non-Ischemic Cardiomyopathy Imaging

Assessment of non-ischemic cardiomyopathies was previously done visually. Patterns of signal enhancement were noticed in the myocardium in the presence of various diseases and the terms "patchy foci, heterogeneous, multifocal, and non-specific" [17] were used. The visual pattern of enhancement in LGE CMR images is a descriptive method that was used to establish if it could be

related to the outcome for patients with non-ischemic cardiomyopathies [159]. Methods to quantify myocardial fibrosis were developed.

Since diffuse myocardial fibrosis is spread out across the myocardium, the area occupied by the signal enhancement might be similar in ischemic and non-ischemic myocardial fibrosis. However, whereas ischemic myocardial fibrosis is concentrated in a relatively well-defined area, diffuse fibrosis is spread out across the myocardium, often creating islands of enhanced signal in LGE CMR images. One way of identifying hyper-enhanced area in this case was to consider the visual structure of the scar in LGE CMR images. O'Donnell et al. [160] identified non-focal myocardial scar by including three physiological components of scar tissue: the border length normalized by the area of scar, the information on transmurality and the percent non-viable scar area.

1.4 Texture Analysis of Fibrosis from other Imaging Modalities

Texture analysis has been exploited to characterize the different patterns of enhancement that are created in the presence of collagen fibers in targeted organ from CT or from MR images. For example, medical imaging methods exist for fibrosis detection in the lung. Pulmonary fibrosis impairs breathing ability and its progression compromises the life of a patient. Automatic detection and grading of pulmonary fibrosis was performed with texture analysis applied to chest radiographs [161-167]. Texture analysis was a successful tool to classify pulmonary diseases on CT images of the chest [168-170] and as well with 3D CT images [171]. The progressive increase of infiltrative collagen fibers also occurs in liver fibrosis and can lead to liver stiffening, with the end stage being liver failure [172]. The different stages of liver fibrosis result in various image characteristics on CT or MR images and have been assessed with texture analysis. House et al. [173] found that texture analysis was not appropriate for the intermediate stages of liver fibrosis, but performed well in discriminating normal cases from those with liver fibrosis. Zhang et al. [174] used Haralick's grey level texture analysis method to successful grade liver fibrosis from MR images. Yokoo et al. [175] found texture analysis of enhanced MR images, obtained with both SPIO and Gd-DTPA contrast agent, could characterize the level of liver fibrosis when compared to liver biopsy. The degree of liver fibrosis was also assessed with different texture analysis methods applied to other modalities, such as double contrast enhanced MR images [176], in diffusion weighed images [177], in proton density MR images [178], and in a comparative study of T_1- and T_2-weighed to contrast enhanced MR images [179]. Texture analysis of ultrasound images was used to automatically classify liver fibrosis [180-182]. The texture analysis methods GLCM, RLM, Law's features and the gray level gradient matrix resulted in liver fibrosis identification from contrast enhanced CT images [183]. The detection and level of presence of collagen fibers by means of texture analysis of medical images has therefore potential in cardiac application. Texture has been extensively used in cardiology in ultrasound images. It was used to evaluate mitral valve regurgitation [184]. Infarcted area was identified by evaluating various texture analysis methods applied to echocardiograms [185]. Texture analysis, namely the run-length matrix, was applied to LGE CMR images in the presence of hypertrophic cardiomyopathies [186].

1.5 Medical Image Classification

1.5.1 General Classification Methodology

In general, texture-based classification is composed of five steps (Figure 0-6). The first step consists of pre-processing the images. This is required in order to extract the region to analyze and to standardize the intensity between images as a common basis for comparison. A choice of features has to be made and we have processed Haralick's texture features from the GLCM. The feature reduction step is performed when the number of features is too big and there is a need to reduce the computation time. Feature selection also reduces the number of features that are given to the classifier by selecting the most significant ones for the problem. We acknowledge that we have a small number of features that were evaluated from the GLCM. Nevertheless a feature reduction algorithm might enhance the classification results if certain significant features influence the classification more than others.

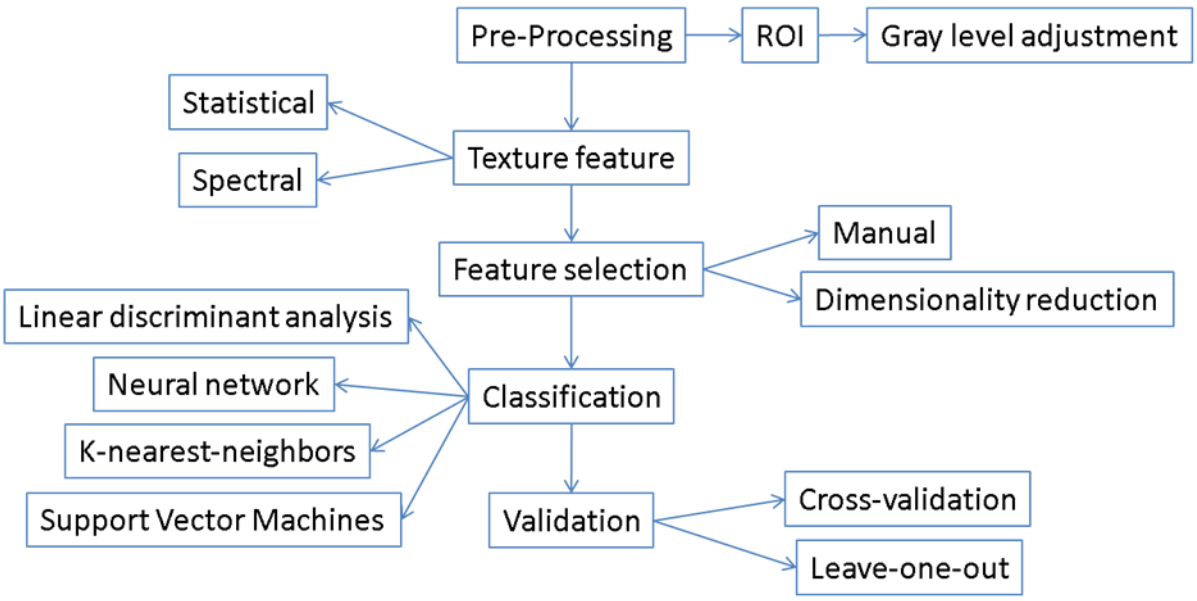

Figure 0-6: Diagram of the different computations involved in texture analysis and classification [187]. A pre-processing step prepares the images to extract the texture features that will be selected to perform classification. Validation of the results is sometimes done simultaneously as the classification step with the cross-validation or leave-one-out methods.

Feature selection can be done by selecting the most discriminant features by comparing classification rates for each individual features or feature reduction techniques can be used. Principal component analysis (PCA) changes the reference axis in the feature space by choosing the orientation of widest distribution of the features. Since the directions with the widest spread of values are used, other dimensions where there is smaller spread can be disregarded. The directions are chosen based on the eigenvectors and the highest associated eigenvectors indicate which components to keep. Linear discriminant analysis (LDA) is another method of feature selection. This process projects features onto a linear component. This linear component is chosen to maximize the distance between the projections of the mean of the different groups of features. Feature reduction is done by projection of the features onto the new feature space and selecting components. Once a feature set has been chosen, a choice of classification method has to be made and relies on many factors. For example, the features could be continuous or discrete, the number of classes (groups) may be known or not, or there might be a need for a parametric or non-parametric method, amongst other considerations [188]. Different classifiers exist that are chosen based on the problem at hand. Validation is the last step in texture analysis and classification to assess the performance of classification. Optimally, a training set of features is determined to give examples to the classifiers and a testing set is provided to estimate the classification performance given as a percentage of correctly classified cases. Cross-validation or the leave-one-out methods are ways in which the classifiers' performance can be established, by taking specific cases out of the training set while training on the rest of the cases and alternating on the cases being removed from the training set.

1.5.2 Classifiers

There are many types of classifiers that solve the general problem of deciding to which class a feature vector belongs, based on the problem at hand. Unsupervised learning is performed when classes are unknown and the classifier determines which feature vector belong to a class. Another type of classifier can assume probabilistic hypothesis on the distribution of the data to help solve classification problems. This section will do a brief overview of methods that have been used in previous studies to address classification as a means of grading diseases.

Unsupervised classifiers are used when specific classes are unknown. This is the case for example of the k-means classifier [188]. The available feature vectors are iteratively grouped into clusters

based on the distances between the feature vectors from the mean of a cluster. The mean is calculated as the centroid of the feature vectors that compose the class. Clusters are iteratively re-calculated so as to have minimal distances between the feature vectors of one cluster while maximizing the distance between clusters. As feature vectors are fed to the classifiers, their distance to the mean of each class is evaluated and the closest mean determines the class it belongs to. In supervised classifiers, classes are known. With the k-NN classifier for example, a feature vector is associated to a class when the majority of its *k*-nearest-neighbors in the feature space belongs to that class [188].

The Bayesian classifier is a statistical method which relies on probabilities. Given a set of feature values, the goal is to find the probability that an instance belongs to a specific class w_i. The Bayes Theorem gives the probability of the feature vector belonging to one class [188]. Let $p(w_i)$ be the prior probability of belonging to class w_i, or the likelihood of belonging to a specific class. The class conditional probability density function is $p(x|w_i)$ and is the probability of having feature x if we are in class w_i. The Bayes theorem gives the posterior probability as: $p(w_i|x) = \frac{p(x|w_i)p(w_i)}{p(x)}$.

The naïve Bayes classifier [188] assumes that the features are independent, and the decision of which class to assign a feature vector is based on the maximal probability obtained amongst the probability computation for each class:

$$argmax_{j=0..d}\left(\prod_{i=1}^{n} p(x_i|w_j)\right).$$

In ischemic cardiomyopathies imaged with LGE CMR, texture analysis has been used with classification methods to differentiate the healthy myocardium from the scar tissue by Kotu et al. [189]. In that study, texture features were evaluated in the remote myocardium and in the infarcted tissues. A combination with the signal intensity feature formed the feature vector. Classification was performed with the maximum likelihood estimator which uses the Bayesian theorem. In another study by Kotu et al. [190], infarcted myocardial tissue was assigned a percentage related to the degree of its fibrosis content. That study used the Bayesian theorem to estimate the probability of assigning a pixel to the scar tissue class.

The support vector machines (SVM) classifier performs a dimensionality augmentation to provide a discriminant boundary, in the form of a hyperplane [188]. Features are converted to the higher dimensionality feature space via a mapping function. The support vectors are the vectors that define the margins around the hyper-plane and the decision boundary is defined. The choice of kernel depends on the problem, linear or not for example. The boundary is chosen so as to maximize the distance of margins to the features provided in the training step (Figure 0-7). The choice of kernel depends on the features separability, for example if they are linearly separable or not. The radial basis function (RBF) kernel can be chosen when there is nonlinear separability of features. A comparison of different classification methods showed that the SVM with the RBF as kernel obtained the best classification result for identification of obstructive lung disease when using texture analysis of CT images [191]. Another comparative study of SVM versus Bayesian classification indicated better diffuse lung disease classification with the SVM method, using the RBF as a kernel, even when the classification was performed on texture features extracted from images obtained through different scanners [192].

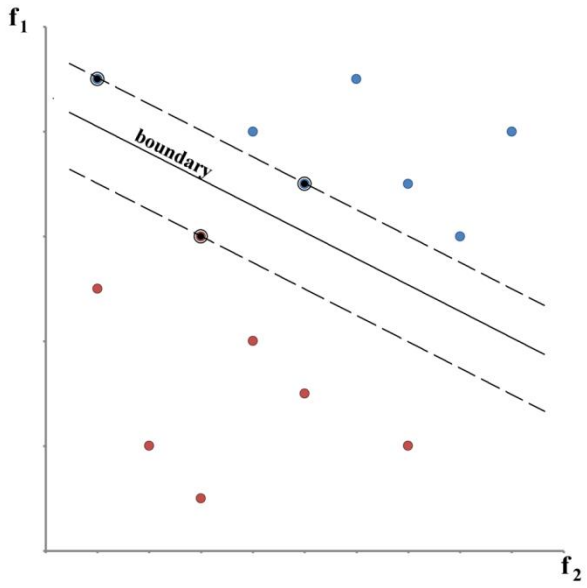

Figure 0-7 : Support vector machine conceptual representation. The support vectors are identified with the black dots. The dashed lines are positioned at a maximal distance between the boundary and the support vectors. *Image inspired from Duda, Hart, Stork [188]*.

Decision trees [188] are non-parametric supervised classifiers. In basic decision trees a sequence of division at the different nodes into the branches is based on the feature vector characteristics and lead to categories associated to a leaf, or class. At each node, there can be a dichotomization or a higher number of splits (branches that emanate from a node). Extra-tree was described as a method which uses randomized decision trees. It was used in a comparative study of automatic versus semi-automatic classification of lung diseases from CT images [193]. That study used volumetric areas for feature calculation and favored the classifier that would adapt to the input from the user, meaning that classification was influenced by the clinician's decision on grading diseases in the training process. The random forest classifier is a method where many decision trees are used. Classification is done by feeding the feature vector to all the trees. A decision is made by choosing the most popular class amongst the classification result of all the decision trees. Random forest was successfully used to classify interstitial lung disease by identifying patterns found in CT images, and surpassed classification results of k-NN and artificial neural networks classifiers [194].

Neural networks [188] are non-linear supervised classifiers that learn from the feature vectors that are initially provided. Neural networks are composed of a combination of nodes that have a weighted input and a bias term. The nodes in the network are distributed in layers, the first one called the input layer which receives the components of the feature vector. The last layer is called the output layer which outputs the components that determine the class to which belongs the input vector. There may be several hidden layers that separate the input and the output layers. The weights of the nodes and the bias term are adjusted by a backpropagation method based on the classification result of the feature vectors in the learning step. Artificial neural networks (ANN) were used to grade lung diseases in CT images [195]. Fukushima et al. [195] found that ANN results were strongly dependent on the amount of examples provided. They stated that the number of cases available for rare diseases could limit their identification with the ANN classifier. Variations of the neural network have been developed. Deep convolutional neural networks, for example, have successfully been used in the classification of interstitial lung disease from CT images [196, 197]. Those neural networks require a large number of feature vectors in the training set. Because of this limitation, some studies rely on previously trained networks.

CHAPTER 3 HYPOTHESES AND OBJECTIVES

LGE CMR images are routinely used to assess myocardial infarctions for patients with ischemic cardiomyopathies. This imaging modality has been extensively studied and used in clinical practice. It offers information on the location and extent of damage in the myocardium following ischemia [2] and has been found useful in other clinical cardiovascular applications [198]. However, quantification of diffuse myocardial fibrosis and discrimination based on the age of infarction remains challenging with conventional signal intensity based methods. The widespread appearance of diffuse fibrosis limits the identification of remote myocardium and the signal intensity threshold method is therefore inapplicable. LGE CMR imaging has been thoroughly validated and it remains a reference in cardiovascular imaging. It would be beneficial to use this imaging method to characterize disease or assess diffuse myocardial fibrosis. Categorizing cardiomyopathies has proven challenging since they exhibit common degrees of enhancement in LGE images. The specific aim of this Ph.D. thesis was to assess the biological characteristics of the myocardium through quantitative texture analysis methods of LGE CMR images. Our hope is that these image analysis methods will offer complementary information to the currently available signal intensity methods. We hypothesize that texture analysis will distinguish different patterns of fibrosis associated with cardiomyopathies.

Texture analysis should be investigated in a high resolution setting to establish its relation to the underlying myocardial tissue structure. The precision of high resolution LGE CMR images in ischemic cardiomyopathy has been proven to approach a cellular level [51]. Validation of texture analysis to measure the myocardial fibrosis content should therefore be applied to microscopy LGE CMR images and compared to a ground truth such as histology. Once the relation between the measured texture features and the underlying myocardium has been established, clinical evaluation can be performed to investigate if quantitative texture analysis could be beneficial for patient diagnosis. The innovative approach of this thesis lies in the application of texture analysis in the diagnostic process, to differentiate between diseases that might be present in the myocardium.

1.6 Hypotheses and Objectives

Quantitative image analysis methods will be investigated to define specific textural features that can be used in the assessment of the myocardium in a more effective way than conventional signal intensity average based methods. These methods should identify the presence of fibrosis when typical or atypical patterns of enhancement are identified in LGE CMR images.

H1: Since high resolution LGE CMR images have been shown to follow myocardial infarction to a cellular level [51], texture analysis of microscopy LGE CMR images may assess the presence of increased myocardial fibrosis in the heart.

H2: Since myocardial infarction includes a myocardial injury that exhibits a heterogeneous pattern previously studied in LGE CMR images of patients [51], texture analysis may be able to characterize myocardial fibrosis in a clinical setting for patients with acute compared to chronic MI.

1.7 Objectives

The following objectives have been identified to verify the hypotheses:

O1: Determine which animal model offers an increase of myocardial fibrosis to model diffuse fibrosis.

O2: Apply quantitative texture analysis to high resolution ex-vivo LGE CMR images as a method to define the underlying microscopic structural distribution of fibrosis in the animal model of myocardial fibrosis.

O3: Compare texture analysis quantification measures of myocardial fibrosis and high resolution LGE CMR images acquired in O2 to the histology images of the animal model of myocardial fibrosis.

O4: Apply the texture features from O2 to LGE CMR images acquired in a clinical setting, to measure the structural discrepancies that are present in different aged ischemic cardiomyopathies.

O5: Classify ischemic cardiomyopathies according to age from the texture features evaluated in O2 applied to LGE CMR patient images.

1.8 General methodology

Computational texture analysis methods have to be validated in a microscopic setting before clinical investigation. The relationship between the biological myocardial structure and the quantitative texture analysis measures from high resolution LGE CMR images has to be established. We investigated the microscopic structural changes that occur in the myocardium during the aging process by quantifying the presence of myocardial fibrosis and comparing those results with texture analysis of microscopy LGE CMR images. It has been shown that older hearts have increased myocardial fibrosis compared to younger ones, both in animal models and in humans [199].

We evaluated how well texture features calculated from high resolution LGE CMR images of ex-vivo rat hearts can assess the changes in the myocardium microstructure that happens with the increase of myocardial fibrosis due to aging. Ex-vivo animal heart LGE CMR images were used to allow for a higher image resolution than in possible for in-vivo imaging. The choice of our animal model was validated by assessing the performance of high LGE CMR images to quantify myocardial fibrosis and more specifically to detect a change in the quantity of collagen fibers present in the heart of young and old rats. Validation of measures was done with histology image quantification stained with a collagen-specific agent to follow myocardial fibrosis. Three

dimensional texture analysis was then applied to LGE CMR images. We used the contrast texture feature extracted from the GLCM built from signal intensity of the LGE CMR images to create contrast texture maps [200]. We compared texture analysis quantification with the quantification obtained from LGE CMR images in the young versus the old rat hearts.

The successful texture analysis method used to assess the increased presence of fibrosis in high resolution LGE CMR images was then applied in a clinical setting to perform a translational study [201]. LGE CMR images of patient with ischemic cardiomyopathy were divided into two groups according to the age of their MI. Regions of interest were segmented automatically [142] and adjusted by an experienced cardiologist to isolate the myocardial infarct, the peri-infarct zone and the remote myocardium. Regions were analyzed with the GLCM matrix and eight of Haralick's defined texture features were computed [104]. Different aged MI seen in LGE CMR images exhibited different heterogeneity pattern unidentified with signal intensity based methods. However, texture analysis of LGE CMR images successfully differentiated acute from chronic MI patients. Structural changes observed during MI progression were assessed by texture features applied to LGE CMR images of patients with acute MI compared to chronic MI.

We obtained preliminary results for the classification LGE CMR images of patients with ischemic cardiomyopathies. The texture features that we obtained in our second study, and presented in our submitted journal paper, were not linearly separable as assessed with the naïve Bayes classifier. Since previous studies indicate a better performance with the SVM classifier when analyzing a diffusive pattern in medical images, we chose this classifier with the radial basis function as kernel. Feature reduction was done with the principal component analysis. A leave-one-out classification validation was performed due to the small number of cases available.

CHAPTER 4 ARTICLE 1: QUANTITATIVE ASSESSMENT OF MYOCARDIAL FIBROSIS IN AN AGE-RELATED RAT MODEL BY EX VIVO LATE GADOLINIUM ENHANCEMENT MAGNETIC RESONANCE IMAGING WITH HISTOPATHOLOGICAL CORRELATION

Pascale Beliveau[1,2], Farida Cheriet[2], Stasia A. Anderson[1],

Joni L. Taylor[1], Andrew E. Arai[1], Li-Yueh Hsu[1]

[1]National Heart, Lung and Blood Institute, National Institutes of Health,

Bethesda, Maryland, USA

[2]Institute of Biomedical Engineering, Ecole Polytechnique of Montreal,

Montreal, Quebec, Canada

1.9 Presentation

This chapter consists of the journal article "*Quantitative Assessment of Myocardial Fibrosis in an Age-Related Rat Model By Ex Vivo Late Gadolinium Enhancement Magnetic Resonance Imaging with Histopathological Validation*" that has been published in the peer-reviewed journal *Computers in Biology and Medicine* on July 29, 2015. This publication was preceded with the conference paper "*Textural Analysis of Diffuse Myocardial Fibrosis in Aging Rats: A Late Gadolinium Enhancement Magnetic Resonance Imaging Study*", that was published in the *International Symposium on Biomedical Imaging: From Nano to Macro,* in April 2013 [202]. In this paper we first show that high resolution LGE CMR imaging is capable of detecting age-related myocardial fibrosis on an ex-vivo animal model and secondly that texture analysis can enhance the location of signal intensity enhancement.

1.10 Abstract

Late gadolinium enhanced (LGE) cardiac magnetic resonance (CMR) imaging can detect the presence of myocardial infarction from ischemic cardiomyopathies (ICM). However, it is more challenging to detect diffuse myocardial fibrosis from non-ischemic cardiomyopathy (NICM) with

this technique due to more subtle and heterogeneous enhancement of the myocardium. This study investigates whether high-resolution LGE CMR can detect age-related myocardial fibrosis using quantitative texture analysis with histological validation. LGE CMR of twenty-four rat hearts (twelve 6-week-old and twelve 2-year-old) was performed using a 7 Tesla MRI scanner. Picrosirius red was used as the histopathology reference for collagen staining. Fibrosis in the myocardium was quantified with standard deviation (SD) threshold methods from the LGE CMR images and 3D *contrast* texture maps that were computed from grey level co-occurrence matrix of the CMR images. There was a significant increase of collagen fibers in the aged compared to the young rat histology slices (2.60±0.27 %LV vs. 1.24±0.29 %LV, $p<0.01$). Both LGE CMR and texture images showed a significant increase of myocardial fibrosis in the elderly compared to the young rats. Fibrosis in the LGE CMR images correlated strongly with histology with the 3 SD threshold ($r=0.84$, $y=0.99x+0.00$). Similarly, fibrosis in the *contrast* texture maps correlated with the histology using the 4 SD threshold ($r=0.89$, $y=1.01x+0.00$). High resolution ex-vivo LGE CMR can detect the presence of diffuse fibrosis that naturally developed in elderly rat hearts. Our results suggest that texture analysis may improve the assessment of myocardial fibrosis in LGE CMR images.

1.11 Introduction

The presence of myocardial fibrosis is associated with the development of cardiomyopathies [17] and has been shown to increase with age [59, 199, 203]. Myocardial fibrosis in non-ischemic cardiomyopathy (NICM) may alter the morphology and function of the myocardium and lead to adverse cardiac outcomes [5, 68, 204]. Non-invasive imaging methods are therefore desirable for the detection and quantification of fibrosis in the myocardium and to stratify the risk of sudden cardiac events.

Currently, myocardial infarction or scar from ischemic cardiomyopathies (ICM) is identified by late gadolinium enhancement (LGE) cardiac magnetic resonance (CMR) imaging [2]. The combination of the contrast agent kinetics and the jeopardized cellular structure of the myocardium result in signal enhancement in the diseased area. Ex-vivo imaging of myocardial infarction can be performed at a near-cellular level and closely match with histologic myocardial fibrosis [51]. Myocardial infarctions are focal, and are seen as concentrated patches of enhancement in LGE CMR images. However in the presence of diffuse fibrosis, there is an intermingling of healthy and

diseased myocardial cells accompanied by an increased extracellular space, which results in subtle non-uniform regions of enhancement across the myocardium in LGE CMR images. It has therefore been challenging to quantify the level of fibrosis in the myocardium from NICM using conventional approaches. For example, clinicians relied on the visual appearance of enhanced regions in LGE CMR images to characterize diffuse myocardial fibrosis, using qualitative descriptions such as: "patchy foci, heterogeneous, multifocal, and non-specific" [17]. Standard quantification methods, such as signal enhancement thresholding, used to detect focal myocardial scars in ICM, may not work for diffuse fibrosis in LGE CMR images [8-11]. Other quantification methods of diffuse fibrosis relied on the non-focal aspect of diffuse fibrosis [160]. More recently, descriptors based on acquisition parameters such as the pre- or post-contrast T_1 and extracellular volume fraction (ECV) imaging techniques have emerged to measure diffuse myocardial fibrosis from various etiologies [8-14, 16, 64, 205]. There are an increasing number of studies assessing the reliability of these methods to detect diffuse myocardial fibrosis. The advantage of these methods is the absolute scale to measure these myocardial tissue properties. CMR diffusion tensor imaging (DTI) has been explored in patients with heart failure to characterize the myocardial microstructure in the presence of diffuse fibrosis [65]. Alternatively, T_2 measurements have been successful in detecting diffuse myocardial fibrosis [206]. However, in former studies when the acquisition methods are not available, an image based analysis method to identify diffuse myocardial fibrosis could be beneficial.

Quantitative texture measures from CMR image have previously been applied to characterize the structural complexity of the myocardium that changes in the presence of disease. Eftestol et al. [207] found texture analysis in the infarct area combined with LV ejection fraction measurement could discriminate patients at higher risks of developing arrhythmia. Kotu et al. [190] studied how texture analysis could segment myocardium infarct region from remote myocardium and as well distinguish higher risk patients with implantable cardioverter defibrillator for the treatment of ischemic cardiomyopathies. More recently, Thornhill et al. [186] applied texture analysis to LGE CMR of patients with hypertrophic cardiomyopathy and found distinct texture features could discriminate those patients from healthy volunteers, even without the presence of significant hyper-enhancement in the myocardium. However, all these studies lacked histological validation.

The specific aim of this study was to determine whether quantitative texture analysis of LGE CMR images can detect subtle myocardial fibrosis.We hypothesize that computational texture analysis

of the LGE CMR images may improve the assessment of more subtle and heterogeneous myocardial fibrosis and may discriminate elderly from young hearts.

1.12 Methods

1.12.1 Animal Model

The animal study was approved by the National Institute of Health Animal Care and Use Committee. Twelve 2-year-old F344 Brown Norway male rat (National Institute of Aging, Bethesda, MD) and twelve 6-week-old Sprague Dawley male rats Charles Rivers Laboratories Inc., Wilmington, MA) were used.

Once the rats were anesthetized with 1-5% isoflurane mixed with oxygen, Gadolinium diethylenetriamine pentaacetic acid (Gd-DTPA, Magnevist, Schering Berlin, Germany) contrast agent at a concentration of 0.6 mL/kg was administered intravenously. The rats were given potassium chloride 10 minutes after administration of the contrast agent to freeze the in-vivo myocardial distribution of gadolinium for subsequent ex-vivo imaging. Immediately, excised hearts were immersed in fomblin perfluoro-polyether (Solvay Solexis, West Deptford, NJ) for CMR imaging. Hearts were then fixed in a 10% Formalin solution for histology processing after the image acquisition.

1.12.2 Image Acquisition

A 7T Vertical Bruker BioSpin small animal scanner (Billerica, MA) was used to obtain the images. A 3D gradient echo image acquisition sequence was performed with a repetition time of 20 ms, an echo time of 3.5 ms, and a flip angle of 30^{o}. The field of view was 1.9-2.0x1.9x1.9cm^{3}, the matrix size was 256-320x256x256 with a pixel bandwidth of 325Hz. The resulting voxel size was ~75x75x75 μm^{3}. For each heart, five to seven 3D images were acquired consecutively over a 3-hour period. Each image acquisition lasted 20 minutes without averaging. Three volumes were manually selected, based on their similarity with each other, and averaged to improve the signal to noise ratio for each individual heart.

1.12.3Histology

Upon completion of the scanning process, all the fixed hearts were embedded in paraffin and cut in 5 µm sections in the short-axis (SA) plane from the apex to the base. Picrosirius red stain, which binds specifically to collagen fibrils (type I, II and III) [208], was used to evaluate fibrosis content in the myocardium. Slices were then digitized with a Leica MZFLIII microscope (Wetzlar, Germany) with a 10x objective lens.

1.12.4Image Analysis

1.12.4.1 Histology Images

Histological image processing was done with a custom software developed with the Interactive Data Language (IDL, Exelis Visual Information Solutions, Boulder, CO). The slice with the most collagen, assessed visually, was chosen for myocardial fibrosis quantification. Quantification of collagen content from the histology images was performed with a multi-channel thresholding method based on the color and illumination contents similar to Yabusaki et al. [209]. The histology image slices were first converted from red-green-blue (RGB) to hue-saturation-value (HSV) channels [210]. In the HSV color space, the *H* channel is defined by a color wheel with primary colors associated to specific angles around the center: 0^o = red, 120^o = green, 240^o = blue Figure 0-1. The *S* channel describes the amount of white in a color given by the *H*. As *S* increases, the distance to the center of the wheel increases and less amount of white gets mixed with the given color. The *V* channel specifies the shading of a color in *H*, with a completely black color associated to 0.

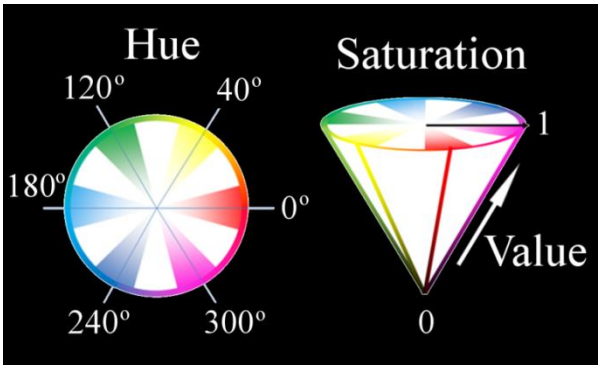

Figure 0-1 : Schematic representation of the color transformation from the RGB to the HSV space.

The conversion of the color space from RGB to HSV is described in Foley et al. [210]. The RGB values are normalized between 0 and 1, and the values of *H* are cycling from 0° to 360°. The Foley et al. equations are:

$$V = max(R, G, B)$$

$$Delta = max(R, G, B) - min(R, G, B)$$

$$S = {Delta}/{V}$$

$$H = \begin{cases} 60 * \left({(G - B)}/{Delta}\right) & , \ if\ R = V \\ 60 * \left(2 + {(B - R)}/{Delta}\right), & if\ G = V \\ 60 * \left(4 + {(R - G)}/{Delta}\right), & if\ B = V \end{cases} \quad (1)$$

The *V* channel contains the illumination component of an image and depicts the lighting variation across such an image. Therefore, the information contained in this channel is discarded from our segmentation process. The myocardium region of interest (ROI) segmentation was performed by removal of the white shades in the background. Since the *S* channel contains the amount of white in a color, a threshold of 0.2 was applied to this channel to eliminate the background pixels. To further isolate red stained collagen fibers in the myocardial ROI, two thresholds, one close to 0° and another close to 360 °, were used to pick up the color red in the *H* channel, and a threshold close to 1 was used for the *S* channel. The results of fibrosis quantification were expressed as the percent area of the left-ventricle (%LV) myocardium.

1.12.4.2 LGE CMR Images

Analysis of the LGE CMR images was performed with custom computer software developed in IDL with a graphical user interface for volume re-slicing and segmentation tasks. LGE CMR images were resliced in the SA direction from each 3D data volume to match the histological sections. The quantification of fibrosis content was performed by first manually tracing the LV endocardial and epicardial contour ROI on the re-sliced LGE CMR images, excluding epicardial fat and ventricular cavity blood pool. To determine the best thresholds for quantifying the amount of fibrosis within the myocardial ROI, a remote region was manually selected to estimate the mean

and standard deviation (SD) of the normal myocardial signal intensity (SI). Semi-automated 2 to 6 SD thresholds above the mean SI were then applied to measure the distribution of bright pixel enhancement in the myocardial ROI and evaluate the amount of diffuse fibrosis in the LGE CMR and texture images quantitatively. The results were compared to the myocardial collagen content measured from the reference histology images to determine the best threshold for CMR and texture image quantification.

1.12.4.3 Texture Analysis

Three dimensional texture analysis was performed in the LGE CMR image volume using the grey level co-occurrence matrix (GLCM) from which texture features were derived following Haralick's method [104]. *Contrast* texture maps of the myocardium were created by computing the GLCM for each pixel Figure 0-2. Quantization of the signal intensity was performed to standardize the comparison of intensity distribution and to improve the computational time. Signal intensity histogram was computed from the myocardial ROI, in which the most prominent distribution was detected as the remote myocardium since it has the largest region in the image. Quantization was then performed by alignment of the peak of the remote myocardial distribution among all rat hearts.

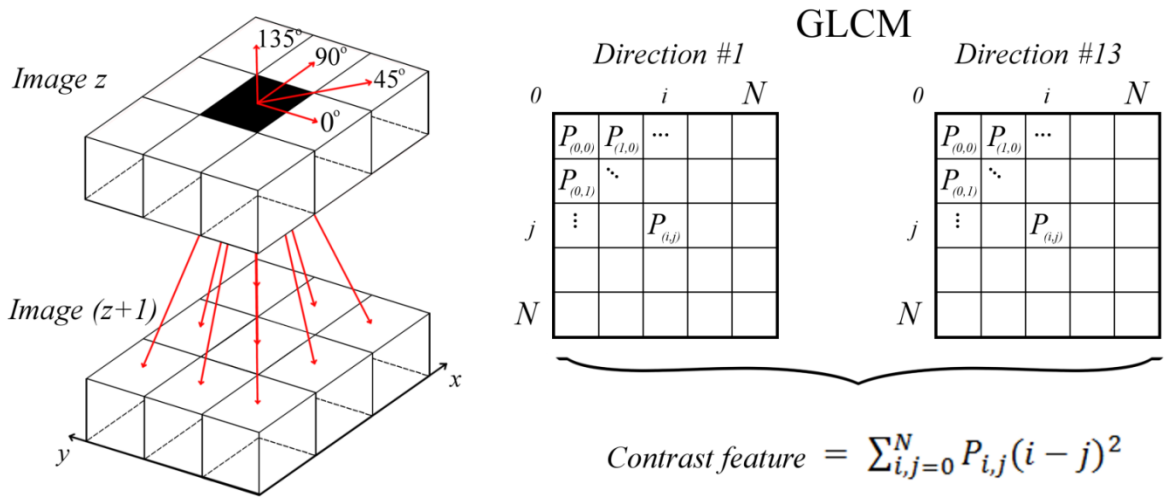

Figure 0-2 : 3D pixel-wise texture map is obtained by computing the GLCM for every pixel in the myocardial region. To derive the GLCM with a spatial distance of one, neighboring pixel pairs in thirteen directions (red arrow) are compared per pixel. The probability of occurrence of signal intensity pairs in a 3x3x3 neighbor region surrounding a position was computed to construct the GLCM for each direction. The final texture value for each pixel is obtained by averaging the *contrast* feature computed from the thirteen GLCMs.

Next, the 3D GLCM were computed in the image volume based on the extension of the 2D GLCM as defined by Haralick [104] to evaluate the probability of signal intensity occurrence among neighboring pixel pairs. For an image I with signal intensity range $[0, N]$, a set of GLCM of size $N \times N$ are derived for every pixel in the myocardial ROI to account for all possible signal intensity relationship among the adjacent neighbors. The GLCM initially contains the number of occurrence of pixel pairs with intensity values (i, j) within a given distance and orientation, defined by a displacement vector $(\Delta_x, \Delta_y, \Delta_z)$, from each other. The L_1-norm is used to avoid signal intensity interpolation and a distance of 1 is used in all directions. The GLCM is, in this state, similar to a histogram of occurrence of intensity pairs (i, j) for all neighboring pixels within the myocardial ROI, with neighbors defined by the displacement vector. The final GLCM is obtained

after normalization of the matrix to obtain the probability of occurrences $P_{i,j}$ for a given pixel I at location (x,y):

$$P_{i,j} = P\left(i,j\middle|I(x,y,z) = i\ and\ I\left(x+\Delta_x, y+\Delta_y, z+\Delta_z\right) = j\right) \quad (2)$$

Since the intensity values in paired neighboring pixels are interchangeable, i.e. (i,j) is considered the same as the intensity pair (j,i), only half of the twenty-six connected pixel neighbors need to be considered and the GLCM is made symmetrical. Therefore, a total of thirteen directions are computed, defined by four in-plane displacement $\left(\Delta_x, \Delta_y, \Delta_z\right)$ = [(1,0,0), (1,1,0), (0,1,0), (-1,1,0)] and that correspond to the orientations 0º, 45º,90º and 135º from the considered position, and as well by the out-of-plane displacements $\left(\Delta_x, \Delta_y, \Delta_z\right) =$ [(0,0,1), (1,0,1), (1,1,1), (0,1,1), (-1,1,1), (-1,0,1),(-1,-1,1), (0,-1,1), (1,-1,1)]. After obtaining the thirteen GLCM, the standard *contrast* texture feature [104], was computed in each direction and then averaged for all pixels in the myocardial ROI:

$$Contrast\ feature = \sum_{i,j=0}^{N} P_{i,j}(i-j)^2 \quad (3)$$

As in the LGE CMR image, myocardial fibrosis content in the *contrast* texture enhanced images was quantified with 2 to 6 SD thresholds in the same myocardial ROIs and compared to the histology reference.

1.12.5 Statistical Analysis

Results are presented as mean ± SD of the %LV in the myocardial ROI for group comparisons. The correspondence of collagen content estimation between histology slices versus LGE CMR and *contrast* texture images were performed with linear regression and Bland-Altman analysis. A two-tailed student t-test was used to determine if significant differences were present between different quantification techniques and the two age groups ($p<0.05$).

1.13 Results

The elderly rats weighed 570±56 grams and were significantly heavier than the young rats at 291±76 grams ($p<0.01$).

1.13.1 Histology Analysis

Histology images showed an increase of collagen fibers in the aged hearts compared to the younger ones Figure 0-3. The fibrous collagen distribution was not typical of ischemic cardiomyopathies [54]. Rather, the presence of interstitial fibrosis was evident in the aging hearts where an increase of collagen fibers was observed in sporadic locations, intermingled with healthy cardiomyocytes Figure 0-4. Perivascular fibrosis was also apparent in the myocardium where collagen fibers surrounded the intra-myocardial blood vessels Figure 0-4. Quantification of the red-stained collagen fibers in histology images was possible with the HSV segmentation method Figure 0-5.

Overall, the red-stained collagen structures occupied approximately 2.60±0.27% LV in the elderly rat hearts, compared to 1.24±0.29% LV in the young rats ($p<0.01$). These were in a similar range of myocardial collagen content as quantified in previous picrosirius studies [211-213].

1.13.2 LGE CMR and Texture Analysis

There was a general agreement of signal enhancement in the matched SA slices of the LGE CMR images that visually corresponded well with location of red-stained collagen fibers in the histology slices for both the elderly and the young rat heats (Figure 0-6 and Figure 0-7, respectively). Figure 0-8 shows an example of myocardial fibrosis quantification on the LGE CMR, and the *contrast* texture images for one of the elderly rats. Different SI thresholds are compared to the histology segmentation. There is a correspondence but not complete correspondence of pixel enhancement between the LGE CMR and the *contrast* texture images as quantified by different thresholds Figure 0-8.

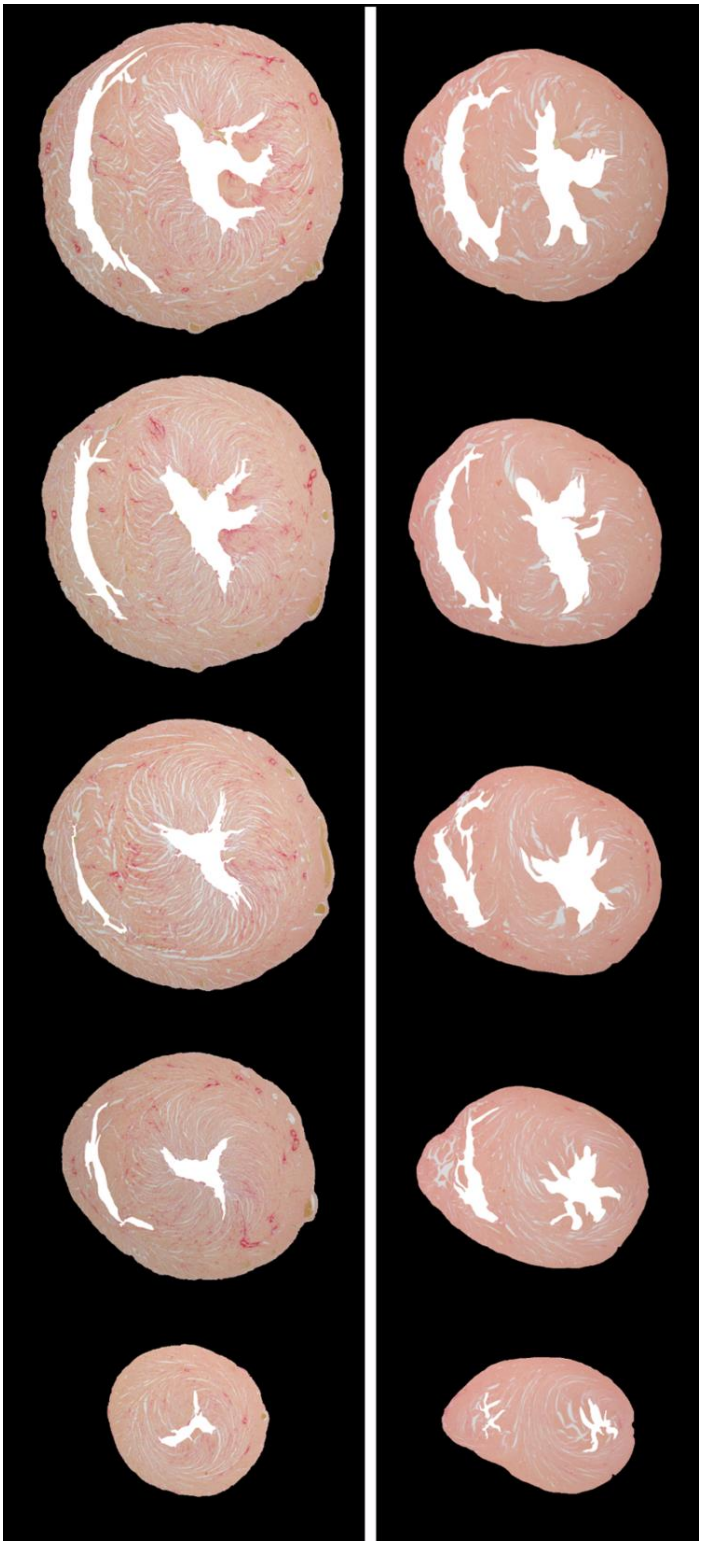

Figure 0-3 : Picrosirius red-stained histology images show an increase of collagen content (stained red) in the elderly rat (left) compared to the young rat (right).

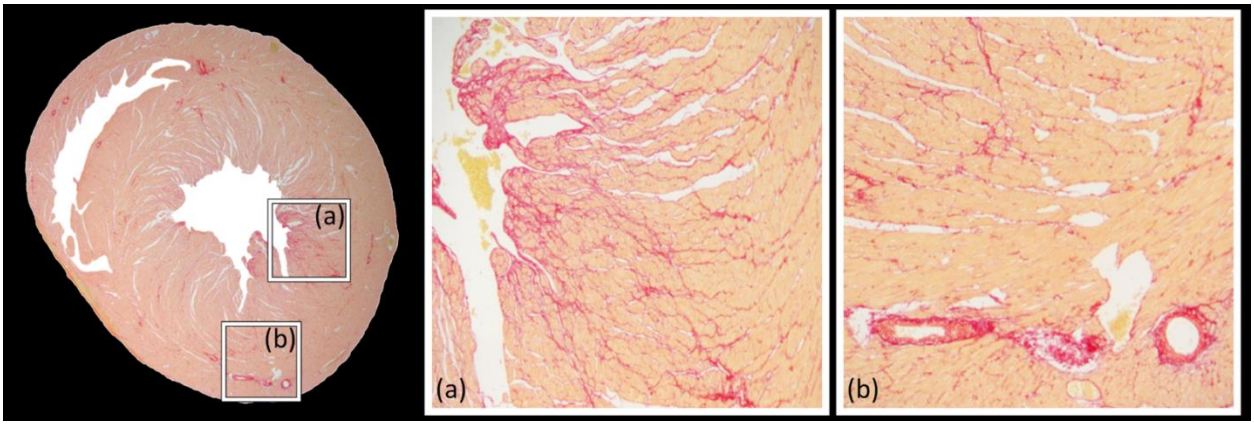

Figure 0-4 : Magnification of a picrosirius red-stained histology slice from an elderly rat heart showing (a) interstitial and (b) perivascular fibrosis. Diffuse interstitial fibrosis appears as an intermingling of pink-salmon color healthy cardiomyocytes and red-stained collagen fibers.

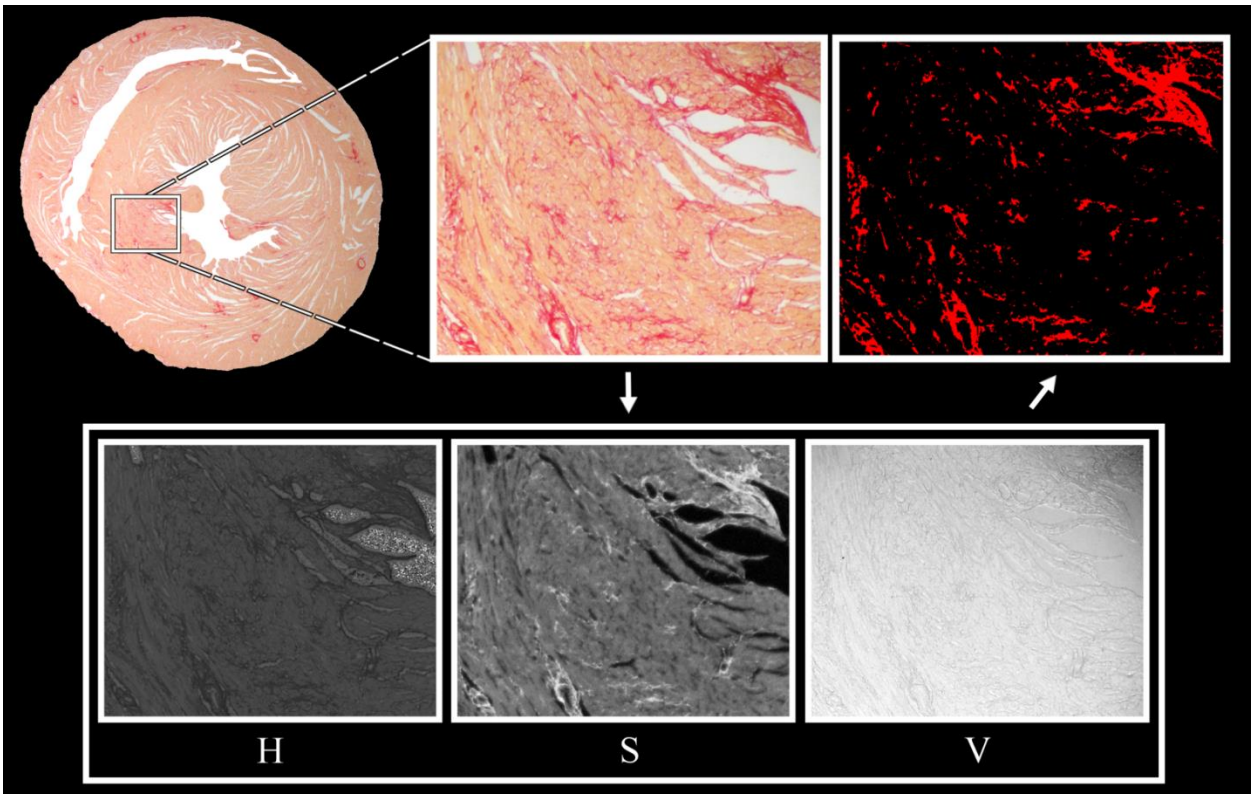

Figure 0-5 : Segmentation of the histology slices was done after transforming the RGB channels into HSV color space. The illuminance variation of the image can be clearly seen in the V channel of the decomposed HSV images. The magnified picrosirius red-stained histology image shows our segmentation can depict detailed red-color collagen content in the myocardium.

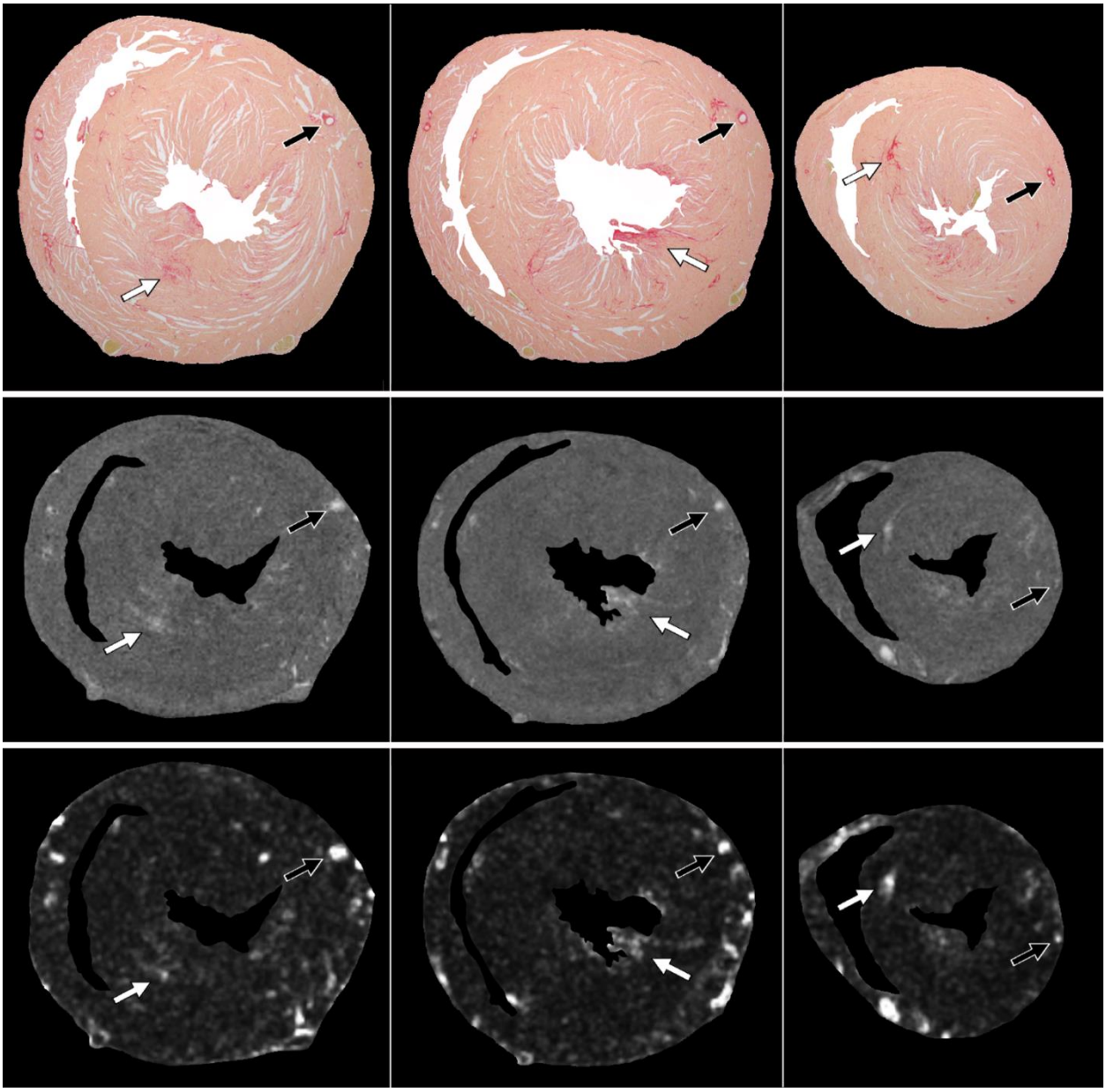

Figure 0-6 : The appearance of collagen fibers in an elderly rat histology slices (top) matches well with the signal enhanced regions in the LGE CMR images (middle) and the corresponding *contrast* texture images (bottom). Regions of interstitial diffuse myocardial fibrosis identified in histology (white arrows) are enhanced in the matched LGE CMR and *contrast* texture images. Perivascular myocardial fibrosis in histology (black arrows) was also enhanced in LGE CMR and in the *contrast* texture image. The corresponding *contrast* texture images show a further increased signal enhancement in locations of myocardial fibrosis.

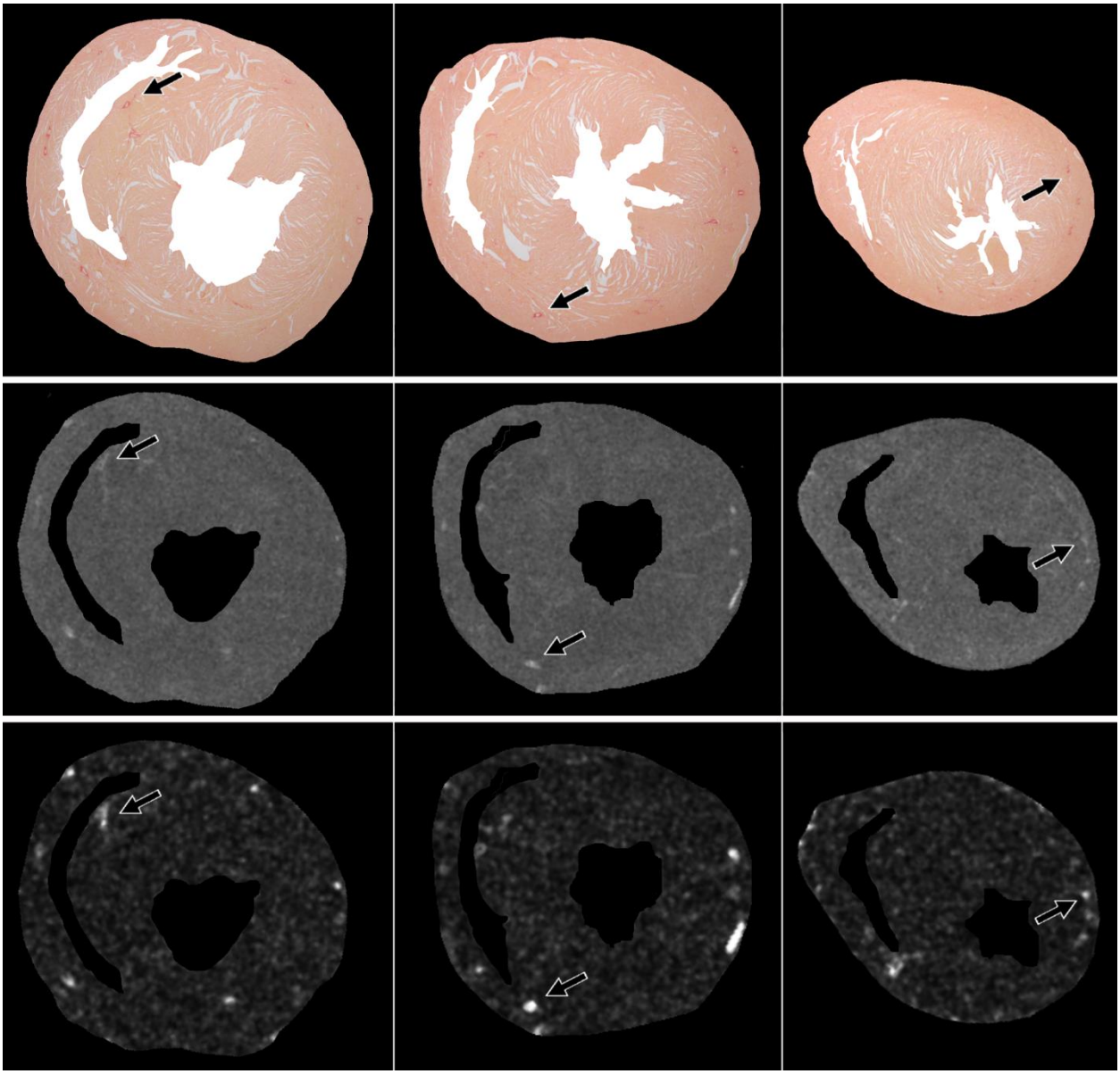

Figure 0-7 : The appearance of collagen fibers in a young rat histology slices (top) also matches closely with the signal enhancement in the LGE CMR images (middle) and *contrast* texture images (bottom). However, there are fewer amounts of collagen fibers compared to the elderly rat in Figure 0-6, and they appeared primarily in the perivascular regions (black arrows).

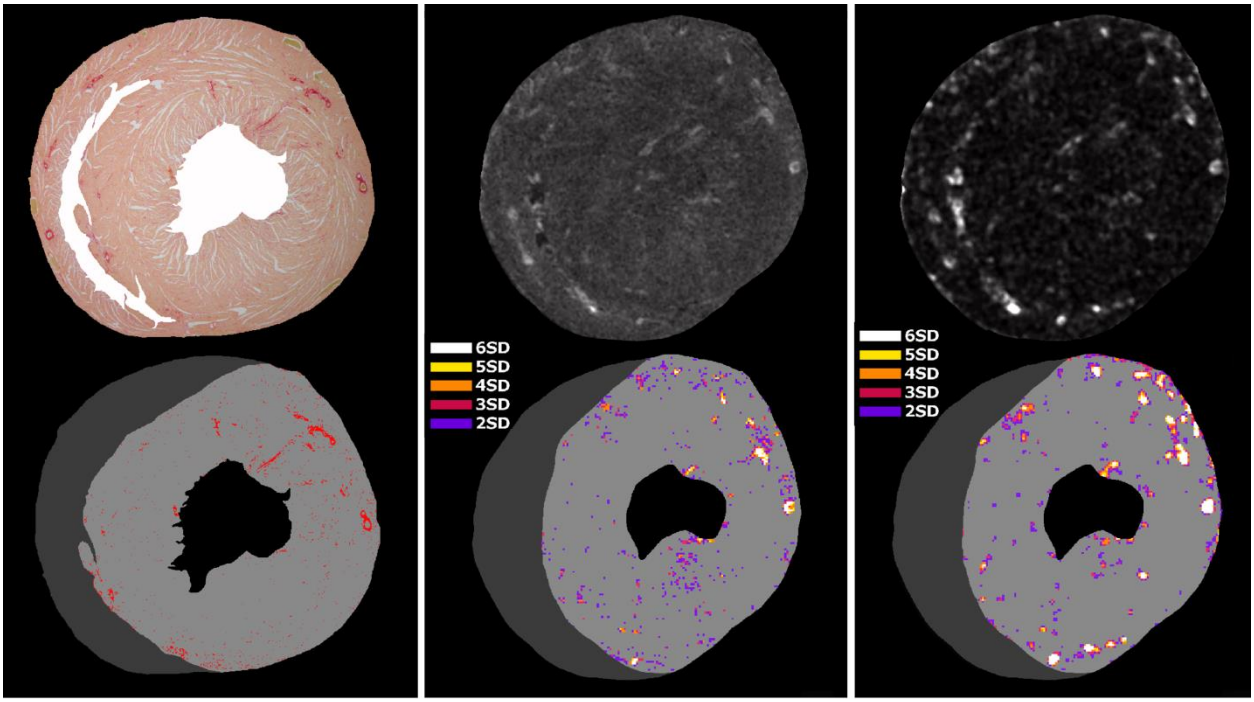

Figure 0-8 : Example of myocardial fibrosis quantification in histology (left), segmented LGE CMR (middle), and segmented *contrast* texture (right) images. The bottom row shows there is a high, but not complete, correspondence of signal enhanced pixels between CMR and the *contrast* texture images as quantified by different SD thresholds. There was a slight over segmentation in the lumen area of the LGE CMR and the *contrast* texture images when compared to histology due to residual contrast in the lumen.

For the LGE CMR images, our comparison showed the 3 SD threshold produced the closest estimation of fibrosis content to that obtained with histology quantification and was therefore retained for subsequent comparisons Figure 0-9. For the elderly group, collagen content was estimated at 2.56±0.52%LV in the LGE CMR images compared to 2.60±0.27% LV fibrosis from the histology (p=NS). In the young rat hearts, fibrosis was estimated at 1.11±0.47% LV compared to 1.24±0.29% LV obtained from the histology (p=NS). With the 3 SD method, linear regression analysis showed a good correlation between LGE CMR and histology quantification for the group overall (r=0.84, y=0.99+0.00, Figure 0-10).

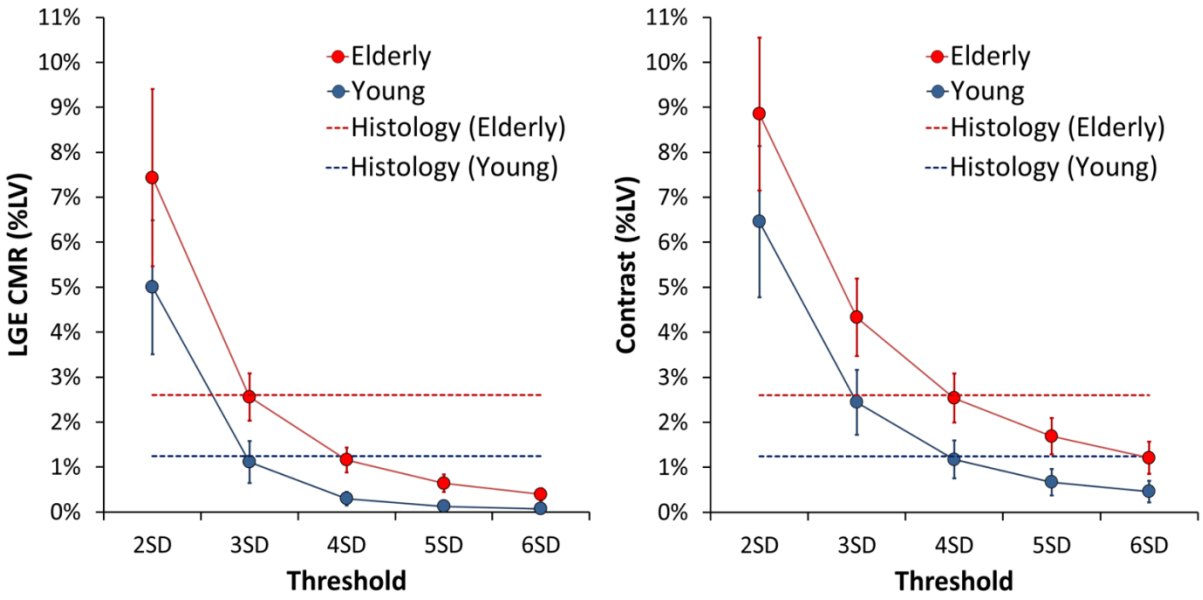

Figure 0-9 : Myocardial collagen content in the elderly versus young rats as estimated by various standard deviation (SD) thresholds from LGE CMR (left) and *contrast* texture (right) images. Dashed lines show collagen estimation from the matched histology references. The optimal threshold values for LGE CMR were obtained with the 3 SD threshold and with the 4 SD for the *contrast* texture images.

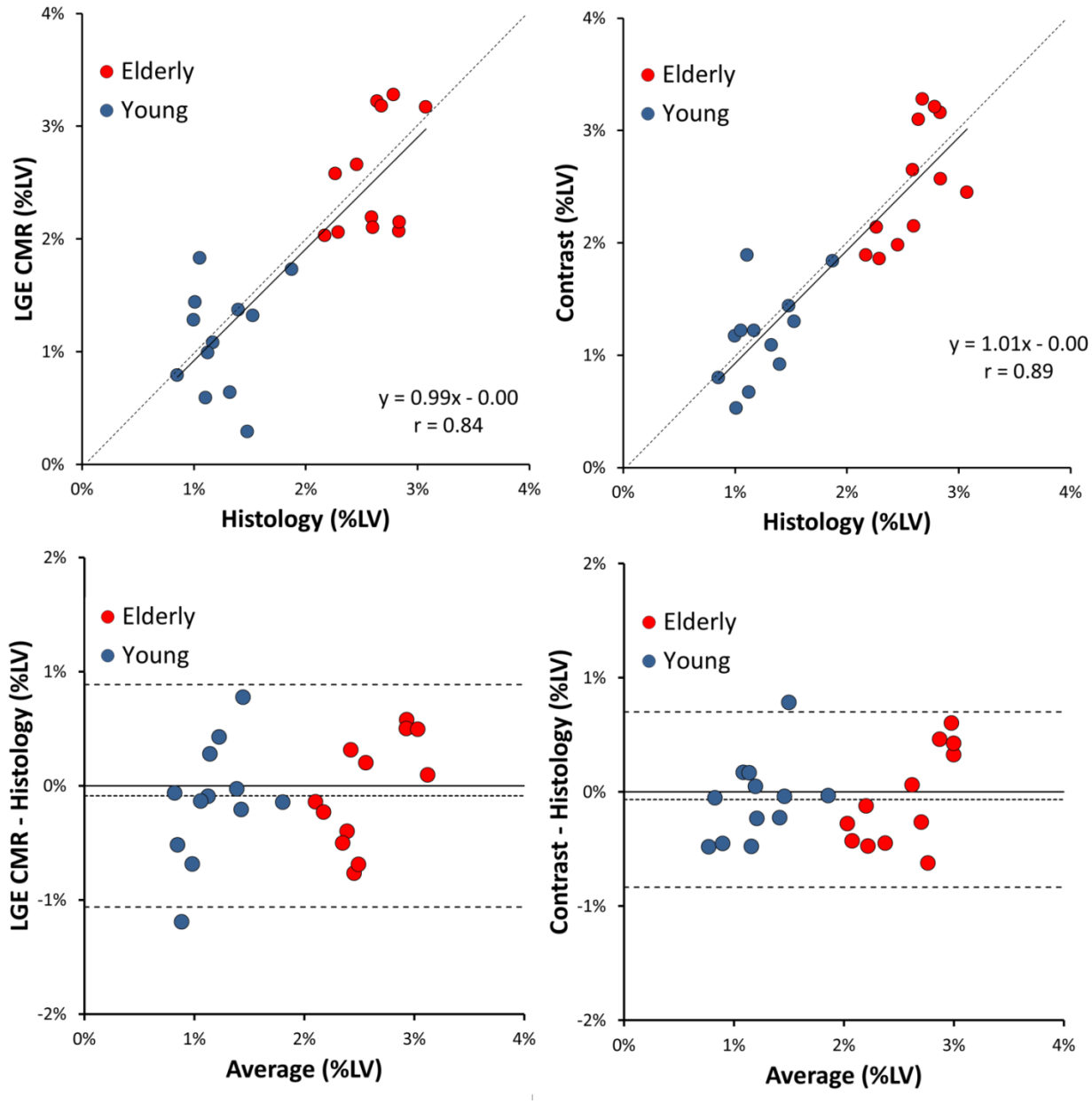

Figure 0-10 : Collagen estimation with the 3 SD threshold for LGE CMR images (left) and the 4 SD threshold for the *contrast* texture images (right) compared to the histology quantification. Linear regression and Bland-Altman analysis showed excellent correlation without significant bias for both LGE CMR and *contrast* texture images. Dashed lines indicate mean ± two standard deviation in the Bland-Altman analysis

For the texture images, our data showed the 4 SD threshold applied to the *contrast* texture feature images resulted in fibrosis estimation that was closest to the histology quantification Figure 0-9. In the elderly rat hearts, collagen content was estimated at 2.60±0.54% LV in the *contrast* feature

images compared to 2.60±0.27% LV fibrosis from the histology (p=NS). For the young rat group, fibrosis estimation in the *contrast* texture feature images was 1.17±0.42% LV compared to 1.24±0.29% LV from the histology (p=NS). For the group overall, linear regression analysis showed a good correlation of fibrosis quantification from the *contrast* texture feature images compared to the histology reference (r=0.89, y=1.01x+0.00, Figure 0-10).

Table 0-1 summarizes the percent difference of fibrosis estimation between elderly and young rat hearts using different threshold levels. There is a larger difference and separation between the two groups using the *contrast* texture maps compared to the LGE CMR images with the 3 SD to 6 SD thresholds. Furthermore, there was a significant increase in SNR (21.9%, p<0.001) measured from the bright fibrotic pixels in the *contrast* texture maps compared to the LGE CMR images (SNR=10.76 and 8.83 respectively).

Table 0-1 : The discrimination between the elderly and the young rat hearts is improved with the contrast texture maps quantification using 3SD to 6SD thresholds when compared to the LGE CMR images. The amount of myocardial fibrosis estimation is expressed in %LV.

Contrast Texture

(% LV)	2SD	3SD	4SD	5SD	6SD
Elderly	8.81%	4.37%	2.60%	1.76%	1.30%
Young	6.46%	2.45%	1.17%	0.67%	0.46%
Difference	**2.35%**	**1.92%**	**1.43%**	**1.10%**	**0.84%**

LGE CMR

(% LV)	2SD	3SD	4SD	5SD	6SD
Elderly	7.43%	2.56%	1.16%	0.64%	0.39%
Young	5.00%	1.11%	0.30%	0.13%	0.07%
Difference	**2.43%**	**1.45%**	**0.86%**	**0.51%**	**0.32%**

1.14Discussion

This study demonstrated that high resolution ex-vivo LGE CMR can detect the presence of age-related interstitial and perivascular myocardial fibrosis in hearts with differing level of collagen content. A significant increase of myocardial fibrosis was found in the elderly group compared to the young rats as shown in our CMR and histology data. Our results show that the signal enhanced regions identified on the LGE CMR images correspond to the fibrosis on the histology. Likewise, the texture analysis also correlated well with fibrosis by histology.

Previous studies have shown that gadolinium contrast agent can delineate myocardial infarction and fibrosis at a near cellular level [51]. We extend this finding to less focal and more subtle, myocardial fibrosis present in the elderly rat hearts. Diffuse fibrosis present in the heart, from various etiologies, has been identified with CMR T_1 mapping, ECV, and DTI methods [9, 11-14, 16, 64, 65, 205]. Moreover the increase of collagen content in the aging heart has been studied in animal models [59-62, 214] and patients [8, 59, 63] using these emerging CMR imaging techniques. It was found that T_1, ECV, and various diffusion parameters in the myocardium have a strong association with age. An elderly animal model was therefore chosen in our study to examine a more subtle increase of diffuse fibrosis in the myocardium. Using high resolution ex-vivo LGE CMR imaging with histopathological correlation, our study indicates that there is a significant increase of patchy interstitial and perivascular fibrosis present in the aged hearts. The increase of diffuse myocardial fibrosis in the older rat hearts compared to the young could be influenced by different factors such as increased sedentary periods, lower metabolism or obesity, which can potentially be attributed to the process of aging. It was important to this study that the increase of fibrosis in our animal model developed naturally without direct intervention. This is consistent with previous studies that link higher amount of fibrosis with aging in animal models. The elderly animal model allowed us to study texture analysis in the presence of more dispersed fibrosis, which is currently challenging to assess with LGE CMR images.

The location of infiltrative collagen fibers as stained by the picrosirius red in the histology references corresponded well with the location of enhanced SI in the myocardium on the LGE CMR images qualitatively. We further showed that the estimation of collagen content in the histology images, as measured by the HSV method, correlated well with the detection and location of myocardial fibrosis on the LGE CMR images. This correlation reflects the accumulation of

gadolinium contrast agent in the extracellular matrix, which in turn indicates an increased presence of collagen fibers. As Schelbert et al. mentioned in the previous study [51], Gd-DTPA accumulates in regions of slight collagen accumulation, a feature critical when imaging particular non-ischemic cardiomyopathies where there is absence of focal alteration to the cellular structure of the myocardium. Our study further confirms that subtle and dispersed accumulation of collagen fibers in the myocardium can be detected with high resolution LGE CMR imaging.

Depending on different clinical and imaging applications, quantification of myocardial fibrosis in LGE CMR images has been performed with SI thresholding that differs among studies [135, 215-217]. We presented a comparative assessment for the amount of fibrosis using various levels of threshold and showed all thresholds achieved a high accuracy separating the two groups. However, there was an increased separation of the two age groups in the *contrast* texture image quantification compared to the LGE CMR images for all threshold comparison (Figure 0-9). With a lower threshold setting such as the 2 SD method, the LGE CMR and *contrast* texture images had a tendency to overestimate fibrosis content as compared to the histology (Figure 0-9). Our results showed the 3 SD threshold applied to the LGE CMR images gave the closest estimation of collagen content to what was estimated in the histology images. These results were consistent with previous findings by Mikami et al. [218] and as well by Moravsky et al. [215] that compared various levels of threshold applied to LGE CMR images with the presence of diffuse fibrosis in hypertrophic cardiomyopathy patients. Moravsky et al. stated that LGE CMR at higher SDs represents the denser fibrosis that probably consists of replacement fibrosis but also the denser interstitial fibrosis.

For the *contrast* texture feature images, our results show that the 4 SD method resulted in the best correlation with histology. We infer this increase of threshold value is due to the effectiveness of the GLCM computation to improve differential SI enhancement patterns among neighboring pixels. The *contrast* texture feature measures textural complexity in a given region by weighing the difference of signal intensity amongst neighbor pixels. Such texture extraction and pattern enhancement process can encapsulate more diffuse pixels with bright and dark neighbors next to each other than just the amount of bright pixels in the image. It not only enhances pixel locations where confluent gadolinium enhancement is present, but also the immediate neighboring regions where pixels are more subtly enhanced. Qualitative analysis of the LGE CMR and the *contrast* texture images Figure 0-6 shows a strong association of enhanced pixels with the location of red-stained collagen fibers in the histology slices. The signal and contrast level of these bright pixel

enhancement regions are markedly enhanced in the *contrast* texture image which have a significantly higher SNR compared to the LGE images. Texture measures can thus be exploited as indicators for the presence of a more complex collagen fibers distribution as depicted by both diffuse and confluent gadolinium enhancement patterns in the myocardium. Furthermore, since texture analysis computes local pixel-to-pixel signal variation, it is less prone to the influence of image artifacts caused by radiofrequency field inhomogeneity.

There are advantages to using LGE CMR images to detect myocardial fibrosis. The significance of signal enhancement found in the myocardium from this modality has been extensively validated and reproduced in many studies including multi-center studies. Acquisition protocols have been extensively tested and precise guidelines have been developed [129]. LGE CMR images are clinically used to diagnose ischemic cardiomyopathies and have been shown to exhibit identifiable enhancement patterns in non-ischemic cardiomyopathies [219]. We have demonstrated that both LGE CMR and *contrast* texture images could successfully discriminate the elderly from the young rat hearts. The subtle but visible increase of red-stained collagen fibers was assessed visually as well as quantitatively in histology images. This increase of fibrosis content was also quantified in LGE CMR images and texture images. Quantification of diffuse fibrosis in LGE CMR images can be challenging in a clinical setting due to an inherent lower spatial resolution. Texture analysis may thus improve the detection of more complex signal enhancement patterns and signal intensity differences of neighboring pixels in the presence of diffuse fibrosis. Although we present texture analysis as a means to quantify myocardial fibrosis on LGE CMR images, this analysis method may also be applied to other types of CMR images, such as T_1 or ECV maps, for tissue characterization and classification.

There are limitations to the current study. Picrosirius red staining allowed the delineation of collagen fibers more closely than would be possible with LGE CMR imaging technique. The lumen was not red stained in the histological images and thus discounted from the HSV segmentation. However the vessel lumen was enhanced by the contrast agent and accounted for false positive fibrosis content in LGE CMR images. Since the amount of diffuse fibrosis in the myocardium is much smaller than focal scars as in myocardium infarctions, these intrinsic differences are not to be overlooked when comparing diffuse fibrosis between different imaging modalities. This might account for part of the overestimation of the collagen content in LGE CMR and texture images

compared to the histological reference. However, this overestimation is consistent throughout all cases in this study and does not impair the enhancement of diffuse fibrosis with texture analysis.

Partial voluming is a well-documented effect that is unavoidable and affects all quantitative analysis of diffuse fibrosis in LGE CMR images due to relatively subtle regional voxel enhancement [51, 143]. The morphological changes of myocardial tissue during histological processing may account for some of the anatomical discrepancy and misalignment between LGE CMR images and the histological slices. In spite of these discrepancies there was visual agreement in the general myocardial structure in LGE CMR images and in the stained histology slices.

Finally, the presence of collagen fibers was assessed with picrosirius red stain under bright light in our study. Polarized light could potentially provide more details about the structures and compositions of the diffuse myocardial fibrosis by exploiting the birefringence property of the stained collagen [220, 221].

The analysis of texture features in this study was performed with the *contrast* texture feature, which was extracted from the GLCM as computed from the LGE CMR images. This feature alone offered the best visual and quantitative assessment of diffuse myocardial fibrosis, compared to other GLCM features. Other texture features and classification methods may be explored in future studies to improve the detection of complex intensity patterns associated with diffuse myocardial fibrosis in LGE CMR images under different image resolution.

1.15 Conclusion

We demonstrated that high resolution LGE CMR images can detect the presence of subtle age-related myocardial fibrosis in ex-vivo rat hearts of different aged groups. Texture feature analysis of those images may add additional value to the assessment of fibrosis in the myocardium. A significant increase of myocardial fibrosis was found in the elderly group compared to the young rats in this study. Our results show both signal intensity and *contrast* texture analysis of the LGE CMR images can separate the two age groups of rats with great accuracy, although the SNR was increased for the *contrast* texture maps. The quantification of fibrosis on both LGE CMR and histology data correlates well. This is the first CMR imaging study that confirms diffuse myocardial fibrosis that occurs due to aging can result in a complex signal intensity pattern in high resolution LGE images and that texture analysis can be successful in identifying fibrotic myocardial regions.

These techniques may be useful for analyzing LGE CMR images in patients with various cardiomyopathies but this will require further studies.

1.16 Acknowledgements

Funded by the Intramural Research Program of National Heart Lung and Blood Institute, Ecole Polytechnique of Montreal and Fonds de Recherche Nature et Technologie du Quebec.

CHAPTER 5 ARTICLE 2: EXPLORATION OF TEXTURE ANALYSIS OF LATE GADOLINIUM ENHANCED CARDIOVASCULAR MAGNETIC RESONANCE IMAGING TO DISCRIMINATE ACUTE VERSUS CHRONIC MYOCARDIAL INFARCTION IN PATIENTS

Pascale Beliveau[1,2], Farida Cheriet[2], W. Patricia Bandettini[1], Andrew E. Arai[1], Li-Yueh Hsu[1]

[1]National Heart, Lung and Blood Institute, National Institutes of Health,

Bethesda, Maryland, USA

[2]Institute of Biomedical Engineering, Ecole Polytechnique of Montreal,

Montreal, Quebec, Canada

1.17Presentation

With the validation of texture features applied to LGE CMR images to assess diffuse myocardial fibrosis, translational research can occur to investigate the performance of texture analysis for patient images. LGE CMR images have been limited to distinguish acute from chronic MI in patients because the analysis relies on signal intensity based methods. The second journal article presented in this chapter has been submitted to the peer-reviewed *Journal of Cardiovascular Magnetic Resonance* on October 14, 2016.

1.18 Abstract

Background: Texture analysis of late gadolinium enhancement (LGE) cardiovascular magnetic resonance (CMR) imaging has been shown to highlight myocardial fibrosis at a cellular level. Differentiating acute from chronic myocardial infarction (MI) could have clinical impact. We

investigated whether texture analysis of LGE CMR images could discriminate patients with acute versus chronic MI.

Methods: LGE CMR images of twenty-two patients were analyzed, including twelve who had acute MI and ten who had chronic MI. The myocardium was classified into remote, MI, and peri-infarct zone (PI) with the full width at half maximum and the two standard deviations intensity threshold methods. Texture features were then computed from a gray level co-occurrence matrix derived from the MI, PI, and the remote regions to compare the two patient groups. The Mann-Whitney-Wilcoxon test was used to determine the difference between the two groups. The area under the curve (AUC) was computed for all texture features following receiver operating characteristics analysis.

Results: Neither the size measured from the MI or from the PI regions differentiated the acute vs. the chronic groups (p=NS). The *mean* texture feature was the only significantly different feature in the MI region between the acute and the chronic groups. However, five of the eight texture features in the PI zone were significantly different. Among those, the four most significant features were *homogeneity*, *dissimilarity*, *contrast*, and *correlation*. Those features all had AUC values greater than 0.80 ($p \leq 0.01$). None of the texture features in the remote myocardium differentiated the two groups (p=NS).

Conclusion: Texture analysis of LGE CMR images can discriminate between acute and chronic MI patients, most prominently from the PI regions. It suggests the PI zone might hold important quantitative textural information in LGE CMR images not detectable with standard signal intensity comparisons.

1.19 Background

The size and transmurality of myocardial infarction (MI) can be reliably estimated from late gadolinium enhanced (LGE) cardiovascular magnetic resonance (CMR) images [2, 50]. However, traditional LGE CMR image analysis methods are unable to estimate the age of myocardial infarction since the level of signal enhancement in both acute and chronic MI have a similar histogram distribution [18]. The thresholding methods used to delineate the myocardial damage in LGE CMR images are insufficient to establish the acuity of an MI [18-21]. It would be clinically

useful if LGE CMR images could distinguish acute from chronic MI independent of other imaging sequences.

Myocardial thinning seen on LGE CMR images and that occurs with remodeling have been found to be a limited discriminant of acute and chronic MI and should be used with other imaging markers [18, 21, 222]. Animal studies using contrast agents that enhanced acute MI but not aged infarctions in combination with standard contrast agent for LGE CMR images have allowed discrimination based on the age of infarction [19, 20, 223, 224]. In spite of those results, the different contrast agents tested in animal studies have not been approved for general use in a patient population. Other manganese based contrast agents have also been investigated to assess the presence of MI in animal models and have been shown to differentiate acute from chronic MI [11, 12]. Methods based on CMR T_2 images have been developed that investigate the presence of edema in acute MI that is absent in chronic MI [3, 8, 13].

LGE CMR is a reference method for myocardial infarct size [129]. LGE CMR corresponds to regions of myocardial fibrosis almost to the cellular level in an animal model imaged ex vivo [200]. The myocardium's cellular structure is altered following MI and this influences the visual pattern of the signal enhancement present in the infarcted region from LGE CMR images. There have been several studies describing the heterogeneity of the infarct scar. A larger peri-infarct (PI) zone was associated with increased risk of mortality or major adverse events [23-26]. Estner et al. [27] found that scar heterogeneity on LGE CMR images corresponded to ablation sites. The myocardium in a chronic MI animal model exhibited a heterogeneous appearance in the border zone while it had denser collagen deposition in the infarct core [225].

Texture features can be used as descriptors of image characteristics and exploited to look for information beyond the simple signal intensity. Texture analysis considers the spatial relationship of the signal intensity and characterizes the relative variation of signal that forms the image. Texture analysis therefore characterizes the signal intensity pattern found in the image to offer a clear interpretation for the clinicians who will analyze the relationship between the metric and their observations of LGE CMR enhancement patterns. Age related myocardial fibrosis has been assessed on explanted animal hearts by texture analysis in high resolution LGE CMR images [200]. Patient imaging offers a much lower image resolution compared to ex-vivo CMR microscopy that

was used in this previous study. The performance of texture analysis remains to be established in a patient population with lower image resolution.

We hypothesized that the texture pattern evaluated in regions of interest from LGE CMR images would vary in the different stages of MI, reflecting the underlying heterogeneity of the tissue characteristics within the myocardial infarction. We also hypothesized that the tissue characteristics of the PI zone would be heterogeneous in ways that might differentiate acute from chronic MI.

1.20 Methods

This retrospective clinical study was approved by the Institutional Review Board of the National Institutes of Health (protocol 09H031). The patient cohort consisted of individuals with acute MI (n=12, age 60.9 ± 11.9) and chronic MI (n=10, age 62.7 ± 20.7). MI was defined based on clinical symptoms consistent with myocardial ischemia, ECG consistent with either ST elevation MI or non-ST elevation MI, and typical rise of troponin I in accordance with guidelines [226]. CMR of acute MI was performed at 4 ± 2 days after presentation for the MI. CMR for chronic MI was done more than 12 months after documented MI. Exclusion criteria included standard contraindication to MRI and an estimated glomerular filtration rate < 30 ml/min/1.73 m^2.

1.20.1 MRI Acquisition

MRI was performed on a Siemens Magnetom Espree (Erlangen, Germany) 1.5 Tesla scanner with 12 surface-coil elements. The MRI acquisition included steady state free precession sequence for cine MRI and phase sensitive inversion recovery sequence for late gadolinium enhancement images [45]. Standard short-axis stacks of LGE images were acquired approximately 10 to 20 minutes after intravenous administration of 0.15 mmol/kg gadolinium diethylenetriamine pentaacetic acid (Gd-DTPA) (Magnevist, Berlex) with the following typical parameters: bandwidth 140Hz/pixel, TE/TR 4.2ms/8.7ms, flip angle 25^o, FOV 360×270mm, matrix size 256 x 125, resolution 1.4×2.2×6mm.

1.20.2 Image Analysis

All image analysis was performed with an in-house developed software using Interactive Data Language (IDL, Exelis Visual Information Solutions, Boulder, CO). Myocardial wall thickness was evaluated on the LGE images in six sectors per slice for all patients. The number of transmural pixels was multiplied by the voxel size to obtain an average wall thickness in millimeters for each sector.

1.20.2.1 Region of Interest

For each patient, the endocardial and epicardial borders were manually traced by an experienced cardiologist on all short-axis LGE slices to isolate the myocardium. The myocardial infarct region was classified by an automated sizing algorithm [142]. The myocardial infarction including the peri-infarct (PI) zone was determined with a threshold of 2 standard deviations (SD) above the mean signal intensity (SI) of the myocardium. The final myocardial infarction (MI) region, without the PI zone, was then identified using the full width at half maximum threshold method. Based on those two regions, the PI zone was derived by removing the MI region from the 2SD region (Figure 0-1). The remote myocardium region was confined to the region inside the endocardium and epicardium after excluding the MI and the PI zones (Figure 0-1).

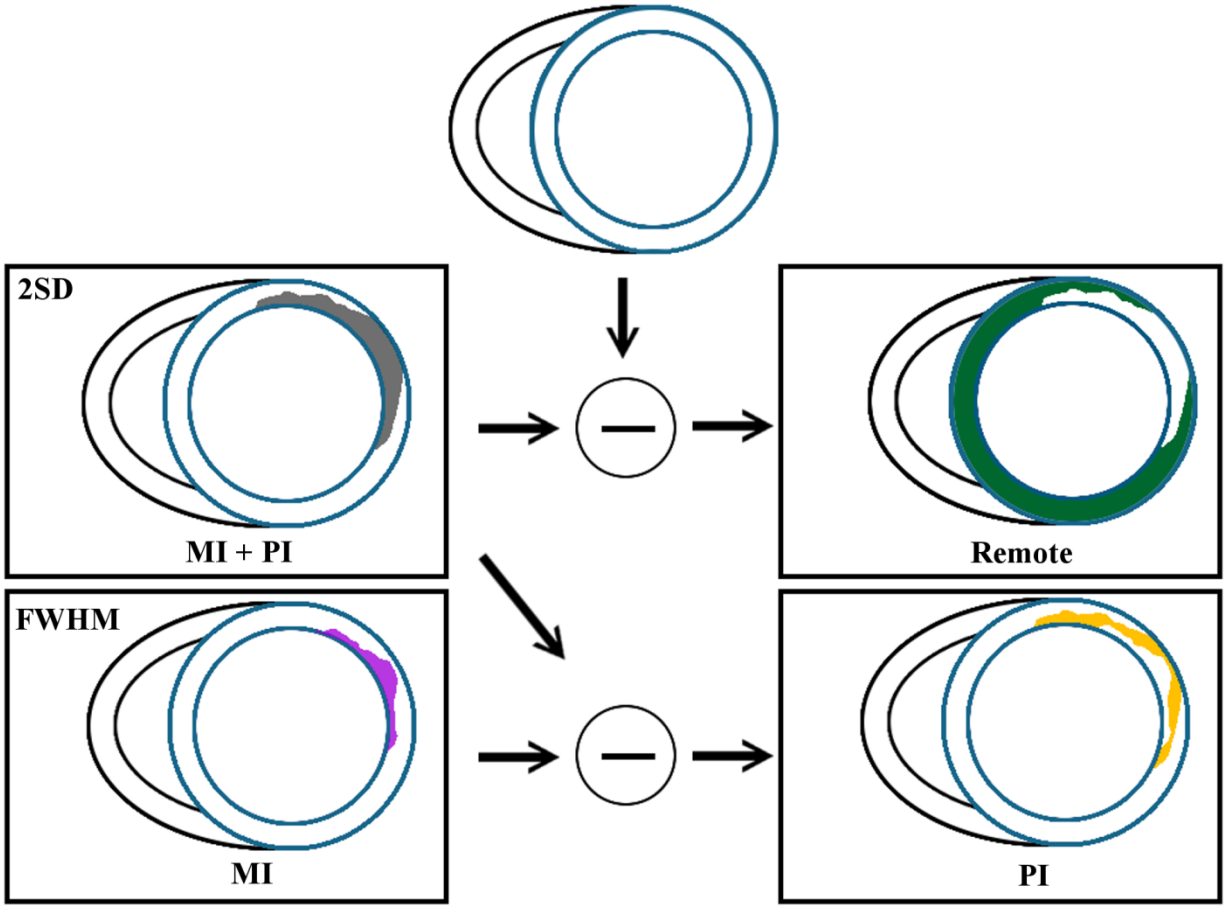

Figure 0-1: Schematic representation of the three myocardial regions of interest segmentations. The whole myocardial region was manually traced on epicardial and endocardial border of the LV (blue circles). The myocardial infarction (MI) including the peri-infarct (PI) zone, here drawn in gray (MI+PI), was determined with a 2SD threshold. The MI region, drawn in magenta, was determined with the full width at half maximum threshold using an automated sizing program. The PI zone, drawn in yellow, was obtained from the difference (⊖) between the MI+PI and the MI zone. The remote myocardium, drawn in green, was obtained from the difference of the whole myocardial region minus the MI+PI zone.

The amount of signal intensity enhancement in the MI and PI zones relative to the remote region were compared between the acute and the chronic groups. The size of each of the three regions was also measured as a percentage of the left ventricular myocardium (%LV) to investigate the existence of any bias between the two groups. As well the myocardial wall thickness (in mm and in number of pixels) was evaluated and compared between the two groups.

1.20.2.2 Texture Analysis

Two dimensional texture analysis was performed over the three myocardial regions of interest for each patient: MI, PI, and on the remote myocardium. Standardization of the signal intensity was applied to the LGE CMR images to compare texture information between patients and to improve computational time. This procedure was performed by alignment of the peak signal intensity from the histogram of the complete myocardial region. Texture features were computed from the gray level co-occurrence matrix (GLCM). This matrix holds the probability of occurrence of two specific signal intensities from neighboring pixels in the image. One GLCM matrix was built for each region of interest and for each patient. For every region R of an image with maximal signal intensity N, a $N \times N$ GLCM matrix was built. For a given pixel I at position (x, y) with signal intensity i that lies within R, the signal intensity values of its neighbors at a distance Δ for each direction [0^o, 45^o, 90^o, 135^o] were examined. A GLCM distance $\Delta = 1$ was chosen in our analysis to consider thinner myocardial walls. The SI values of neighboring pixels were added into the corresponding j^{th} columns of the GLCM. Pixels whose neighbors were located outside of the myocardial borders were ignored. Only half of the possible directions were considered since the GLCM was made symmetric. The final GLCM, as shown in Figure 0-2, contains the probability of occurrence of the signal intensity pairs after performing normalization over all the initial entries such as to obtain probabilities $P_{i,j}$ of:

$$P_{i,j} = P\big(i, j \big| I(x, y) = i \; and \; I\big(x + \Delta_x, y + \Delta_y\big) = j\big).$$

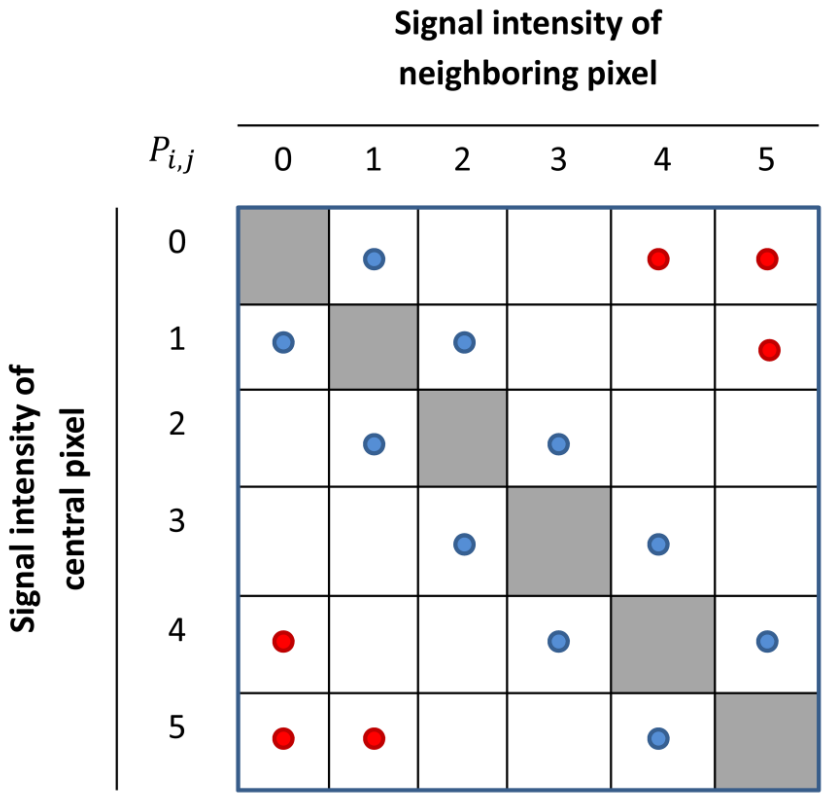

Figure 0-2 : Diagram of a gray level co-occurrence matrix (GLCM). This illustration shows the probability ($P_{i,j}$) of occurrence that a central pixel with signal intensity i will be neighboring a pixel with signal intensity j. The diagonal of the GLCM matrix (shaded in gray in the diagram image) indicates if the same signal intensity is found around the central pixel analyzed and its neighbors. If all entries of the GLCM are found on the diagonal, this indicates a uniform region in the image. The further away an entry is off the diagonal (red dots in the GLCM) the higher the signal intensity difference will be between the two pixels. Positions closest to the diagonal indicate small intensity variation between a pixel and its neighbors (blue dots in the GLCM).

Table 0-1 lists eight of Haralick's [104] texture features that were derived from the GLCM: the *contrast*, the *homogeneity*, the *dissimilarity*, the *energy*, the *entropy*, the *mean*, the *variance* and the *correlation*. Those features were selected and used in our study as they are the most commonly used GLCM texture features. The *contrast*, the *homogeneity* and the *dissimilarity* are related

features since they quantify the relative differences that exist between neighbor signal intensities. High values of *contrast* and *dissimilarity* occur with high differences of neighbor signal intensities ($i - j$), which occurs when a heterogeneous region is present in the image. This will be related to low values for the *homogeneity* feature since the difference of signal intensity is found in the denominator of the feature computation. The predictability of the pattern, how repetitive is a pattern found in the region, is described with the *energy* feature, the opposite of the *entropy* features.

Table 0-1: Description of texture features**.** Description of the eight texture features from Haralick [104] computed from the GLCM.

Texture Features	**Equation**	**Details**
Contrast	$\sum_{i,j=0}^{N} P_{i,j}(i-j)^2$	Indicates the presence of high signal intensity differences among neighboring pixels.
Dissimilarity	$\sum_{i,j=0}^{N} P_{i,j}\lvert i-j\rvert$	Indicates the presence of different pixel signal intensities among neighboring pixels.
Homogeneity	$\sum_{i,j=0}^{N} \frac{P_{i,j}}{1+(i-j)^2}$	Indicates the smoothness of signal intensity transitions among neighboring pixels.
Energy	$\sum_{i,j=0}^{N} \sqrt{P_{i,j}{}^2}$	Indicates the presence of repetitive structure among neighboring pixels (occurrence of signal intensity combinations).
Entropy	$\sum_{i,j=0}^{N} P_{i,j}\left(-\ln P_{i,j}\right)$	Indicates signal intensity disorder among neighboring pixels (opposite of the *energy*).
Mean	$\mu = \sum_{i,j=0}^{N} i\left(P_{i,j}\right)$	Indicates the mean of signal intensity occurrence among neighboring pixels.
Variance	$\sum_{i,j=0}^{N} P_{i,j}(i-\mu)^2$	Indicates the variation around the mean of signal intensity occurrence among neighboring pixels.
Correlation	$\sum_{i,j=0}^{N} \frac{P_{i,j}(ij)-\mu_x\mu_y}{\sigma_x\sigma_y}$	Indicates the independence of signal intensity among neighboring pixels.

1.20.2.3 Statistical Analysis

The size of each region of interest in the myocardium is reported as mean ± standard deviation of the %LV. Wall thickness is reported as mean ± standard deviation in millimeters. The Mann-Whitney-Wilcoxon U test was used to determine if significant differences were present from the signal intensity enhancement and as well from the eight texture feature values between the two patient groups ($p<0.05$). The discrimination performance of texture features was evaluated with the ROC analysis and the area under the curve (AUC) reported.

1.21 Results

An example of manual segmentation of the endocardium and the epicardium by an experienced cardiologist is presented alongside the different color coded regions of interest in Figure 0-3. The amount of signal enhancement in both MI and the PI regions were not significantly different between the two patient groups. In the MI region, the acute group had an average SI increase of 315.8 ± 81.1 vs. 387.5 ± 80.7 for the chronic group ($p=0.07$). Likewise, an average SI increase of 150.8 ± 31.2 was found in the PI region for the acute group vs. 162.7 ± 32.9 for the chronic group ($p=0.47$).

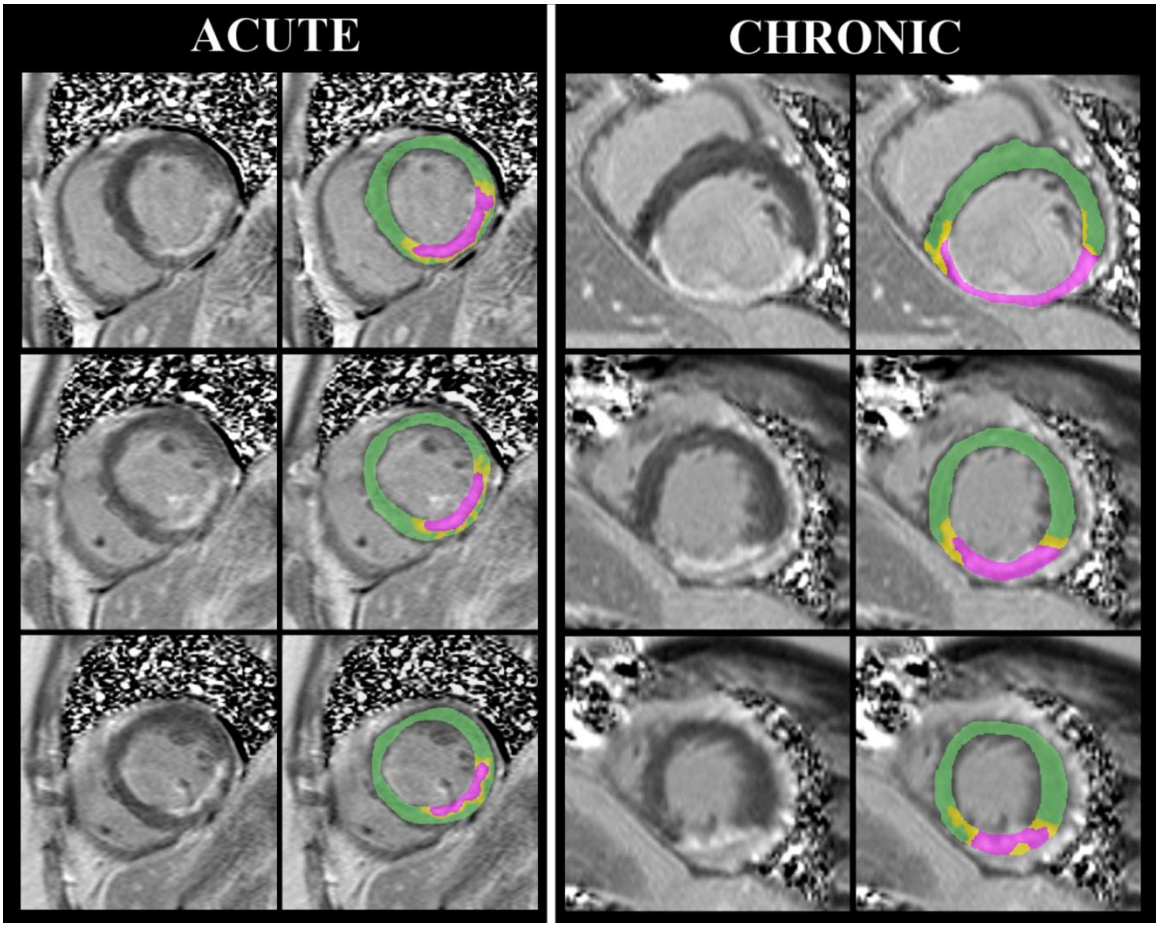

Figure 0-3 : Example LGE CMR images of an acute and a chronic MI patient. The original LGE CMR image is shown next to the myocardial segmentation. The magenta area identifies the myocardial infarction (MI) area, the yellow shows the peri-infarct (PI) zone and the green identifies the remote myocardium. It is difficult to visually assess the difference in SI between the acute and the chronic MI patients. However, there was a more uniform SI variation in the PI zone of the acute patient, as compared with a more complex signal intensity variation as measured with the texture features in the PI zone of the chronic patient.

There was no significant difference in the size of MI between the acute and the chronic groups. The size of the MI averaged 18.4 ± 7.9 %LV for the acute group and 21.7 ± 6.6 %LV for the chronic group ($p=0.17$). The size of PI zone was not significantly different neither between the two groups with 12.5 ± 8.0 %LV for the acute group and 9.7 ± 2.6 %LV for the chronic group ($p=0.43$). The myocardial wall thickness measured from the LGE images was different between the two groups with 7.8 ± 2.2 mm for the acute group and 8.2 ± 2.1 mm for the chronic group ($p\leq0.01$). The myocardial wall thickness, where there was presence of infarction, was 7.9mm on average and ranged from 3.5mm to 14.8mm for all patients.

Table 0-2 summarizes the p-values from the Mann-Whitney-Wilcoxon U test for texture feature comparisons between the acute and the chronic groups as stratified by measurements in the remote myocardium, the MI, and the PI zone. None of the texture feature values found in the remote myocardium distinguished between the two groups. Within the MI region, only the *mean* texture feature was significantly different between the two groups. For the PI region, five of the eight texture features were statistically significantly different between the acute and the chronic groups. The *homogeneity*, the *dissimilarity*, the *contrast*, and the *correlation* were the four most significant texture features ($p \leq 0.01$).

Table 0-2: P-value from the Mann-Whitney-Wilcoxon U test. P-value from the Mann-Whitney-Wilcoxon U test were evaluated for the eight Haralick texture features computed from the peri-infarct (PI), myocardial infarction (MI) and the remote myocardium region of interest comparing the acute versus the chronic MI patient groups. The p-value is also shown for comparing the size of all three regions (PI, MI and remote) in the two groups. Significantly different texture features are identified with asterisks (* $p \leq 0.05$; ** $p \leq 0.01$; *** $p \leq 0.001$).

		PI	MI	Remote
Size	**%LV**	0.429	0.166	0.429
Texture features	**Homogeneity**	0.002 ***	0.429	0.291
	Dissimilarity	0.005 **	0.553	0.323
	Contrast	0.007 **	0.644	0.356
	Correlation	0.008 **	0.553	0. 4680
	Variance	0.048 *	0.692	0.356
	Energy	0.056	0.210	0.644
	Entropy	0.065	0.210	0.391
	Mean	0.468	0.048 *	0.166

The AUC results for all features distinguishing acute from chronic group in the different ROIs are presented in Table 0-3. The highest AUCs were found in the PI zone. The *homogeneity*, *dissimilarity*, *contrast* and *correlation* texture features had the highest and statistically significant AUC in the PI zone for discriminating the two groups. The *homogeneity* texture feature had a

sensitivity of 100.0%, a specificity of 80.0% with an AUC of 0.90. The *dissimilarity* and the *contrast* texture feature both had a sensitivity of 80.0%, a specificity of 91.7%, and an AUC of 0.86 and 0.84 respectively. The *correlation* feature had an AUC 0.83, a sensitivity of 91.7% and a specificity of 80.0%. The *mean* texture feature measured in the MI region was the only significantly different texture feature.

Table 0-3 : AUC from ROC Analysis. The area under the curve (AUC) for each of the computed texture features in the peri-infarct (PI), the myocardial infarction (MI) and the remote region for the acute versus the chronic MI patient groups. The *homogeneity*, the *dissimilarity* and the *contrast* and the *correlation* texture features have the highest AUC. Significantly different texture features are identified with asterisks (* p≤0.05; ** p≤0.01; *** p≤0.005).

		PI	MI	Remote
Size	**%LV**	0.600	0.675	0.423
Texture features	**Homogeneity**	0.900 *	0.600	0.633
	Dissimilarity	0.858***	0.575	0.625
	Contrast	0.842 **	0.558	0.617
	Correlation	0.833 **	0.575	0.592
	Variance	0.750 *	0.550	0.617
	Energy	0.742	0.658	0.558
	Entropy	0.733	0.658	0.608
	Mean	0.592	0.750 *	0.675

Figure 0-4 shows the normalized values of all texture features comparing different myocardial regions in the acute and the chronic groups. The PI zone had the largest separation of texture measurements between the two groups: whereas there was a significant increase of the *contrast* and the *dissimilarity* features, as well as a significant decrease of the *homogeneity* and the *correlation* features, in the chronic group compared to the acute group. The *entropy* and the *variance* texture features were increased whereas the *energy* texture feature was decreased in the chronic group compared to the acute group. The separation of texture features in the two groups was not as clear in the MI and remote regions compared to the PI zone.

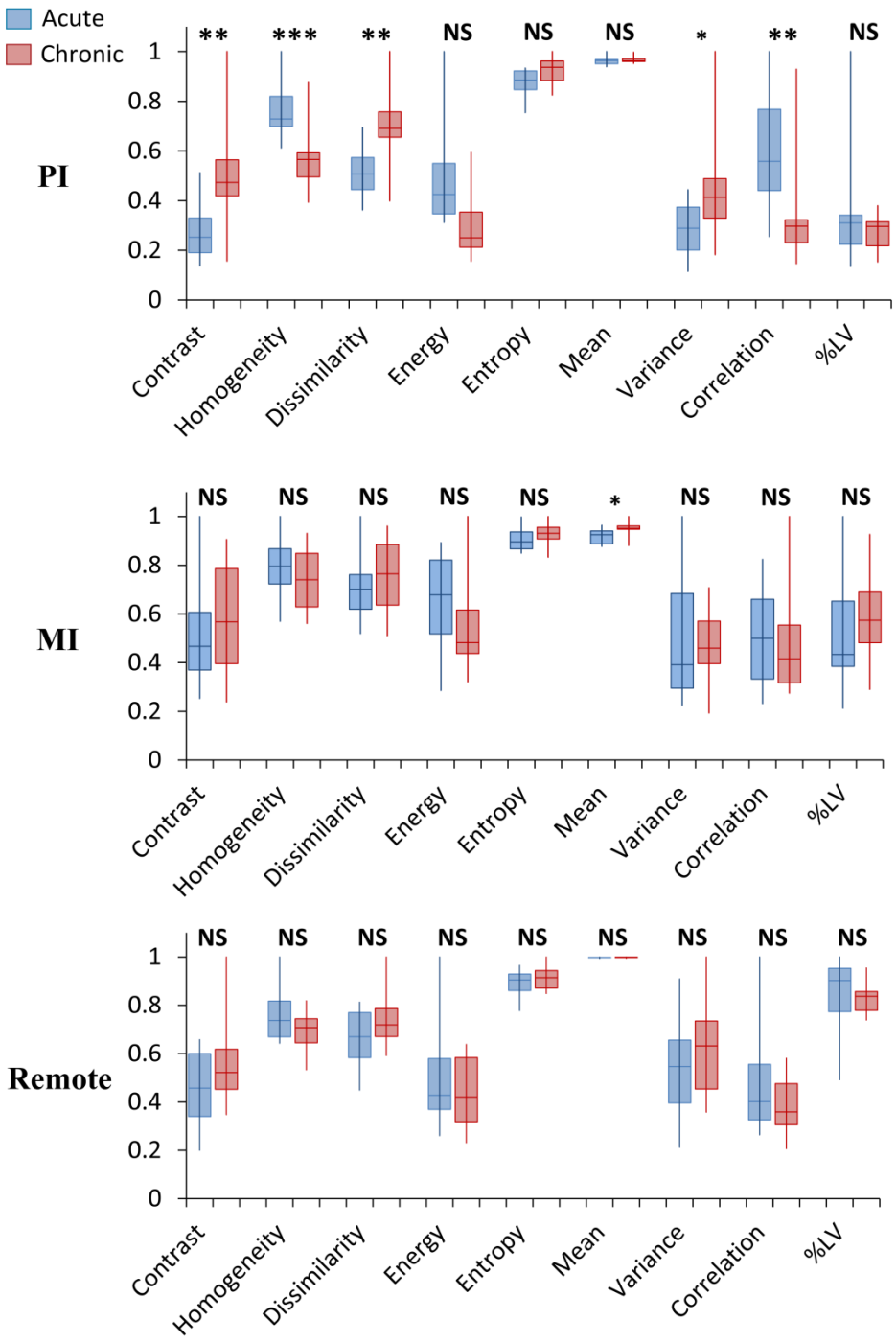

Figure 0-4: Comparison of texture features in the three myocardial regions. The box plots shows the normalized values of different texture features in the peri-infarct (PI), the myocardial infarction (MI) and the remote region between the acute and the chronic MI patients. The features from the PI region show the most separation between the two groups of patients. Significantly different texture features are identified with asterisks (* $p \leq 0.05$; ** $p \leq 0.01$; *** $p \leq 0.001$).

1.22Discussion

Quantitative texture analysis of LGE CMR images showed a significant difference in patients with acute versus chronic MI while simple measurements of signal intensity enhancement or the size of the MI did not. Our study showed five of the eight texture features measured within the PI zone could discriminate acute from chronic MI in patients. Within the MI core, only the *mean* texture feature differentiated the two groups. This could indicate a subtle difference between acute and aged MI as evaluated with the textural pattern in that region. As expected, texture measurements in the remote myocardium did not show significant differences between the two patient groups. Thus, the peri-infarct zone of acute and chronic MI contains textural information that may be useful in differentiating the age of an MI.

In LGE CMR images, the PI zone is characterized by intermediate levels of signal intensity related to the underlying tissue structure, which Hervas et al. described as a disorganized cellular structure of collagen fibers [227]. In non-transmural acute MI, there is a rim of edematous myocardium corresponding to salvaged myocardium in a large fraction of patients [228]. Moreover, the cellular organization of the border zone is progressively altered as MI evolves [227]. Therefore, the PI zone is a region where one might expect differences between the acute MI and the chronic MI LGE CMR patient images. The PI heterogeneity was related to patient outcome in ischemic cardiomyopathies in many studies [26, 229-231]. However, other results are not congruent with studies on patients suffering from ischemic cardiomyopathies [232]. Gouda et al. [232] attributed these discrepancies to the inconsistency in delineating the PI zone. Nevertheless, the PI heterogeneity was able to assess the variation in outcome following targeted therapies in a diabetic mouse model of myocardial infarction [233]. We found the PI zone in LGE images was a more discriminative region compared to the MI region based on texture analysis (Figure 0-4). There were significantly higher values of *contrast* and *dissimilarity* texture features in the PI region of the chronic MI patients. This indicates an increase of signal intensity complexity in the PI region for a chronic MI. As shown by the equations in Table 0-1, these two texture values will increase if there is greater difference between the signal intensity of neighboring pixels. A previous study also found that higher *contrast* texture feature values existed in an animal model of increased myocardial

fibrosis [200]. This could be attributed to the increased collagen deposition intermingled with healthy cardiomyocytes in the fibrotic region. Conversely, we found the *homogeneity* texture feature in the PI region was lower in the chronic than the acute MI patients. This indicates the appearance of a more uniform contrast agent distribution in the PI region of the acute patients can be characterized by a smoothness measurement such as the *homogeneity* texture feature.

In our study, microvascular obstruction (MVO) was observed within the MI region of some of the acute patients. We expected a higher textural complexity for those infarctions. However, such a structured pattern of enhancement, a dark region inside the bright myocardial infarction, was not as discriminant as we initially thought. As a large, dense region of MVO may contain homogeneously dark pixels, it may thus reduce the complexity of the signal intensity distribution and texture contents. Moreover, the size of the MVO varies between patients and even between slices, possibly limiting its discrimination power for texture analysis to differentiate the acute from the chronic MI. The small number of patients in each group, coupled with the fact that not all acute MI have MVO might also explain our results.

Texture analysis has been previously used in LGE CMR images. Automatic segmentation of the MI region was possible based on the difference in textural pattern found in the MI region and in the remote myocardium on LGE CMR patient images [189]. A probability map was generated from LGE CMR images to assess the degree of tissue scarring in 24 patients with MI [234]. Another study using LGE CMR images was performed on 44 patients with MI that identified the probability of a myocardium region being infarcted [190]. Texture analysis has also been used in the presence of non-ischemic cardiomyopathies to identify patients with hypertrophic cardiomyopathies in LGE CMR images [186]. Our study furthers the usage of texture analysis to discriminate between acute and chronic MI in patients which was previously limited with conventional signal intensity analysis methods applied to LGE CMR images alone.

1.23Limitations

Our study had several limitations. First, the low number of patient cases included was a limitation of this study. An increased sample size would be preferable for statistical purposes and to solidify our findings. Second, the patients included in the two groups were different for this study. A longitudinal study of the same patients who underwent acute and chronic MI stages would allow

comparing the patient-specific progression of signal intensity patterns in the myocardium more unbiasedly. This would investigate texture analysis further as a means to grade myocardial infarction in LGE CMR images. Further studies are needed to investigate the effect of image resolution on texture features from LGE CMR images. The robustness of texture analysis between imaging scanners should also be investigated.

1.24 Conclusion

We found texture analysis of LGE CMR images could differentiate between acute and chronic MI patients. Such differences were more prominent in the peri-infarct zone than the infarct region or the remote myocardium. Texture analysis should be further investigated with more patient cases, and in a longitudinal study, to solidify this exploratory study.

CHAPTER 6 CLASSIFICATION OF ISCHEMIC CARDIOMYOPATHIES

Texture analysis of LGE CMR images gave significantly different texture feature values in different aged MI. It remains to be validated if using those texture features from LGE CMR images could automatically classify patients with acute from those with chronic MI. Medical image classification can have different applications, ranging from identification of tissue types for organ segmentation to disease grading based on the different alterations that organs undergo in the presence of disease. We will concentrate on classification with the aim of grading diseases to differentiate between patients with acute versus chronic MI using texture features evaluated in the different regions of interest in LGE CMR images. Pattern classification is a complex process with many possible schemes to analyze the feature space [188]. The choice of classifier can be made by reviewing the literature and by conceptualizing the problem. This chapter presents the classification method that was chosen and the preliminary results that we have obtained to classify acute versus chronic MI patients with LGE CMR images only.

1.25 Acute Versus Chronic MI Classification

1.25.1 Classification Method

The support vector machine (SVM) method was chosen based on previous studies [191, 192]. This method finds a hyper-plane in the feature space that separates the data into groups, in our case the acute and the chronic MI groups. We used the Gaussian radial basis function (RBF) as the SVM kernel with parameters C and gamma that define the cost function for margin selection and the Gaussian parameter in the RBF, respectively. Principal component analysis (PCA) was used to perform feature reduction prior to the automatic classification with SVM. Classification rates were evaluated for each combination of the x^{th} first principal component associated with the x^{th} highest eigenvalues. We performed classification with 2 to 7 PCA components ($x = [2\,..\,7]$). Cross validation with n=2 was performed during the SVM training process. Classification rates are presented as a percentage of correctly classified cases.

1.25.2 Classification Results

The eigenvalues and the associated percent variance from the PCA analysis are shown in Table-0-1. Automatic classification results with the SVM classifier, PCA for feature reduction and using the texture features extracted from the GLCM (d=1) are presented in Table-0-2. We obtained our classification results after having selected the *C* and *gamma* parameters that resulted in the highest classification rate. The highest classification rate of 86.95% was obtained in the PI zone, when using 5 principal components with the RBF SVM. A classification rate of 82.60% was obtained in the PI area using 3 or 4 principal components. The same classification rate was obtained in the remote myocardium with all the original texture features (no feature reduction process) and as well when 6 principal components were used. When the GLCM distance was set to 2, the MI region had a highest classification rate of 82.60%, using 5 principal components (Table-0-3). When the GLCM distance was set to 3, the highest classification rate of 82.60% was obtained in the MI region without feature selection (Table 0-4).

Table-0-1: Eigen values and percent variance per PCA components.

Principal components	**Eigen values**	**Percent Variance (%)**
1	6.753	84.41
2	0.584	7.30
3	0.334	4.17
4	0.156	1.95
5	0.118	1.48
6	0.038	0.48
7	0.015	0.19
8	0.001	0.01

Table-0-2: Classification rate (%) with texture features obtained from the GLCM matrix built with d=1, with all features or with a specified number of PCA components.

		Classification rate (%)		
		PI	**MI**	**Remote**
no feature selection		73.91	69.95	82.60
Number of PCA components	**2**	73.91	60.86	60.86
	3	82.60	69.56	69.56
	4	82.60	69.56	69.56
	5	86.95	73.91	65.21
	6	69.56	65.21	82.60
	7	69.56	65.21	78.26

Table-0-3: Classification rate (%) with texture features obtained from the GLCM matrix built with d=2**,** with all features or with a specified number of PCA components.

		Classification rate (%)		
		PI	**MI**	**Remote**
no feature selection		78.26	78.26	69.56
Number of PCA components	**2**	69.56	69.56	56.52
	3	69.56	65.21	56.52
	4	69.56	65.21	56.52
	5	73.91	82.60	69.56
	6	73.91	69.56	78.26
	7	69.56	69.56	73.91

Table 0-4: Classification rate (%) with texture features obtained from the GLCM matrix built with d=3, with all features or with a specified number of PCA components.

		Classification rate (%)		
		PI	**MI**	**Remote**
no feature selection		69.56	82.60	60.86
Number of PCA components	**2**	56.52	56.52	56.52
	3	60.86	65.21	65.21
	4	60.86	65.21	65.21
	5	65.21	69.56	60.86
	6	65.21	60.86	56.52
	7	56.52	65.21	52.17

1.25.3 Discussion

The highest classification rate of 86.95% was obtained when texture analysis was applied in the peri-infarct region (GLCM d=1). The fact that the classification rate was over 80% indicates the existence of a difference in the signal intensity pattern from LGE CMR images and that classification methods can detect if a patient has an acute or chronic MI scar. Interestingly, there was also a high classification rate of 82.60% in the remote myocardium when using a GLCM distance of d=1. There have been studies relating changes to the remote myocardium in the presence of ischemia [235] that could explain this result. Those studies point to an increase of extracellular space that could be related to an increase amount of diffuse fibrosis in this region. However, the association of those changes to the measured differences in texture features and classification results remains to be investigated.

A variation of GLCM distance influenced the classification results. The presence of microvascular obstruction (MVO) in the acute MI group made us expect a higher textural complexity in that region when compared to the chronic MI patients. However, such a structural pattern of enhancement, a dark region inside the bright myocardial infarct, did not allow the texture measures to discriminate the patients of the two groups as well as other regions, with a GLCM d=1, and a maximal classification rate of 73.91%. However, automatic classification using features obtained from GLCM distances of d=2 and d=3 could correctly differentiate a majority of acute from chronic cases in the MI region (Table-0-3 and Table 0-4). This can indicate texture analysis could measure patterns at different scales. The peri-infarct zone could require a small GLCM distance to detect the rapid variation of signal intensity as a result of the underlying structure of the myocardium which consists of an intermingling of healthy and diseased cells. At higher GLCM distances, texture analysis could be influenced by the presence of grosser patterns as a result of contrast agent dynamics in the myocardium, such as the presence of MVO. Care must be taken to consider the image resolution and thickness of the myocardial wall while selecting a distance to compute the GLCM. These limited results are interesting but it should be noted that not all acute patients have MVO. Moreover the size of the MVO varies as well between patients and even between slices, possibly limiting its discrimination power between the acute and the chronic MI groups. However, classification might be improved if the presence of MVO could be assessed as a feature in itself. A region of darker intensities inside the MI could be assessed for size and may influence the classification results. Moreover, the stability of the textural analysis might be influenced by other image factors than the underlying structural composition of the myocardium. As we vary the GLCM distances, there might be an influence from image resolution and the size of the structures we are measuring that needs to be further analyzed.

Caution should be taken in interpreting these results since we have a small number of cases. We obtained higher classification rates when using the principal component analysis. However it is clear that the number of features that we have tested do not warrant a feature reduction process. As a matter of fact, we also observed a variation in the classification rate that doesn't stabilize as we increase the number of PCA components used for automatic classification (Table-0-2, Table-0-3 and Table 0-4). We can argue that a higher number of features would allow for such a stabilization of classification rate.

We have chosen the SVM classifier as our first test for the classifier. However other methods should be tested as well. Neural networks were successfully studied in the classification of liver fibrosis in a comparative study of the most performant feature selection process [236]. They analyzed texture features evaluated from regions of interest of healthy patients compared to those having liver disease. They subsequently classified the group of liver disease patients into those having a cyst or not. The individuals from the group which didn't have cyst were divided as having hemangioma or as having liver cancer. Another option consists of using a combination of classifiers. This was suggested as a means of obtaining the most accurate classification result while limiting the sensitivity of a particular classifier to biased features [237]. Combining classifiers was done for liver fibrosis classification by weighing the response of each classifier [238]. They compared two of such combined classifiers, one with a five layer perceptron with each receiving different types of features as input, and another classifier composed of a multi-layer perceptron neural network, a probabilistic neural network, and three variations of the k-NN classifier.

CHAPTER 7 GENERAL DISCUSSION AND FUTURE DIRECTIONS

In this thesis we aimed to exploit texture analysis method by which LGE CMR images could be used to improve the myocardium characterization. More specifically, we wanted to assess the presence of diffuse myocardial fibrosis and as well discriminate acute from chronic MI cases from LGE CMR images alone. This chapter discusses our findings with regards to our initial objectives. In the first part, we will make an overview of our findings from our first animal study regarding the use of texture analysis on high resolution LGE CMR images and with histological validation. In the second part of this chapter we will discuss our findings from the application of texture analysis to LGE CMR images of patients with ischemic cardiomyopathies and present how these computational methods were a discriminant measure of acute versus chronic MI. We will also briefly review our initial classification results.

1.26Texture Analysis of Diffuse Myocardial Fibrosis in LGE images

The first study of this thesis aimed at detecting subtle increases in collagen content seen from LGE CMR microscopy of different aged rat hearts. Quantification of those changes was done with texture analysis methods and validated with histology images. Our first objective was to identify an animal model of diffuse myocardial fibrosis. We found that aged rat hearts contained an increase in collagen fibers in the myocardium compared to younger rat hearts. Histological analysis of the heart slices stained with picrosirius red showed there was an increase in both perivascular and diffusive myocardial fibrosis. Quantitative analysis of the histology images was performed by isolating collagen fibers in the myocardium with an HSV thresholding method. Our second objective was to detect an increase in diffuse myocardial fibrosis with texture analysis from high resolution LGE CMR images of the different aged rat hearts. Texture analysis method applied to the LGE CMR images enhanced the quantitative assessment of the slight increase in myocardial fibrosis from the aged myocardium compared to that of the younger rat hearts. Histological validation confirmed the underlying microstructure of the myocardium showed collagen fibers location, as assessed with picrosirius red staining of the hearts, corresponded to enhanced regions in LGE CMR and in the *contrast* texture images. We have therefore shown in our first article that high resolution LGE CMR images can depict locations of myocardial fibrosis and that texture analysis enhanced those locations. To our knowledge, this study is the first to confirm that texture

analysis of LGE CMR images can assess the underlying myocardial structure and more precisely detect even slight increases in collagen fibers in the heart.

Ex-vivo imaging of rat hearts offered the possibility of acquiring high resolution LGE CMR images which showed structural details of the myocardium that was not available with in-vivo imaging. Diffuse myocardial fibrosis was previously challenging to detect with signal intensity based methods in LGE CMR images [7, 14]. When fibrosis is present in all the myocardium, the remote region cannot be defined. There is therefore no baseline to evaluate the enhancement of signal intensity and the SD method above the mean signal intensity of the remote region cannot be applied. Even if texture analysis methods enhance locations where collagen fibers are present, we still used the signal intensity method to isolate island of enhancement in the *contrast* texture maps that we obtained in our first study. This requires the identification of remote myocardium to isolate the enhanced signal. To resolve this issue, a comparative analysis of texture feature measures from many healthy hearts is needed to establish a baseline value of texture features. Establishing this baseline will allow a direct comparison of the texture feature values in health and disease. Texture analysis describes the signal intensity patterns in the image and the increased value of contrast in the feature maps of our first article indicates a higher complexity in the locations of increased collagen fiber. We performed a comparative study of low and high collagen fibers in the heart. It should be investigated if the native value of texture features could be used to characterize the myocardium in health and disease.

As discussed in our first paper, Schelbert et al [51] found focal fibrosis could be identified with LGE CMR images and our study extended their findings to diffuse myocardial fibrosis. Slight alterations to the myocardium caused by collagen fiber infiltration were depicted in high resolution LGE CMR images. This finding was interesting since it was believed that LGE CMR images were limited in showing diffuse myocardial fibrosis and could only reliably enhance focal fibrosis, or more concentrated regions of collagen accumulation.

Alternative acquisition methods, such as T_1 maps and ECV, have been successfully presented to assess fibrosis in the heart. The use of texture analysis and those alternative images is not exclusive. In fact, we have found texture analysis of T_1 maps have been investigated in images of the knee cartilage [239]. It was moreover recently found that fibrosis in the liver could be characterized by

texture analysis applied to T_1 and T_2 maps [240]. There is therefore potential in the application of texture analysis methods to T_1, T_2 maps and ECV. This should be considered in future studies.

The prognostic importance of LGE CMR images was shown in NICM [241], for example in DCM [242, 243], in myocarditis [244], and particularly in HCM [245-247]. The presence and as well the absence of enhancement in LGE CMR images was shown to be related to prognosis. Since we now know that even the subtle presence of collagen fibers in the heart can be depicted by LGE CMR images and that texture analysis enhances those locations, we assume that texture analysis can help in the quantification of non-typical patterns of enhancement in NICM. If we concentrate on HCM for example, both the presence and the area occupied by enhancement in LGE CMR images, as assessed with the SD above the mean of the remote myocardium method, was related to patient outcome [248, 249]. Based on that knowledge, Maron et al. [250] stressed the importance of finding better ways than the SD above the mean signal intensity of the remote myocardium to characterize diffuse fibrosis in LGE CMR images in the presence of HCM. Texture analysis could assess the enhancement of those non-typical, non-focal patterns of enhancement that are seen in LGE CMR images in HCM. In fact, during this thesis, Thornhill et al. [186] did find that enhancement distribution across the myocardium in the presence of HCM could be quantified with texture analysis and related to patient outcome. Our first study complements their findings and confirms that texture analysis does characterize diffuse fibrosis in LGE CMR images. Other interesting application of texture analysis would be on images of patients with an increase of extracellular space, for example with amyloidosis, where the infiltration of amyloid increases the extracellular space and creates areas of enhancement in LGE CMR images. We believe that texture analysis of LGE CMR images could, in a similar way, characterize other non-ischemic diseases that sparsely affect the entire myocardium.

1.27 Texture Analysis of Myocardial Infarction in LGE images

Our second submitted research paper showed texture analysis could successfully be applied to LGE CMR images of patients with ischemic cardiomyopathies. We found texture analysis allowed discrimination of patients with acute or with chronic MI. This second translational study indicates that texture analysis of LGE CMR images can be used in a clinical setting. This is important knowing that image resolution is much lower in patient imaging. The texture analysis method we used in the LGE CMR imaging of patients was computed on image slices. Therefore, the GLCM

was built with the neighborhood of a central pixel determined in a 2D region, as opposed to a 3D region around a position in the animal study of the first journal paper. There is the possibility to perform 3D texture analysis in patient images by interpolation of the existing data. The reliability of such new values remains to be validated but could be promising since three dimensional analysis of LGE CMR patient images with ischemic cardiomyopathies was shown to characterize scar following multi-planar reformatting [251]. Nevertheless we were able to extract interesting information from our planar analysis. Mainly, texture analysis could differentiate patients with different aged infarcts.

To our knowledge, differentiating acute from chronic MI has not been done on LGE CMR images alone. Previous methods used infarct characteristics that occur according to infarct age, such as the presence of edema, detected in T_2 images, in acute but not in chronic MI. Other methods used specific contrast agent with varying enhancement result in the two infarct aged groups, requiring more image acquisitions. Our study is the first to differentiate MI by its age using only LGE CMR images, by analyzing the textural information contained in one image. The importance of this discrimination comes as more patients survive acute MI and might be re-admitted when other cardiac events occur. Our method might be particularly useful in patient populations more at risk of having unrecognized MI, such as people with diabetes [22]. The presence of unrecognized scar has prognostic implications [252-254]. There have been limited means to identify patients with unrecognized MI [255]. CMR has emerged as a tool for such an assessment [254]. Patients with these types of MI could present with symptoms and acute MI but also have previous myocardial scars that our texture analysis method could characterize. The existing myocardial scars could be discerned from more recent myocardial damage. Since we found in our first study that areas containing an intermingling of healthy and diseased cells were associated to texture feature values, and knowing that such areas are related to arrhythmia events [256], we could present the clinician with a means to better characterize the myocardial scar as opposed to simply estimating its size and extent from LGE CMR images. This could potentially influence how patients are treated, with aggressive interventions aimed at more recent myocardial damage.

Visual assessment of complex signal intensity patterns was previously done for LGE CMR images when describing heterogeneity of the infarct scar. The term *heterogeneity* was associated to the peri-infarct zone characteristics such as its size [257], or its evolution [258]. Our texture analysis computation is consistent with the visual assessment of clinicians and the histological analysis of

the PI zone [227]. A comparison of different intensity based analysis methods of the heterogeneity of the peri-infarct zone found there was a high variability of results between these studies to isolate that region [259]. We are presenting a consistent mean of analyzing the peri-infarct zone in ischemic cardiomyopathies. The peri-infarct zone, also referenced as the border zone in the literature, identifies a region with intermediate levels of grey values in LGE CMR images that correspond to a mixture of healthy and diseased cardiomyocytes along with collagen fibers. Schelbert et al. [51] discussed imaging of the peri-infarct zone with LGE CMR images. They showed the border zone, as seen in histology images of rat hearts, was composed of healthy cardiomyocytes intermingled with collagen fibers. They also showed, from histological slices stained with Masson Trichrome, that islands of enhancement in LGE CMR images were present in that region. Moreover, Hervas et al. [227] recognized that the physiological structure of that region was particularly different than the infarct core following histological analysis. Therefore, these areas are of particular interest because of the propagation of contraction signal in the heart that is perturbed in that region, leaving the patient at risk of arrhythmias [256]. This is of particular interest since it was shown that the existence of island of healthy cardiomyocytes surrounded by collagen fibers in that region was found to be an indicator of adverse cardiac events such as ventricular arrhythmias [229] or a predictor of mortality [24, 231] for patients with ischemic cardiomyopathies. However in these studies, the heterogeneity of the PI zone was assessed with the size of the area and not the intensity pattern of the region. The texture analysis of this region allowed discriminating MI by its age and this shows the PI region offers physiological differences in young versus old myocardial scars. Characterizing the myocardial infarct according to its age opens the door to grading of ischemic cardiomyopathies, and offers the potential to estimate the prognosis for patients based on the border zone's textural content from the LGE CMR images. Future studies should investigate how texture analysis would grade intermediate aged MI, and follow progression of the disease. In patients with acute MI, different texture feature quantification might discriminate areas previously infarcted from others damaged by more recent events.

We used the GLCM to analyze LGE CMR images because of its extensive use in medical imaging. Usage of the GLCM with MRI images has been successful in other diseases such as for cancer characterization [260-264], cartilage analysis [265] and brain imaging [266]. Engan et al. [267] moreover found that the GLCM matrix and its extracted features from LGE CMR images were characteristic of infarct scar in patients with ischemic cardiomyopathy. GLCM allows studying the

inter-relation of intensity in a given sub-region, as a characteristic for a broader textural pattern. Moreover the simplicity of the mathematically computed features from the grey level matrix and their descriptive names made it a relatable method for clinicians who were familiar with heterogeneities seen on LGE CMR images. Thornhill et al. [186] used the RLM [111] as texture method to extract features from LGE CMR images of patients with HCM. It was found that using a combination of texture analysis methods increased classification rate of multiple sclerosis lesions in brain images, compared to using the GLCM texture alone [268]. An investigation of different individual texture analysis methods and a combination of those methods from LGE CMR images in ischemic and non-ischemic cardiomyopathies should be done in the future. Such a combination of texture features could be of particular interest when performing the classification step.

Much information can be obtained by analyzing the GLCM matrix itself [269] without extracting the typical texture features described by Haralick [104]. Nanni et al. [269] found the GLCM matrix itself held more information and was more discriminative than the initial texture features described by Haralick [104]. Such an analysis is interesting but comes with the computational load of the GLCM matrices. GPU acceleration [270, 271] of the GLCM texture analysis method were developed to counter this limitation and could be considered for further analysis.

Another interesting approach to consider when using texture analysis is the directional component in the calculation of the GLCM. Different GLCM matrices can be computed according to a specified direction. Since we know that texture features are related to collagen fiber content, it would be interesting to investigate if directional measures of texture features could relate to fiber orientation in the heart. Since the myocardium in the short axis direction is circular, relative orientation could be measured from the insertion points of the RV as a reference orientation.

Patient classification into different MI aged groups is a first step to grading of ischemic cardiomyopathies. Automatic classification of patients into different non-ischemic cardiomyopathy groups could also be of interest. Our initial classification results are promising and could lead to the characterization of different enhancement patterns that have been identified in LGE CMR images [241].

Patient specific retrospective study of texture features in chronic MI compared to the first onset of the disease in acute MI is planned for the near future. It will be interesting to verify the difference in myocardial structure that texture analysis will be able to enhance with different aged MI images

from the same patient. Progression of fibrosis infiltration could be followed and we hope texture analysis will quantify those myocardial structure changes through time.

We have found relative measures of texture features could differentiate groups with different levels of fibrosis in the heart and it remains to be seen if quantifiable measures could also stand alone as an indication of disease. In the aged rat study, feature values were compared in the normal and in the aged rat hearts, and for the patients with ischemic cardiomyopathy it was the relative measure between the acute and the chronic MI groups that differentiated them. Future work is necessary to investigate if specific values of texture features from LGE CMR images could hold information on the structure of the myocardium. We have not evaluated the absolute values of the features for each groups and this requires further analysis.

It is important to know that if a region is entirely occupied by collagen fibers, the contrast agent will spread uniformly in that region, which could result in low values of contrast in the contrast feature map for example. It is therefore possible that texture analysis might be limited in distinguishing regions of uniformly distributed contrast agent such as in ischemic scar. A complex pattern of signal intensity variation is only obtained in the presence of intermingling of healthy cardiomyocytes and collagen infiltration. We can notice that in agreement with this statement, in our second study we have obtained discrimination from acute and chronic MI patients in the border zone of the infarct more so than in the MI scar region. In the presence of enhancement, a weighing factor indicating the level of signal intensity in a region could be considered. In its present state, the application of texture analysis in the infarct core could be of interest as an indicator of the structure of the underlying myocardium. It could indicate if there could be the existence of healthy cardiomyocytes in a scar region by indicating a location of higher signal intensity variation.

It also should be investigated if absolute values would remain consistent across MR scanners. It would require an increased number of studies reporting consistent measures of texture features from different MR scanners to consider the possibility of associating a myocardial status to specific texture values. However, in the near future, since the precise values of the texture features are used only in comparison to basis measures, we foresee the need to acquire baseline images to extract texture features in control cases. This will allow for texture feature comparison when LGE CMR images are acquired in the presence of disease on the same scanner.

Since our preliminary classification results are interesting, a comparative study testing classification schemes with images originating from different imaging scanners would be interesting to test. A previous classification study found the SVM classifier, with a RBF kernel, could successfully grade lung diseases with images obtained across different scanners [192]. Their regional analysis was done on square regions identified from high resolution CT images of the lungs. They used a relatively low number of features, twenty two, originating from histogram analysis, gradient calculation, RLM, GLCM amongst others. A multi-scanner approach would increase chances that our computer aided diagnostic method could be used in a clinical setting, if classification results are standardized across scanners.

CHAPTER 8 CONCLUSION

The aim of this thesis was to enhance LGE CMR images through texture analysis methods to discern subtle changes in myocardial collagen content in the presence of cardiomyopathies. We have shown that pattern of enhancement through texture analysis of LGE CMR images could characterize myocardial fibrosis in both an animal model of diffuse myocardial fibrosis and for patients with ischemic cardiomyopathy. The histological validation of texture analysis from high resolution LGE CMR images and moreover its application in LGE CMR patient images, indicate texture is a reliable analysis method to characterize alteration of the myocardial structure in the presence of disease. Histological validation was lacking for texture analysis of LGE CMR images. High resolution LGE CMR images were necessary to investigate if texture analysis methods could follow myocardial fibrosis at a cellular level. The findings from our first study, comparing different aged rat hearts, showed that it is possible to quantify a subtle increase in myocardial fibrosis in high resolution LGE CMR images and with texture analysis. Histological validation with picrosirius red staining showed texture analysis quantification was indeed related to the underlying tissue structure and was correlated to collagen content in the myocardium. This study established the link between quantification by texture analysis measures of LGE CMR images and the presence of fibrosis in the myocardium. The second translational study was therefore necessary to investigate how this method would hold in clinical imaging, where typical images offer much lower resolution. Our second study presented texture analysis methods applied to LGE CMR images of patient with ischemic cardiomyopathy. Our findings showed that texture features were significantly different for patients with acute compared with chronic MI, allowing what was previously limited with signal intensity based methods applied to LGE CMR images. We have provided validation of texture analysis as a measure of fibrosis content variation in the myocardium in an animal model of diffuse fibrosis and to characterize acute and chronic MI scars. Our findings can serve as reference for studies using texture analysis in cardiology to confirm the measures are related to the underlying tissue structure.

Other application of our texture analysis method include staging of myocardial fibrosis which is important in forensic science, where CMR is gaining in popularity because it allows myocardial analysis without autopsy [272]. Although contrast agent cannot be used in this context, if texture analysis is successful in contrast free in-vivo CMR images, which should also be investigated, there could be potential applications in forensic science.

The texture analysis we have presented is a consistent and reproducible image analysis method that is easily transferable between centers. Multi-center trials can therefore easily be planned to assess the performance of texture analysis methods with LGE CMR images from different scanners. In the near future we do foresee the need to acquire baseline images from different scanners that would give typical values of texture analysis from which enhanced texture analysis could be compared.

Our hope is that texture analysis could become a consistent indicator of myocardial structure alteration in cardiomyopathies from different etiologies. Since texture analysis is a computational method it can easily be applied to patient images retrospectively and with disregard to the cardiomyopathy. This increases the number of images that can be analyzed in future studies and in comparing non-ischemic diseases. Texture analysis could be used as an additional marker to assess the state of the myocardium in the occurrence of cardiomyopathies from various etiologies either through a more developed classification scheme than our initial study, or through the direct use of relative texture values with regards to pre-established baseline values. In this way, specific patterns of enhancement would be quantified through texture analysis and could guide the diagnosis to specific cardiomyopathies. In clinical practice, knowing the severity of the myocardium's structure alteration is important to establish a prognosis and to plan a personalized intervention. Complex pattern of enhancement is the result of the interwoven cardiomyocytes with collagen fibers. Such a structural arrangement in the myocardium is associated to higher risk of arrhythmia. Our texture analysis method could be a measure of the presence of such complex myocardial structure and guide the clinician to find such locations in the heart. Grading of myocardial infarction scar could be an indicator of the progression of disease in patients. It could monitor different cardiac involvement following heart transplant for example. Unrecognized MI could be detected more easily, specifically in the presence of recent scar where rapid intervention could lead to partial recovery whereas chronic MI would not benefit from therapeutic intervention.

BIBLIOGRAPHY

[1] D. Mozaffarian, E. J. Benjamin, A. S. Go, D. K. Arnett, M. J. Blaha, M. Cushman, *et al.*, "Heart disease and stroke statistics--2015 update: a report from the American Heart Association," *Circulation,* vol. 131, pp. e29-322, Jan 27 2015.

[2] R. J. Kim, D. S. Fieno, T. B. Parrish, K. Harris, E. L. Chen, O. Simonetti, *et al.*, "Relationship of MRI delayed contrast enhancement to irreversible injury, infarct age, and contractile function," *Circulation,* vol. 100, pp. 1992-2002, Nov 9 1999.

[3] S. Bohl, R. Wassmuth, H. Abdel-Aty, A. Rudolph, D. Messroghli, R. Dietz, *et al.*, "Delayed enhancement cardiac magnetic resonance imaging reveals typical patterns of myocardial injury in patients with various forms of non-ischemic heart disease," *Int J Cardiovasc Imaging,* vol. 24, pp. 597-607, Aug 2008.

[4] K. W. Cummings, S. Bhalla, C. Javidan-Nejad, A. J. Bierhals, F. R. Gutierrez, and P. K. Woodard, "A Pattern-based Approach to Assessment of Delayed Enhancement in Nonischemic Cardiomyopathy at MR Imaging," *RadioGraphics,* vol. 29, pp. 89-103, 2009.

[5] D. A. Bluemke, "MRI of nonischemic cardiomyopathy," *AJR Am J Roentgenol,* vol. 195, pp. 935-40, Oct 2010.

[6] J. A. Gonzalez and C. M. Kramer, "Role of Imaging Techniques for Diagnosis, Prognosis and Management of Heart Failure Patients: Cardiac Magnetic Resonance," *Curr Heart Fail Rep,* vol. 12, pp. 276-83, Aug 2015.

[7] R. J. Everett, C. G. Stirrat, S. I. Semple, D. E. Newby, M. R. Dweck, and S. Mirsadraee, "Assessment of myocardial fibrosis with T1 mapping MRI," *Clin Radiol,* vol. 71, pp. 768-78, Aug 2016.

[8] M. Ugander, A. J. Oki, L. Y. Hsu, P. Kellman, A. Greiser, A. H. Aletras, *et al.*, "Extracellular volume imaging by magnetic resonance imaging provides insights into overt and sub-clinical myocardial pathology," *Eur Heart J,* vol. 33, pp. 1268-78, May 2012.

[9] D. R. Messroghli, S. Nordmeyer, T. Dietrich, O. Dirsch, E. Kaschina, K. Savvatis, *et al.*, "Assessment of diffuse myocardial fibrosis in rats using small-animal Look-Locker inversion recovery T1 mapping," *Circ Cardiovasc Imaging,* vol. 4, pp. 636-40, Nov 2011.

[10] M. Salerno and C. M. Kramer, "Advances in parametric mapping with CMR imaging," *JACC Cardiovasc Imaging,* vol. 6, pp. 806-22, Jul 2013.

[11] C. S. Broberg, S. S. Chugh, C. Conklin, D. J. Sahn, and M. Jerosch-Herold, "Quantification of diffuse myocardial fibrosis and its association with myocardial dysfunction in congenital heart disease," *Circ Cardiovasc Imaging,* vol. 3, pp. 727-34, Nov 2010.

[12] D. M. Sado, A. S. Flett, S. M. Banypersad, S. K. White, V. Maestrini, G. Quarta, *et al.*, "Cardiovascular magnetic resonance measurement of myocardial extracellular volume in health and disease," *Heart,* vol. 98, pp. 1436-41, 2012.

[13] A. S. Flett, M. P. Hayward, M. T. Ashworth, M. S. Hansen, A. M. Taylor, P. M. Elliott, *et al.*, "Equilibrium contrast cardiovascular magnetic resonance for the measurement of diffuse myocardial fibrosis: preliminary validation in humans," *Circulation,* vol. 122, pp. 138-44, Jul 13 2010.

[14] L. Iles, H. Pfluger, A. Phrommintikul, J. Cherayath, P. Aksit, S. N. Gupta, *et al.*, "Evaluation of diffuse myocardial fibrosis in heart failure with cardiac magnetic resonance contrast-enhanced T1 mapping," *J Am Coll Cardiol,* vol. 52, pp. 1574-80, Nov 4 2008.

[15] P. Kellman, J. R. Wilson, H. Xue, W. P. Bandettini, S. M. Shanbhag, K. M. Druey, *et al.*, "Extracellular volume fraction mapping in the myocardium, part 2: initial clinical experience," *Journal of Cardiovascular Magnetic Resonance,* vol. 14, Sep 11 2012.

[16] C. T. Sibley, R. A. Noureldin, N. Gai, M. S. Nacif, S. Liu, E. B. Turkbey, *et al.*, "T1 Mapping in cardiomyopathy at cardiac MR: comparison with endomyocardial biopsy," *Radiology,* vol. 265, pp. 724-32, Dec 2012.

[17] N. Mewton, C. Y. Liu, P. Croisille, D. Bluemke, and J. A. Lima, "Assessment of myocardial fibrosis with cardiovascular magnetic resonance," *J Am Coll Cardiol,* vol. 57, pp. 891-903, Feb 22 2011.

[18] H. Abdel-Aty, A. Zagrosek, J. Schulz-Menger, A. J. Taylor, D. Messroghli, A. Kumar, *et al.*, "Delayed enhancement and T2-weighted cardiovascular magnetic resonance imaging differentiate acute from chronic myocardial infarction," *Circulation,* vol. 109, pp. 2411-6, May 25 2004.

[19] M. Saeed, O. Weber, R. Lee, L. Do, A. Martin, D. Saloner, *et al.*, "Discrimination of Myocardial Acute and Chronic (Scar) Infarctions on Delayed Contrast Enhanced Magnetic Resonance Imaging With Intravascular Magnetic Resonance Contrast Media," *Journal of the American College of Cardiology,* vol. 48, pp. 1961-1968, Nov 21 2006.

[20] R. Kirschner, L. Toth, A. Varga-Szemes, T. Simor, P. Suranyi, P. Kiss, *et al.*, "Differentiation of acute and four-week old myocardial infarct with Gd(ABE-DTTA)-enhanced CMR," *J Cardiovasc Magn Reson,* vol. 12, p. 22, Apr 7 2010.

[21] K. A. Kim, J. B. Seo, K. H. Do, J. N. Heo, Y. K. Lee, J. W. Song, *et al.*, "Differentiation of recently infarcted myocardium from chronic myocardial scar: the value of contrast-enhanced SSFP-based cine MR imaging," *Korean J Radiol,* vol. 7, pp. 14-9, Jan-Mar 2006.

[22] R. Y. Kwong, H. Sattar, H. Wu, G. Vorobiof, V. Gandla, K. Steel, *et al.*, "Incidence and prognostic implication of unrecognized myocardial scar characterized by cardiac magnetic resonance in diabetic patients without clinical evidence of myocardial infarction," *Circulation,* vol. 118, pp. 1011-20, Sep 2 2008.

[23] S. D. Roes, C. J. Borleffs, R. J. van der Geest, J. J. Westenberg, N. A. Marsan, T. A. Kaandorp, *et al.*, "Infarct tissue heterogeneity assessed with contrast-enhanced MRI predicts spontaneous ventricular arrhythmia in patients with ischemic cardiomyopathy and implantable cardioverter-defibrillator," *Circ Cardiovasc Imaging,* vol. 2, pp. 183-90, May 2009.

[24] A. T. Yan, A. J. Shayne, K. A. Brown, S. N. Gupta, C. W. Chan, T. M. Luu, *et al.*, "Characterization of the peri-infarct zone by contrast-enhanced cardiac magnetic resonance imaging is a powerful predictor of post-myocardial infarction mortality," *Circulation,* vol. 114, pp. 32-9, Jul 4 2006.

[25] F. Demirel, A. Adiyaman, J. R. Timmer, J. H. Dambrink, M. Kok, W. J. Boeve, *et al.*, "Myocardial scar characteristics based on cardiac magnetic resonance imaging is associated

with ventricular tachyarrhythmia in patients with ischemic cardiomyopathy," *Int J Cardiol,* vol. 177, pp. 392-9, Dec 15 2014.

[26] D. H. Kwon, L. Asamoto, Z. B. Popovic, K. Kusunose, M. Robinson, M. Desai, *et al.*, "Infarct characterization and quantification by delayed enhancement cardiac magnetic resonance imaging is a powerful independent and incremental predictor of mortality in patients with advanced ischemic cardiomyopathy," *Circ Cardiovasc Imaging,* vol. 7, pp. 796-804, Sep 2014.

[27] H. L. Estner, M. M. Zviman, D. Herzka, F. Miller, V. Castro, S. Nazarian, *et al.*, "The critical isthmus sites of ischemic ventricular tachycardia are in zones of tissue heterogeneity, visualized by magnetic resonance imaging," *Heart Rhythm,* vol. 8, pp. 1942-9, Dec 2011.

[28] NHLBI. (2016). *How the Heart Works*. Available: http://www.nhlbi.nih.gov/health/health-topics/topics/chd/heartworks

[29] K. T. Weber, "Cardiac interstitium in health and disease: The fibrillar collagen network," *Journal of the American College of Cardiology,* vol. 13, pp. 1637-1652, Jun 1989.

[30] A. J. Pope, G. B. Sands, B. H. Smaill, and I. J. LeGrice, "Three-dimensional transmural organization of perimysial collagen in the heart," *American Journal of Physiology - Heart and Circulatory Physiology,* vol. 295, pp. H1243-H1252, Sep 2008.

[31] G. Macchiarelli, O. Ohtani, S. A. Nottola, T. Stallone, A. Camboni, I. M. Prado, *et al.*, "A micro-anatomical model of the distribution of myocardial endomysial collagen," *Histol Histopathol,* vol. 17, pp. 699-706, 2002.

[32] A. M. Segura, O. H. Frazier, and L. M. Buja, "Fibrosis and heart failure," *Heart Fail Rev,* vol. 19, pp. 173-85, Mar 2014.

[33] A. Biernacka and N. G. Frangogiannis, "Aging and Cardiac Fibrosis," *Aging Dis,* vol. 2, pp. 158-173, Apr 2011.

[34] J. G. Mill, I. Stefanon, L. dos Santos, and M. P. Baldo, "Remodeling in the ischemic heart: the stepwise progression for heart," *Braz J Med Biol Res,* vol. 44, pp. 890-8, Sep 2011.

[35] R. H. Falk, "Diagnosis and Management of the Cardiac Amyloidoses," *Circulation,* vol. 112, p. 2047, Sep 27 2005.

[36] M. R. Hazebroek, K. Everaerts, and S. Heymans, "Diagnostic approach of myocarditis: strike the golden mean," *Neth Heart J,* vol. 22, pp. 80-4, Feb 2014.

[37] A. G. Japp, A. Gulati, S. A. Cook, M. R. Cowie, and S. K. Prasad, "The Diagnosis and Evaluation of Dilated Cardiomyopathy," *Journal of the American College of Cardiology,* vol. 67, pp. 2996-3010, Jun 28 2016.

[38] C. Prinz, M. Farr, D. Hering, D. Horstkotte, and L. Faber, "The Diagnosis and Treatment of Hypertrophic Cardiomyopathy," *Deutsches Ärzteblatt International,* vol. 108, pp. 209-215, Apr 2011.

[39] J. P. Ridgway, "Cardiovascular magnetic resonance physics for clinicians: part I," *J Cardiovasc Magn Reson,* vol. 12, p. 71, Apr 2010.

[40] R. J. Kim, D. J. Shah, and R. M. Judd, "How we perform delayed enhancement imaging," *Journal of Cardiovascular Magnetic Resonance,* vol. 5, pp. 505-514, Jul 2003.

[41] J. D. Biglands, A. Radjenovic, and J. P. Ridgway, "Cardiovascular magnetic resonance physics for clinicians: part II," *Journal of Cardiovascular Magnetic Resonance,* vol. 14, p. 66, Sep 20 2012.

[42] M. J. Allen, K. W. MacRenaris, P. N. Venkatasubramanian, and T. J. Meade, "Cellular delivery of MRI contrast agents," *Chem Biol,* vol. 11, pp. 301-7, Mar 2004.

[43] M.-F. Bellin and A. J. Van Der Molen, "Extracellular gadolinium-based contrast media: An overview," *European Journal of Radiology,* vol. 66, pp. 160-167, May 2008.

[44] C. F. Geraldes and S. Laurent, "Classification and basic properties of contrast agents for magnetic resonance imaging," *Contrast Media Mol Imaging,* vol. 4, pp. 1-23, Jan-Feb 2009.

[45] P. Kellman, A. E. Arai, E. R. McVeigh, and A. H. Aletras, "Phase-sensitive inversion recovery for detecting myocardial infarction using gadolinium-delayed hyperenhancement," *Magn Reson Med,* vol. 47, pp. 372-83, Feb 2002.

[46] A. Franco, S. Javidi, and S. G. Ruehm, "Delayed Myocardial Enhancement in Cardiac Magnetic Resonance Imaging," *Journal of Radiology Case Reports,* vol. 9, pp. 6-18, Jun 30 2015.

[47] H. W. Kim, A. Farzaneh-Far, and R. J. Kim, "Cardiovascular Magnetic Resonance in Patients With Myocardial Infarction: Current and Emerging Applications," *Journal of the American College of Cardiology,* vol. 55, pp. 1-16, Dec 29 2010.

[48] C. Berry, P. Kellman, C. Mancini, M. Y. Chen, W. P. Bandettini, T. Lowrey, *et al.*, "Magnetic resonance imaging delineates the ischemic area at risk and myocardial salvage in patients with acute myocardial infarction," *Circ Cardiovasc Imaging,* vol. 3, pp. 527-35, Sep 2010.

[49] A. E. Arai, "The cardiac magnetic resonance (CMR) approach to assessing myocardial viability," *J Nucl Cardiol,* Dec 2011.

[50] R. J. Kim, E. Wu, A. Rafael, E. L. Chen, M. A. Parker, O. Simonetti, *et al.*, "The use of contrast-enhanced magnetic resonance imaging to identify reversible myocardial dysfunction," *N Engl J Med,* vol. 343, pp. 1445-53, Nov 16 2000.

[51] E. B. Schelbert, L. Y. Hsu, S. A. Anderson, B. D. Mohanty, S. M. Karim, P. Kellman, *et al.*, "Late gadolinium-enhancement cardiac magnetic resonance identifies postinfarction myocardial fibrosis and the border zone at the near cellular level in ex vivo rat heart," *Circ Cardiovasc Imaging,* vol. 3, pp. 743-52, Nov 2010.

[52] A. E. Stillman, M. Oudkerk, D. Bluemke, J. Bremerich, F. P. Esteves, E. V. Garcia, *et al.*, "Assessment of acute myocardial infarction: current status and recommendations from the North American society for Cardiovascular Imaging and the European Society of Cardiac Radiology," *Int J Cardiovasc Imaging,* vol. 27, pp. 7-24, Jan 2011.

[53] H. Vogelsberg, H. Mahrholdt, C. C. Deluigi, A. Yilmaz, E. M. Kispert, S. Greulich, *et al.*, "Cardiovascular magnetic resonance in clinically suspected cardiac amyloidosis: noninvasive imaging compared to endomyocardial biopsy," *J Am Coll Cardiol,* vol. 51, pp. 1022-30, Mar 11 2008.

[54] K. A. Reimer, J. E. Lowe, M. M. Rasmussen, and R. B. Jennings, "The wavefront phenomenon of ischemic cell death. 1. Myocardial infarct size vs duration of coronary occlusion in dogs," *Circulation,* vol. 56, pp. 786-94, Nov 1977.

[55] M. Fontana, S. Pica, P. Reant, A. Abdel-Gadir, T. A. Treibel, S. M. Banypersad, *et al.*, "Prognostic Value of Late Gadolinium Enhancement Cardiovascular Magnetic Resonance in Cardiac Amyloidosis," *Circulation,* vol. 132, p. 1570, Oct 20 2015.

[56] NHLBI. (2016). *Diseases and Conditions Index - Cardiomyopathy*. Available: http://www.nhlbi.nih.gov/health/dci/Diseases/cm/cm_types.html

[57] R. S. Jiji and C. M. Kramer, "Cardiovascular Magnetic Resonance Applications in Daily Practice," *Cardiology in Review,* vol. 19, pp. 246-254, Sep-Oct 2011.

[58] D. Lin, J. R. Lesser, and B. J. Maron, "Coexistence of late gadolinium enhancement due to myocardial infarction and hypertrophic cardiomyopathy," *Heart,* vol. 97, pp. 861-862, May 2011.

[59] T. G. Neilan, O. R. Coelho-Filho, R. V. Shah, S. A. Abbasi, B. Heydari, E. Watanabe, *et al.*, "Myocardial extracellular volume fraction from T1 measurements in healthy volunteers and mice: relationship to aging and cardiac dimensions," *JACC Cardiovasc Imaging,* vol. 6, pp. 672-83, Jun 2013.

[60] P. Anversa and J. M. Capasso, "Cellular basis of aging in the mammalian heart," *Scanning Microsc,* vol. 5, pp. 1065-73; discussion 1073-4, Dec 1991.

[61] S. J. Sangaralingham, E. L. Ritman, P. M. McKie, T. Ichiki, A. Lerman, C. G. Scott, *et al.*, "Cardiac micro-computed tomography imaging of the aging coronary vasculature," *Circ Cardiovasc Imaging,* vol. 5, pp. 518-24, Jul 2012.

[62] E. M. Walker, Jr., M. S. Nillas, E. I. Mangiarua, S. Cansino, R. G. Morrison, R. R. Perdue, *et al.*, "Age-associated changes in hearts of male Fischer 344/Brown Norway F1 rats," *Ann Clin Lab Sci,* vol. 36, pp. 427-38, Automn 2006.

[63] C. Y. Liu, Y. C. Liu, C. Wu, A. Armstrong, G. J. Volpe, R. J. van der Geest, *et al.*, "Evaluation of age-related interstitial myocardial fibrosis with cardiac magnetic resonance contrast-enhanced T1 mapping: MESA (Multi-Ethnic Study of Atherosclerosis)," *J Am Coll Cardiol,* vol. 62, pp. 1280-7, Oct1 2013.

[64] P. Kellman, J. R. Wilson, H. Xue, W. P. Bandettini, S. M. Shanbhag, K. M. Druey, *et al.*, "Extracellular volume fraction mapping in the myocardium, part 2: initial clinical experience," *J Cardiovasc Magn Reson,* vol. 14, p. 64, 2012.

[65] O. M. Abdullah, S. G. Drakos, N. A. Diakos, O. Wever-Pinzon, A. G. Kfoury, J. Stehlik, *et al.*, "Characterization of diffuse fibrosis in the failing human heart via diffusion tensor imaging and quantitative histological validation," *NMR Biomed,* vol. 27, pp. 1378-86, Nov 2014.

[66] N. A. Ntusi, S. K. Piechnik, J. M. Francis, V. M. Ferreira, P. M. Matthews, M. D. Robson, *et al.*, "Diffuse Myocardial Fibrosis and Inflammation in Rheumatoid Arthritis: Insights From CMR T1 Mapping," *JACC Cardiovasc Imaging,* vol. 8, pp. 526-36, May 2015.

[67] F. aus dem Siepen, S. J. Buss, D. Messroghli, F. Andre, D. Lossnitzer, S. Seitz, *et al.*, "T1 mapping in dilated cardiomyopathy with cardiac magnetic resonance: quantification of

diffuse myocardial fibrosis and comparison with endomyocardial biopsy," *Eur Heart J Cardiovasc Imaging,* vol. 16, pp. 210-6, Feb 2015.

[68] A. H. Ellims, L. M. Iles, L. H. Ling, J. L. Hare, D. M. Kaye, and A. J. Taylor, "Diffuse myocardial fibrosis in hypertrophic cardiomyopathy can be identified by cardiovascular magnetic resonance, and is associated with left ventricular diastolic dysfunction," *J Cardiovasc Magn Reson,* vol. 14, p. 76, Oct 29 2012.

[69] C. J. Yi, E. Yang, S. Lai, N. Gai, C. Liu, S. Liu, *et al.*, "Progression of diffuse myocardial fibrosis assessed by cardiac magnetic resonance T(1) mapping," *Int J Cardiovasc Imaging,* vol. 30, pp. 1339-46, Oct 2014.

[70] Y. J. Hong, C. H. Park, Y. J. Kim, J. Hur, H. J. Lee, S. R. Hong, *et al.*, "Extracellular volume fraction in dilated cardiomyopathy patients without obvious late gadolinium enhancement: comparison with healthy control subjects," *Int J Cardiovasc Imaging,* vol. 31 Suppl 1, pp. 115-22, Jun 2015.

[71] A. Florian, A. Ludwig, S. Rosch, H. Yildiz, U. Sechtem, and A. Yilmaz, "Myocardial fibrosis imaging based on T1-mapping and extracellular volume fraction (ECV) measurement in muscular dystrophy patients: diagnostic value compared with conventional late gadolinium enhancement (LGE) imaging," *Eur Heart J Cardiovasc Imaging,* vol. 15, pp. 1004-12, Sep 2014.

[72] R. J. Perea, J. T. Ortiz-Perez, M. Sole, M. T. Cibeira, T. M. de Caralt, S. Prat-Gonzalez, *et al.*, "T1 mapping: characterisation of myocardial interstitial space," *Insights Imaging,* vol. 6, pp. 189-202, Apr 2015.

[73] C. de Meester de Ravenstein, C. Bouzin, S. Lazam, J. Boulif, M. Amzulescu, J. Melchior, *et al.*, "Histological Validation of measurement of diffuse interstitial myocardial fibrosis by myocardial extravascular volume fraction from Modified Look-Locker imaging (MOLLI) T1 mapping at 3 T," *J Cardiovasc Magn Reson,* vol. 17, p. 48, Jun 11 2015.

[74] R. Lopes, A. Ayache, N. Makni, P. Puech, A. Villers, S. Mordon, *et al.*, "Prostate cancer characterization on MR images using fractal features," *Med Phys,* vol. 38, pp. 83-95, Jan 2011.

[75] A. Madabhushi, M. D. Feldman, D. N. Metaxas, J. Tomaszeweski, and D. Chute, "Automated detection of prostatic adenocarcinoma from high-resolution ex vivo MRI," *IEEE Trans Med Imaging,* vol. 24, pp. 1611-25, Dec 2005.

[76] W. Chen, M. L. Giger, H. Li, U. Bick, and G. M. Newstead, "Volumetric texture analysis of breast lesions on contrast-enhanced magnetic resonance images," *Magn Reson Med,* vol. 58, pp. 562-71, Sep 2007.

[77] J. Yao, J. Chen, and C. Chow, "Breast Tumor Analysis in Dynamic Contrast Enhanced MRI Using Texture Features and Wavelet Transform," *Ieee Journal of Selected Topics in Signal Processing,* vol. 3, pp. 94-100, 2009.

[78] Y. Zheng, S. Englander, S. Baloch, E. I. Zacharaki, Y. Fan, M. D. Schnall, *et al.*, "STEP: spatiotemporal enhancement pattern for MR-based breast tumor diagnosis," *Med Phys,* vol. 36, pp. 3192-204, Jul 2009.

[79] M. E. Mayerhoefer, W. Schima, S. Trattnig, K. Pinker, V. Berger-Kulemann, and A. Ba-Ssalamah, "Texture-based classification of focal liver lesions on MRI at 3.0 Tesla: a feasibility study in cysts and hemangiomas," *J Magn Reson Imaging,* vol. 32, pp. 352-9, Aug 2010.

[80] G. Chen, M. Strzelecki, Q. Pang, H. Kim, and H. Stodkilde-Jorgensen, "Textures in magnetic resonance images of the ischemic rat brain treated with an anti-inflammatory agent," *Clin Imaging,* vol. 34, pp. 7-13, Jan-Feb 2010.

[81] "Texture". (2016). *Merriam-Webster Dictionary* [Online]. Available: http://www.merriam-webster.com/dictionary/texture

[82] B. Julesz, "Textons, the elements of texture perception, and their interactions," *Nature,* vol. 290, pp. 91-7, Mar 12 1981.

[83] A. Materka, "Texture analysis methodologies for magnetic resonance imaging," *Dialogues in Clinical Neuroscience,* vol. 6, pp. 243-250, Jun 2004.

[84] G. Castellano, L. Bonilha, L. M. Li, and F. Cendes, "Texture analysis of medical images," *Clin Radiol,* vol. 59, pp. 1061-9, Dec 2004.

[85] A. Depeursinge, A. Foncubierta-Rodriguez, D. Van De Ville, and H. Muller, "Three-dimensional solid texture analysis in biomedical imaging: review and opportunities," *Med Image Anal,* vol. 18, pp. 176-96, Jan 2014.

[86] R. M. Haralick, "Statistical and Structural Approaches to Texture," *Proceedings of the Ieee,* vol. 67, pp. 786-804, May 1979.

[87] L. Carlucci, "A formal system for texture languages," *Pattern Recognition,* vol. 4, pp. 53-72, 1972.

[88] F. Vilnrotter, R. Nevatia, and K. E. Price, "Structural-Analysis of Natural Textures," *Proceedings of the Society of Photo-Optical Instrumentation Engineers,* vol. 281, pp. 246-253, Jan 1981.

[89] M. H. Bharati, J. J. Liu, and J. F. MacGregor, "Image texture analysis: methods and comparisons," *Chemometrics and Intelligent Laboratory Systems,* vol. 72, pp. 57-71, Jun 28 2004.

[90] B. Mandelbrot, *Fractal Geometry of Nature*. Moscow: Inst computer, 1983.

[91] J. M. Keller, S. Chen, and R. M. Crownover, "Texture description and segmentation through fractal geometry," *Computer Vision, Graphics and Image Processing,* vol. 45, pp. 150-166, 1989.

[92] S. S. Chen, J. M. Keller, and R. M. Crownover, "On the Calculation of Fractal Features from Images," *IEEE Transactions on Pattern Analysis and Machine Intelligence,* vol. 15, pp. 1087-1090, 1993.

[93] R. Lopes, P. Dubois, I. Bhouri, H. Akkari-Bettaieb, S. Maouche, and N. Betrouni, "Fractal geometry for medical signal analysis: A review," *Irbm,* vol. 31, pp. 189-208, Aug 2010.

[94] M. Borowska, J. Szarmach, and E. Oczeretko, "Fractal texture analysis of the healing process after bone loss," *Computerized Medical Imaging and Graphics,* vol. 46, pp. 191-196, Dec 2015.

[95] G. R. Cross and A. K. Jain, "Markov Random Field Texture Models," *IEEE Transactions on Pattern Analysis and Machine Intelligence,* vol. PAMI-5, pp. 25-39, Jan 1983.

[96] R. L. Kashyap and A. Khotanzad, "A Model-Based Method for Rotation Invariant Texture Classification," *IEEE Transactions on Pattern Analysis and Machine Intelligence,* vol. PAMI-8, pp. 472-481, July 1986.

[97] G. Finet, M. Gilard, B. Perrenot, G. Rioufol, P. Motreff, L. Gavit, *et al.*, "Fractal geometry of arterial coronary bifurcations: a quantitative coronary angiography and intravascular ultrasound analysis," *EuroIntervention,* vol. 3, pp. 490-8, Jan 2008.

[98] E. Santos Filho, Y. Saijo, A. Tanaka, T. Yambe, and M. Yoshizawa, "Fractal dimension of 40 MHz intravascular ultrasound radio frequency signals," *Ultrasonics,* vol. 48, pp. 35-9, Mar 2008.

[99] G. Captur, A. L. Karperien, C. Li, F. Zemrak, C. Tobon-Gomez, X. Gao, *et al.*, "Fractal frontiers in cardiovascular magnetic resonance: towards clinical implementation," *J Cardiovasc Magn Reson,* vol. 17, p. 80, Sep 7 2015.

[100] H. V. Huikuri and P. K. Stein, "Clinical application of heart rate variability after acute myocardial infarction," *Front Physiol,* vol. 3, p. 41, Feb 27 2012.

[101] F. Beckers, B. Verheyden, and A. E. Aubert, "Aging and nonlinear heart rate control in a healthy population," *Am J Physiol Heart Circ Physiol,* vol. 290, pp. H2560-70, Jun 2006.

[102] J. S. Perkiomaki, "Heart rate variability and non-linear dynamics in risk stratification," *Front Physiol,* vol. 2, p. 81, Nov 9 2011.

[103] I. Sedjelmaci and F. Bereksi-Reguig, "Fractal Analysis of the Electrocardiogram Signal," *Journal of Mechanics in Medicine and Biology,* vol. 14, 2014.

[104] R. M. Haralick, K. Shanmugam, and I. H. Dinstein, "Textural Features for Image Classification," *Systems, Man and Cybernetics, IEEE Transactions on,* vol. 3, pp. 610-621, Nov 1973.

[105] S. W. C. Lam, "Texture feature extraction using gray level gradient based co-occurence matrices," in *Systems, Man, and Cybernetics, 1996. IEEE International Conference on*, 14-17 Oct 1996, pp. 267-271.

[106] D. A. Clausi, Y. P. Zhao, Ieee, and Ieee, "Rapid determination of co-occurrence texture features," in *Igarss 2001: Scanning the Present and Resolving the Future, Vols 1-7, Proceedings*, ed, 2001, pp. 1880-1882.

[107] M. A. Tahir, M. A. Roula, A. Bouridane, E. Kurugollu, A. Amira, and Ieee, *An FPGA based co-processor for GLCM texture features measurement*, 2003.

[108] R. F. Walker, P. T. Jackway, and D. Longstaff, "Genetic algorithm optimization of adaptive multi-scale GLCM features," *International Journal of Pattern Recognition and Artificial Intelligence,* vol. 17, pp. 17-39, Aug 06 2003.

[109] F. R. de Siqueira, W. R. Schwartz, and H. Pedrini, "Multi-scale gray level co-occurrence matrices for texture description," *Neurocomputing,* vol. 120, pp. 336-345, 2013.

[110] A. Gelzinis, A. Verikas, and M. Bacauskiene, "Increasing the discrimination power of the co-occurrence matrix-based features," *Pattern Recognition,* vol. 40, pp. 2367-2372, Sept 2007.

[111] M. M. Galloway, "Texture analysis using gray level run lengths," *Computer Graphics and Image Processing,* vol. 4, pp. 172-179, Jun 1975.

[112] X. Tang, "Texture information in run-length matrices," *IEEE Trans Image Process,* vol. 7, pp. 1602-9, 1998.

[113] T. Ojala, M. Pietikäinen, and D. Harwood, "A comparative study of texture measures with classification based on featured distributions," *Pattern Recognition,* vol. 29, pp. 51-59, Jan 1996.

[114] K. I. Laws, "Rapid Texture Identification," 1980, pp. 376-381.

[115] L. Wang and D.-C. He, "Texture classification using texture spectrum," *Pattern Recognition,* vol. 23, pp. 905-910, 1990.

[116] D.-C. He and L. Wang, "Texture features based on texture spectrum," *Pattern Recognition,* vol. 24, pp. 391-399, 1991.

[117] T. Ojala, M. Pietikainen, and T. Maenpaa, "Multiresolution gray-scale and rotation invariant texture classification with local binary patterns," *IEEE Transactions on Pattern Analysis and Machine Intelligence,* vol. 24, pp. 971-987, Aug 07 2002.

[118] H. Zhou, R. Wang, and C. Wang, "A novel extended local-binary-pattern operator for texture analysis," *Information Sciences,* vol. 178, pp. 4314-4325, Nov 15 2008.

[119] L. Nanni, A. Lumini, and S. Brahnam, "Local binary patterns variants as texture descriptors for medical image analysis," *Artificial Intelligence in Medicine,* vol. 49, pp. 117-125, Jun 2010.

[120] A. Hafiane, G. Seetharaman, K. Palaniappan, and B. Zavidovique, "Rotationally Invariant Hashing of Median Binary Patterns for Texture Classification," in *Image Analysis and Recognition: 5th International Conference, ICIAR 2008, Póvoa de Varzim, Portugal, June 25-27, 2008. Proceedings*, A. Campilho and M. Kamel, Eds., ed Berlin, Heidelberg: Springer Berlin Heidelberg, 2008, pp. 619-629.

[121] A. Hafiane, K. Palaniappan, and G. Seetharaman, "Joint Adaptive Median Binary Patterns for texture classification," *Pattern Recognition,* vol. 48, pp. 2609-2620, Aug 2015.

[122] Y. Kaya, Ö. F. Ertuğrul, and R. Tekin, "Two novel local binary pattern descriptors for texture analysis," *Applied Soft Computing,* vol. 34, pp. 728-735, Sep 2015.

[123] Z. Zhu, X. You, C. L. P. Chen, D. Tao, W. Ou, X. Jiang, *et al.*, "An adaptive hybrid pattern for noise-robust texture analysis," *Pattern Recognition,* vol. 48, pp. 2592-2608, Aug 2015.

[124] A. Barcelo, E. Montseny, and P. Sobrevilla, "Fuzzy Texture Unit and Fuzzy Texture Spectrum for texture characterization," *Fuzzy Sets and Systems,* vol. 158, pp. 239-252, Feb 01 2007.

[125] T. Matsuyama, S.-I. Miura, and M. Nagao, "Structural analysis of natural textures by Fourier transformation," *Computer Vision, Graphics, and Image Processing,* vol. 24, pp. 347-362, Dec 1983.

[126] T. Chang and C. C. Jay Kuo, "Texture Analysis and Classification with Tree-Structured Wavelet Transform," *IEEE Transactions on Image Processing*, vol. 2, pp. 429-441, Aug 06 1993.

[127] M. Unser, "Texture Classification and Segmentation Using Wavelet Frames," *IEEE Transactions on Image Processing*, vol. 4, pp. 1549-1560, Nov 1995.

[128] A. C. Bovik, M. Clark, and W. S. Geisler, "Multichannel Texture Analysis Using Localized Spatial Filters," *IEEE Transactions on Pattern Analysis and Machine Intelligence*, vol. 12, pp. 55-73, Aug 06 1990.

[129] B. Ambale-Venkatesh and J. A. Lima, "Cardiac MRI: a central prognostic tool in myocardial fibrosis," *Nat Rev Cardiol*, vol. 12, pp. 18-29, Jan 2015.

[130] R. Kirschner, A. Varga-Szemes, B. C. Brott, S. Litovsky, A. Elgavish, G. A. Elgavish, *et al.*, "Quantification of myocardial viability distribution with Gd(DTPA) bolus-enhanced, signal intensity-based percent infarct mapping," *Magnetic Resonance Imaging*, vol. 29, pp. 650-658, Jun 2011.

[131] K. H. Stensaeth, P. Hoffmann, E. Fossum, A. Mangschau, L. Sandvik, and N. E. Klow, "Cardiac magnetic resonance visualizes acute and chronic myocardial injuries in myocarditis," *Int J Cardiovasc Imaging*, Feb 2011.

[132] E. Dall'Armellina, N. Karia, A. C. Lindsay, T. D. Karamitsos, V. Ferreira, M. D. Robson, *et al.*, "Dynamic Changes of Edema and Late Gadolinium Enhancement After Acute Myocardial Infarction and Their Relationship to Functional Recovery and Salvage Index," *Circulation-Cardiovascular Imaging*, vol. 4, pp. 228-U67, May 2011.

[133] A. Wagner, H. Mahrholdt, L. Thomson, S. Hager, G. Meinhardt, W. Rehwald, *et al.*, "Effects of time, dose, and inversion time for acute myocardial infarct size measurements based on magnetic resonance imaging-delayed contrast enhancement," *Journal of the American College of Cardiology*, vol. 47, pp. 2027-2033, May 16 2006.

[134] A. Welinder, N. Hakacova, T. Martin, and H. Engblom, "Importance of standardized assessment of late gadolinium enhancement for quantification of infarct size by cardiac magnetic resonance: implications for comparison with electrocardiogram," *J Electrocardiol*, vol. 44, pp. 538-43, Sep-Oct 2011.

[135] A. S. Flett, J. Hasleton, C. Cook, D. Hausenloy, G. Quarta, C. Ariti, *et al.*, "Evaluation of techniques for the quantification of myocardial scar of differing etiology using cardiac magnetic resonance," *JACC Cardiovasc Imaging*, vol. 4, pp. 150-6, Feb 2011.

[136] R. Goetti, S. Kozerke, O. F. Donati, D. Surder, P. Stolzmann, P. A. Kaufmann, *et al.*, "Acute, subacute, and chronic myocardial infarction: quantitative comparison of 2D and 3D late gadolinium enhancement MR imaging," *Radiology*, vol. 259, pp. 704-11, Jun 2011.

[137] L. C. Amado, B. L. Gerber, S. N. Gupta, G. Szarf, R. Schock, K. Nasir, *et al.*, "Accurate and objective infarct sizing by contrast-enhanced magnetic resonance imaging in a canine myocardial infarction model," *Journal of the American College of Cardiology*, vol. 44, pp. 2383-2389, Dec 21 2004.

[138] M. Neizel, M. Katoh, E. Schade, T. Rassaf, G. A. Krombach, M. Kelm, *et al.*, "Rapid and accurate determination of relative infarct size in humans using contrast-enhanced magnetic resonance imaging," *Clin Res Cardiol,* vol. 98, pp. 319-24, May 2009.

[139] B. Ruzsics, P. Suranyi, P. Kiss, B. C. Brott, A. Elgavish, T. Simor, *et al.*, "Head-to-Head Comparison Between Delayed Enhancement and Percent Infarct Mapping for Assessment of Myocardial Infarct Size in a Canine Model," *Journal of Magnetic Resonance Imaging,* vol. 28, pp. 1386-1392, Dec 2008.

[140] T. Simor, P. Suranyi, B. Ruzsics, A. Toth, L. Toth, P. Kiss, *et al.*, "Percent Infarct Mapping for Delayed Contrast Enhancement Magnetic Resonance Imaging to Quantify Myocardial Viability by Gd(DTPA)," *Journal of Magnetic Resonance Imaging,* vol. 32, pp. 859-868, Oct 2010.

[141] E. Heiberg, M. Ugander, H. Engblom, M. Gotberg, G. K. Olivecrona, D. Erlinge, *et al.*, "Automated quantification of myocardial infarction from MR images by accounting for partial volume effects: animal, phantom, and human study," *Radiology,* vol. 246, pp. 581-8, Feb 2008.

[142] L. Y. Hsu, W. P. Ingkanisorn, P. Kellman, A. H. Aletras, and A. E. Arai, "Quantitative myocardial infarction on delayed enhancement MRI. Part II: Clinical application of an automated feature analysis and combined thresholding infarct sizing algorithm," *Journal of Magnetic Resonance Imaging,* vol. 23, pp. 309-314, Mar 2006.

[143] L. Y. Hsu, A. Natanzon, P. Kellman, G. A. Hirsch, A. H. Aletras, and A. E. Arai, "Quantitative myocardial infarction on delayed enhancement MRI. Part I: Animal validation of an automated feature analysis and combined thresholding infarct sizing algorithm," *J Magn Reson Imaging,* vol. 23, pp. 298-308, Mar 2006.

[144] M. T. Wu, M. Y. Su, Y. L. Huang, K. R. Chiou, P. Yang, H. B. Pan, *et al.*, "Sequential changes of myocardial microstructure in patients postmyocardial infarction by diffusion-tensor cardiac MR: correlation with left ventricular structure and function," *Circ Cardiovasc Imaging,* vol. 2, pp. 32-40, 6 p following 40, Jan 2009.

[145] U. P. Sechtem and H. Mahrholdt, "Myocardial Viability," in *Cardiovascular Magnetic Resonance (Second Edition)*, J. M. Warren, Md, J. P. Dudley, Frcp, Facc, and Fesc, Eds., ed Philadelphia: Churchill Livingstone, 2010, pp. 267-283.

[146] A. Hamdy, K. Kitagawa, M. Ishida, and H. Sakuma, "Native Myocardial T1 Mapping, Are We There Yet?," *International Heart Journal,* vol. 57, pp. 400-407, Jul 27 2016.

[147] J. C. Moon, D. R. Messroghli, P. Kellman, S. K. Piechnik, M. D. Robson, M. Ugander, *et al.*, "Myocardial T1 mapping and extracellular volume quantification: a Society for Cardiovascular Magnetic Resonance (SCMR) and CMR Working Group of the European Society of Cardiology consensus statement," *Journal of Cardiovascular Magnetic Resonance,* vol. 15, Oct 14 2013.

[148] P. Kellman and M. S. Hansen, "T1-mapping in the heart: accuracy and precision," *Journal of Cardiovascular Magnetic Resonance,* vol. 16, Jan 4 2014.

[149] E. B. Schelbert, K. M. Piehler, K. M. Zareba, J. C. Moon, M. Ugander, D. R. Messroghli, *et al.*, "Myocardial Fibrosis Quantified by Extracellular Volume Is Associated With

Subsequent Hospitalization for Heart Failure, Death, or Both Across the Spectrum of Ejection Fraction and Heart Failure Stage," *J Am Heart Assoc,* vol. 4, Dec 18 2015.

[150] F. von Knobelsdorff-Brenkenhoff, M. Prothmann, M. A. Dieringer, R. Wassmuth, A. Rudolph, W. Utz, *et al.*, "Current T(1) and T(2) mapping techniques applied with simple thresholds cannot discriminate acute from chronic myocadial infarction on an individual patient basis: a pilot study," *BMC Med Imaging,* vol. 16, p. 35, Apr 29 2016.

[151] A. J. McLellan, A. H. Ellims, S. Prabhu, A. Voskoboinik, L. M. Iles, J. L. Hare, *et al.*, "Diffuse Ventricular Fibrosis on Cardiac Magnetic Resonance Imaging Associates with Ventricular Tachycardia in Patients with Hypertrophic Cardiomyopathy," *J Cardiovasc Electrophysiol,* May 2016.

[152] A. Chiribiri, S. Leuzzi, M. R. Conte, S. Bongioanni, K. Bratis, L. Olivotti, *et al.*, "Rest perfusion abnormalities in hypertrophic cardiomyopathy: correlation with myocardial fibrosis and risk factors for sudden cardiac death," *Clin Radiol,* vol. 70, pp. 495-501, May 2015.

[153] M. Perazzolo Marra, M. De Lazzari, A. Zorzi, F. Migliore, F. Zilio, C. Calore, *et al.*, "Impact of the presence and amount of myocardial fibrosis by cardiac magnetic resonance on arrhythmic outcome and sudden cardiac death in nonischemic dilated cardiomyopathy," *Heart Rhythm,* vol. 11, pp. 856-63, May 2014.

[154] M. Chimura, K. Kiuchi, K. Okajima, A. Shimane, T. Sawada, T. Onishi, *et al.*, "Distribution of ventricular fibrosis associated with life threatening ventricular tachyarrhythmias in patients with nonishcemic dilated cardiomyopathy," *J Cardiovasc Electrophysiol,* Jul 29 2015.

[155] E. Hookana, M. J. Junttila, K. S. Kaikkonen, K. Porvari, H. Kaija, J. Risteli, *et al.*, "Increased type I collagen synthesis in victims of sudden cardiac death due to idiopathic myocardial fibrosis," *Ann Med,* vol. 46, pp. 318-23, Aug 2014.

[156] B. Y. Cheong, R. Muthupillai, M. Nemeth, B. Lambert, D. Dees, S. Huber, *et al.*, "The utility of delayed-enhancement magnetic resonance imaging for identifying nonischemic myocardial fibrosis in asymptomatic patients with biopsy-proven systemic sarcoidosis," *Sarcoidosis Vasc Diffuse Lung Dis,* vol. 26, pp. 39-46, Jul 2009.

[157] R. J. Taylor, F. Umar, E. L. Lin, A. Ahmed, W. E. Moody, W. Mazur, *et al.*, "Mechanical effects of left ventricular midwall fibrosis in non-ischemic cardiomyopathy," *J Cardiovasc Magn Reson,* vol. 18, p. 1, Jan 05 2016.

[158] T. G. Neilan, O. R. Coelho-Filho, S. B. Danik, R. V. Shah, J. A. Dodson, D. J. Verdini, *et al.*, "CMR quantification of myocardial scar provides additive prognostic information in nonischemic cardiomyopathy," *JACC Cardiovasc Imaging,* vol. 6, pp. 944-54, Sep 2013.

[159] D. G. Shin, H. J. Lee, J. Park, J. S. Uhm, H. N. Pak, M. H. Lee, *et al.*, "Pattern of late gadolinium enhancement predicts arrhythmic events in patients with non-ischemic cardiomyopathy," *Int J Cardiol,* vol. 222, pp. 9-15, Nov 01 2016.

[160] R. M. Setser, D. G. Bexell, T. P. O'Donnell, A. E. Stillman, M. L. Lieber, P. Schoenhagen, *et al.*, "Quantitative assessment of myocardial scar in delayed enhancement magnetic resonance imaging," *J Magn Reson Imaging,* vol. 18, pp. 434-41, Oct 2003.

[161] S. Katsuragawa, K. Doi, and H. MacMahon, "Image feature analysis and computer-aided diagnosis in digital radiography: classification of normal and abnormal lungs with interstitial disease in chest images," *Med Phys,* vol. 16, pp. 38-44, Jan-Feb 1989.

[162] R. Uppaluri, E. A. Hoffman, M. Sonka, P. G. Hartley, G. W. Hunninghake, and G. McLennan, "Computer recognition of regional lung disease patterns," *Am J Respir Crit Care Med,* vol. 160, pp. 648-54, Aug 1999.

[163] S. Katsuragawa, K. Doi, N. Nakamori, and H. MacMahon, "Image feature analysis and computer-aided diagnosis in digital radiography: effect of digital parameters on the accuracy of computerized analysis of interstitial disease in digital chest radiographs," *Med Phys,* vol. 17, pp. 72-8, Jan-Feb 1990.

[164] S. Delorme, M. A. Keller-Reichenbecher, I. Zuna, W. Schlegel, and G. Van Kaick, "Usual interstitial pneumonia. Quantitative assessment of high-resolution computed tomography findings by computer-assisted texture-based image analysis," *Invest Radiol,* vol. 32, pp. 566-74, Sep 1997.

[165] I. C. Sluimer, M. Prokop, I. Hartmann, and B. van Ginneken, "Automated classification of hyperlucency, fibrosis, ground glass, solid, and focal lesions in high-resolution CT of the lung," *Med Phys,* vol. 33, pp. 2610-20, Jul 2006.

[166] I. O. Rosas, J. Yao, N. A. Avila, C. K. Chow, W. A. Gahl, and B. R. Gochuico, "Automated quantification of high-resolution CT scan findings in individuals at risk for pulmonary fibrosis," *Chest,* vol. 140, pp. 1590-7, Dec 2011.

[167] M. B. Huber, M. B. Nagarajan, G. Leinsinger, R. Eibel, L. A. Ray, and A. Wismuller, "Performance of topological texture features to classify fibrotic interstitial lung disease patterns," *Med Phys,* vol. 38, pp. 2035-44, Dec 2011.

[168] J. Yao, A. Dwyer, R. M. Summers, and D. J. Mollura, "Computer-aided diagnosis of pulmonary infections using texture analysis and support vector machine classification," *Acad Radiol,* vol. 18, pp. 306-14, Mar 2011.

[169] S. O. Park, J. B. Seo, N. Kim, Y. K. Lee, J. Lee, and D. S. Kim, "Comparison of usual interstitial pneumonia and nonspecific interstitial pneumonia: quantification of disease severity and discrimination between two diseases on HRCT using a texture-based automated system," *Korean J Radiol,* vol. 12, pp. 297-307, May-Jun 2011.

[170] J. H. Wang, F. Li, K. Doi, and Q. Li, "Computerized detection of diffuse lung disease in MDCT: the usefulness of statistical texture features," *Physics in Medicine and Biology,* vol. 54, pp. 6881-6899, Nov 21 2009.

[171] H. F. Boehm, C. Fink, U. Attenberger, C. Becker, J. Behr, and M. Reiser, "Automated classification of normal and pathologic pulmonary tissue by topological texture features extracted from multi-detector CT in 3D," *Eur Radiol,* vol. 18, pp. 2745-55, Dec 2008.

[172] E. Arriazu, M. Ruiz de Galarreta, F. J. Cubero, M. Varela-Rey, M. P. Perez de Obanos, T. M. Leung*, et al.*, "Extracellular matrix and liver disease," *Antioxid Redox Signal,* vol. 21, pp. 1078-97, Sep 01 2014.

[173] M. J. House, S. J. Bangma, M. Thomas, E. K. Gan, O. T. Ayonrinde, L. A. Adams, *et al.*, "Texture-based classification of liver fibrosis using MRI," *J Magn Reson Imaging,* vol. 41, pp. 322-8, Feb 2015.

[174] X. Zhang, H. Fujita, M. Kanematsu, X. Zhou, T. Hara, H. Kato, *et al.*, "Improving the Classification of Cirrhotic Liver by using Texture Features," *Conf Proc IEEE Eng Med Biol Soc,* vol. 1, pp. 867-70, 2005.

[175] T. Yokoo, T. Wolfson, K. Iwaisako, M. R. Peterson, H. Mani, Z. Goodman, *et al.*, "Evaluation of Liver Fibrosis Using Texture Analysis on Combined-Contrast-Enhanced Magnetic Resonance Images at 3.0T," *Biomed Res Int,* vol. 2015, p. 387653, 2015.

[176] G. Bahl, I. Cruite, T. Wolfson, A. C. Gamst, J. M. Collins, A. D. Chavez, *et al.*, "Noninvasive classification of hepatic fibrosis based on texture parameters from double contrast-enhanced magnetic resonance images," *J Magn Reson Imaging,* vol. 36, pp. 1154-61, Nov 2012.

[177] B. Barry, K. Buch, J. A. Soto, H. Jara, A. Nakhmani, and S. W. Anderson, "Quantifying liver fibrosis through the application of texture analysis to diffusion weighted imaging," *Magn Reson Imaging,* vol. 32, pp. 84-90, Jan 2014.

[178] H. S. Yu, K. Buch, B. J. Li, M. O'Brien, J. Soto, H. Jara, *et al.*, "Utility of texture analysis for quantifying hepatic fibrosis on proton density MRI," *Journal of Magnetic Resonance Imaging,* vol. 42, pp. 1259-1265, Nov 2015.

[179] Z. Wu, O. Matsui, A. Kitao, K. Kozaka, W. Koda, S. Kobayashi, *et al.*, "Hepatitis C related chronic liver cirrhosis: feasibility of texture analysis of MR images for classification of fibrosis stage and necroinflammatory activity grade," *PLoS One,* vol. 10, p. e0118297, Mar 5 2015.

[180] C. Vicas, M. Lupsor, M. Socaciu, S. Nedevschi, and R. Badea, "Influence of expert-dependent variability over the performance of noninvasive fibrosis assessment in patients with chronic hepatitis C by means of texture analysis," *Comput Math Methods Med,* vol. 2012, p. 346713, 2012.

[181] A. V. Kvostikov, A. S. Krylov, and U. R. Kamalov, "Ultrasound image texture analysis for liver fibrosis stage diagnostics," *Programming and Computer Software,* vol. 41, pp. 273-278, Sep 2015.

[182] U. R. Acharya, O. Faust, F. Molinari, S. V. Sree, S. P. Junnarkar, and V. Sudarshan, "Ultrasound-based tissue characterization and classification of fatty liver disease: A screening and diagnostic paradigm," *Knowledge-Based Systems,* vol. 75, pp. 66-77, Feb 2015.

[183] N. Daginawala, B. J. Li, K. Buch, H. S. Yu, B. Tischler, M. M. Qureshi, *et al.*, "Using texture analyses of contrast enhanced CT to assess hepatic fibrosis," *European Journal of Radiology,* vol. 85, pp. 511-517, Mar 2016.

[184] A. Balodi, M. L. Dewal, R. S. Anand, and A. Rawat, "Texture based classification of the severity of mitral regurgitation," *Computers in Biology and Medicine,* vol. 73, pp. 157-164, Jun 1 2016.

[185] V. K. Sudarshan, U. R. Acharya, E. Y. Ng, R. S. Tan, S. M. Chou, and D. N. Ghista, "An integrated index for automated detection of infarcted myocardium from cross-sectional echocardiograms using texton-based features (Part 1)," *Comput Biol Med,* vol. 71, pp. 231-40, Apr 1 2016.

[186] R. E. Thornhill, M. Cocker, G. Dwivedi, C. Dennie, L. Fuller, A. Dick, *et al.*, "Quantitative texture features as objective metrics of enhancement heterogeneity in hypertrophic cardiomyopathy," *J Cardiovasc Magn Reson,* vol. 16, p. P351, Jan 16 2014.

[187] A. Kassner and R. E. Thornhill, "Texture analysis: a review of neurologic MR imaging applications," *AJNR Am J Neuroradiol,* vol. 31, pp. 809-16, 2010.

[188] R. O. Duda, P. E. Hart, and D. G. Stork, *Pattern Classification*, 2nd Edition ed.: Wiley, 2000.

[189] L. P. Kotu, K. Engan, T. Eftestol, S. Orn, and L. Woie, "Segmentation of scarred and non-scarred myocardium in LG enhanced CMR images using intensity-based textural analysis," *Conf Proc IEEE Eng Med Biol Soc,* vol. 2011, pp. 5698-701, 2011.

[190] L. P. Kotu, K. Engan, K. Skretting, F. Maloy, S. Orn, L. Woie, *et al.*, "Probability mapping of scarred myocardium using texture and intensity features in CMR images," *Biomed Eng Online,* vol. 12, p. 91, 2013.

[191] Y. Lee, J. B. Seo, J. G. Lee, S. S. Kim, N. Kim, and S. H. Kang, "Performance testing of several classifiers for differentiating obstructive lung diseases based on texture analysis at high-resolution computerized tomography (HRCT)," *Computer Methods and Programs in Biomedicine,* vol. 93, pp. 206-215, 2009.

[192] Y. Chang, J. Lim, N. Kim, J. B. Seo, and D. A. Lynch, "A support vector machine classifier reduces interscanner variation in the HRCT classification of regional disease pattern in diffuse lung disease: comparison to a Bayesian classifier," *Med Phys,* vol. 40, p. 051912, 2013.

[193] T. T. Kockelkorn, P. A. de Jong, C. M. Schaefer-Prokop, R. Wittenberg, A. M. Tiehuis, H. A. Gietema, *et al.*, "Semi-automatic classification of textures in thoracic CT scans," *Phys Med Biol,* vol. 61, pp. 5906-24, Aug 21 2016.

[194] M. Anthimopoulos, S. Christodoulidis, A. Christe, and S. Mougiakakou, "Classification of interstitial lung disease patterns using local DCT features and random forest," *Conf Proc IEEE Eng Med Biol Soc,* vol. 2014, pp. 6040-3, 2014.

[195] A. Fukushima, K. Ashizawa, T. Yamaguchi, N. Matsuyama, H. Hayashi, I. Kida, *et al.*, "Application of an artificial neural network to high-resolution CT: usefulness in differential diagnosis of diffuse lung disease," *AJR Am J Roentgenol,* vol. 183, pp. 297-305, Aug 2004.

[196] M. Anthimopoulos, S. Christodoulidis, L. Ebner, A. Christe, and S. Mougiakakou, "Lung Pattern Classification for Interstitial Lung Diseases Using a Deep Convolutional Neural Network," *IEEE Trans Med Imaging,* Feb 29 2016.

[197] H. C. Shin, H. R. Roth, M. Gao, L. Lu, Z. Xu, I. Nogues, *et al.*, "Deep Convolutional Neural Networks for Computer-Aided Detection: CNN Architectures, Dataset Characteristics and Transfer Learning," *IEEE Trans Med Imaging,* vol. 35, pp. 1285-98, May 2016.

[198] W. G. Hundley, D. A. Bluemke, J. P. Finn, S. D. Flamm, M. A. Fogel, M. G. Friedrich, *et al.*, "ACCF/ACR/AHA/NASCI/SCMR 2010 expert consensus document on cardiovascular magnetic resonance: a report of the American College of Cardiology Foundation Task Force on Expert Consensus Documents," *J Am Coll Cardiol,* vol. 55, pp. 2614-62, 2010.

[199] S. Cheng, V. R. Fernandes, D. A. Bluemke, R. L. McClelland, R. A. Kronmal, and J. A. Lima, "Age-related left ventricular remodeling and associated risk for cardiovascular outcomes: the Multi-Ethnic Study of Atherosclerosis," *Circ Cardiovasc Imaging,* vol. 2, pp. 191-8, 2009.

[200] P. Beliveau, F. Cheriet, S. A. Anderson, J. L. Taylor, A. E. Arai, and L. Y. Hsu, "Quantitative assessment of myocardial fibrosis in an age-related rat model by ex vivo late gadolinium enhancement magnetic resonance imaging with histopathological correlation," *Comput Biol Med,* vol. 65, pp. 103-13, 2015.

[201] P. C. Beliveau, F.; W. Bandettini, P.; Arai, A.E.; Hsu, L.Y, "Exploration of texture analysis of late gadolinium enhanced cardiovascular magnetic resonance imaging to discriminate acute versus chronic myocardial infarction in patients," *Journal of Cardiovascular Magnetic Resonance,* vol. [Submitted, October 2016], 2016.

[202] P. Beliveau, F. Cheriet, S. A. Anderson, J. Taylor, S. Berul, A. E. Arai, *et al.*, "Textural Analysis of Diffuse Myocardial Fibrosis in Aging Rats: a Late Gadolinium Enhancement Magnetic Resonance Imaging Study," *2013 IEEE 10th International Symposium on Biomedical Imaging,* pp. 109-112, 2013.

[203] M. Eghbali, T. F. Robinson, S. Seifter, and O. O. Blumenfeld, "Collagen accumulation in heart ventricles as a function of growth and aging," *Cardiovasc Res,* vol. 23, pp. 723-9, Aug 1989.

[204] J. Shirani, R. Pick, W. C. Roberts, and B. J. Maron, "Morphology and significance of the left ventricular collagen network in young patients with hypertrophic cardiomyopathy and sudden cardiac death," *J Am Coll Cardiol,* vol. 35, pp. 36-44, Jan 2000.

[205] M. Y. Su, V. C. Wu, H. Y. Yu, Y. H. Lin, C. C. Kuo, K. L. Liu, *et al.*, "Contrast-enhanced MRI index of diffuse myocardial fibrosis is increased in primary aldosteronism," *J Magn Reson Imaging,* vol. 35, pp. 1349-55, Jun 2012.

[206] S. S. Bun, F. Kober, A. Jacquier, L. Espinosa, J. Kalifa, M. F. Bonzi, *et al.*, "Value of in vivo T2 measurement for myocardial fibrosis assessment in diabetic mice at 11.75 T," *Invest Radiol,* vol. 47, pp. 319-23, May 2012.

[207] T. Eftestol, L. Woie, K. Engan, J. T. Kvaloy, D. W. T. Nilsen, and S. Orn, "Texture Analysis to Assess Risk of Serious Arrhythmias after Myocardial Infarction," *2012 Computing in Cardiology, Vol 39,* pp. 365-368, 2012.

[208] A. Lopez-De Leon and M. Rojkind, "A simple micromethod for collagen and total protein determination in formalin-fixed paraffin-embedded sections," *J Histochem Cytochem,* vol. 33, pp. 737-43, Aug 1985.

[209] K. Yabusaki, T. Faits, E. McMullen, J. L. Figueiredo, M. Aikawa, and E. Aikawa, "A novel quantitative approach for eliminating sample-to-sample variation using a hue saturation value analysis program," *Plos One,* vol. 9, p. e89627, 2014.

[210] J. D. Foley and A. VanDam, *Fundamentals of interactive computer graphics*: Addison-Wesley Longman Publishing Co., Inc., 1982.

[211] W. Y. Ding, L. Liu, Z. H. Wang, M. X. Tang, Y. Ti, L. Han, *et al.*, "FP-receptor gene silencing ameliorates myocardial fibrosis and protects from diabetic cardiomyopathy," *J Mol Med (Berl),* vol. 92, pp. 629-40, Jun 2014.

[212] J. Caudron, P. Mulder, L. Nicol, V. Richard, C. Thuillez, and J. N. Dacher, "MR relaxometry and perfusion of the myocardium in spontaneously hypertensive rat: correlation with histopathology and effect of anti-hypertensive therapy," *Eur Radiol,* vol. 23, pp. 1871-81, Jul 2013.

[213] T. Ishizu, Y. Seo, Y. Kameda, R. Kawamura, T. Kimura, N. Shimojo, *et al.*, "Left ventricular strain and transmural distribution of structural remodeling in hypertensive heart disease," *Hypertension,* vol. 63, pp. 500-6, Mar 2014.

[214] W. Li, M. Lu, S. Banerjee, J. Zhong, A. Ye, J. Molter, *et al.*, "Ex vivo diffusion tensor MRI reflects microscopic structural remodeling associated with aging and disease progression in normal and cardiomyopathic Syrian hamsters," *NMR Biomed,* vol. 22, pp. 819-25, Oct 2009.

[215] G. Moravsky, E. Ofek, H. Rakowski, J. Butany, L. Williams, A. Ralph-Edwards, *et al.*, "Myocardial fibrosis in hypertrophic cardiomyopathy: accurate reflection of histopathological findings by CMR," *JACC Cardiovasc Imaging,* vol. 6, pp. 587-96, May 2013.

[216] A. M. Beek, O. Bondarenko, F. Afsharzada, and A. C. van Rossum, "Quantification of late gadolinium enhanced CMR in viability assessment in chronic ischemic heart disease: a comparison to functional outcome," *J Cardiovasc Magn Reson,* vol. 11, p. 6, 2009.

[217] N. Baron, N. Kachenoura, P. Cluzel, F. Frouin, A. Herment, P. Grenier, *et al.*, "Comparison of various methods for quantitative evaluation of myocardial infarct volume from magnetic resonance delayed enhancement data," *Int J Cardiol,* vol. 167, pp. 739-44, Aug 10 2013.

[218] Y. Mikami, L. Kolman, S. X. Joncas, J. Stirrat, D. Scholl, M. Rajchl, *et al.*, "Accuracy and reproducibility of semi-automated late gadolinium enhancement quantification techniques in patients with hypertrophic cardiomyopathy," *J Cardiovasc Magn Reson,* vol. 16, p. 85, 2014.

[219] H. Mahrholdt, A. Wagner, R. M. Judd, U. Sechtem, and R. J. Kim, "Delayed enhancement cardiovascular magnetic resonance assessment of non-ischaemic cardiomyopathies," *Eur Heart J,* vol. 26, pp. 1461-74, Aug 2005.

[220] P. Whittaker, R. A. Kloner, D. R. Boughner, and J. G. Pickering, "Quantitative assessment of myocardial collagen with picrosirius red staining and circularly polarized light," *Basic Res Cardiol,* vol. 89, pp. 397-410, Sep-Oct 1994.

[221] S. de Jong, T. A. van Veen, J. M. de Bakker, and H. V. van Rijen, "Monitoring cardiac fibrosis: a technical challenge," *Neth Heart J,* vol. 20, pp. 44-8, Jan 2012.

[222] M. W. Smulders, S. C. Bekkers, H. W. Kim, L. M. Van Assche, M. A. Parker, and R. J. Kim, "Performance of CMR Methods for Differentiating Acute From Chronic MI," *JACC Cardiovasc Imaging,* vol. 8, pp. 669-79, Jun 2015.

[223] R. Kirschner, A. Varga-Szemes, T. Simor, P. Suranyi, P. Kiss, B. Ruzsics, *et al.*, "Acute infarct selective MRI contrast agent," *Int J Cardiovasc Imaging,* vol. 28, pp. 285-93, 2012.

[224] J. Wang, B. Xiang, H. Y. Lin, H. Liu, D. Freed, R. C. Arora, *et al.*, "Differential MR delayed enhancement patterns of chronic myocardial infarction between extracellular and intravascular contrast media," *PLoS One,* vol. 10, p. e0121326, 2015.

[225] M. Pop, N. R. Ghugre, V. Ramanan, L. Morikawa, G. Stanisz, A. J. Dick, *et al.*, "Quantification of fibrosis in infarcted swine hearts by ex vivo late gadolinium-enhancement and diffusion-weighted MRI methods," *Phys Med Biol,* vol. 58, pp. 5009-28, Aug 7 2013.

[226] E. M. Antman, D. T. Anbe, P. W. Armstrong, E. R. Bates, L. A. Green, M. Hand, *et al.*, "ACC/AHA guidelines for the management of patients with ST-elevation myocardial infarction; A report of the American College of Cardiology/American Heart Association Task Force on Practice Guidelines (Committee to Revise the 1999 Guidelines for the Management of patients with acute myocardial infarction)," *J Am Coll Cardiol,* vol. 44, pp. E1-E211, Aug 4 2004.

[227] A. Hervas, A. Ruiz-Sauri, E. de Dios, M. J. Forteza, G. Minana, J. Nunez, *et al.*, "Inhomogeneity of collagen organization within the fibrotic scar after myocardial infarction: results in a swine model and in human samples," *J Anat,* Oct 29 2015.

[228] S. Hammer-Hansen, M. Ugander, L. Y. Hsu, J. Taylor, J. J. Thune, L. Kober, *et al.*, "Distinction of salvaged and infarcted myocardium within the ischaemic area-at-risk with T2 mapping," *Eur Heart J Cardiovasc Imaging,* vol. 15, pp. 1048-53, Sep 2014.

[229] A. Schmidt, C. F. Azevedo, A. Cheng, S. N. Gupta, D. A. Bluemke, T. K. Foo, *et al.*, "Infarct tissue heterogeneity by magnetic resonance imaging identifies enhanced cardiac arrhythmia susceptibility in patients with left ventricular dysfunction," *Circulation,* vol. 115, pp. 2006-14, Apr 17 2007.

[230] B. L. Nguyen, L. Capotosto, A. Persi, A. Placanica, A. Rafique, G. Piccirillo, *et al.*, "Global and regional left ventricular strain indices in post-myocardial infarction patients with ventricular arrhythmias and moderately abnormal ejection fraction," *Ultrasound Med Biol,* vol. 41, pp. 407-17, Feb 2015.

[231] E. Watanabe, S. A. Abbasi, B. Heydari, O. R. Coelho-Filho, R. Shah, T. G. Neilan, *et al.*, "Infarct tissue heterogeneity by contrast-enhanced magnetic resonance imaging is a novel predictor of mortality in patients with chronic coronary artery disease and left ventricular dysfunction," *Circ Cardiovasc Imaging,* vol. 7, pp. 887-94, 2014.

[232] S. Gouda, A. Abdelwahab, M. Salem, and M. A. Hamid, "Scar characteristics for prediction of ventricular arrhythmia in ischemic cardiomyopathy," *Pacing Clin Electrophysiol,* vol. 38, pp. 311-8, Mar 2015.

[233] I. Toma, P. J. Kim, R. Dash, M. V. McConnell, D. Nishimura, P. Harnish, *et al.*, "Telmisartan in the diabetic murine model of acute myocardial infarction: dual contrast manganese-enhanced and delayed enhancement MRI evaluation of the peri-infarct region," *Cardiovasc Diabetol,* vol. 15, p. 24, 2016.

[234] L. P. Kotu, K. Engan, K. Skretting, #xd8, S. rn, L. Woie, *et al.*, "Segmentation of Scarred Myocardium in Cardiac Magnetic Resonance Images," *ISRN Biomedical Imaging,* vol. 2013, p. 12, 2013.

[235] W. Chan, S. J. Duffy, D. A. White, X.-M. Gao, X.-J. Du, A. H. Ellims, *et al.*, "Acute Left Ventricular Remodeling Following Myocardial Infarction: Coupling of Regional Healing With Remote Extracellular Matrix Expansion," *JACC: Cardiovascular Imaging,* vol. 5, pp. 884-893, Sept 2012.

[236] M. Gletsos, S. G. Mougiakakou, G. K. Matsopoulos, K. S. Nikita, A. S. Nikita, and D. Kelekis, "A computer-aided diagnostic system to characterize CT focal liver lesions: design and optimization of a neural network classifier," *IEEE Trans Inf Technol Biomed,* vol. 7, pp. 153-62, Sep 2003.

[237] M. Y. Kiang, "A comparative assessment of classification methods," *Decision Support Systems,* vol. 35, pp. 441-454, July 2003.

[238] S. G. Mougiakakou, I. K. Valavanis, A. Nikita, and K. S. Nikita, "Differential diagnosis of CT focal liver lesions using texture features, feature selection and ensemble driven classifiers," *Artif Intell Med,* vol. 41, pp. 25-37, Sep 2007.

[239] M. E. Mayerhoefer, G. H. Welsch, G. Riegler, T. C. Mamisch, A. Materka, M. Weber, *et al.*, "Feasibility of texture analysis for the assessment of biochemical changes in meniscal tissue on T1 maps calculated from delayed gadolinium-enhanced magnetic resonance imaging of cartilage data: comparison with conventional relaxation time measurements," *Invest Radiol,* vol. 45, pp. 543-7, 2010.

[240] H. Yu, A. S. Touret, B. Li, M. O'Brien, M. M. Qureshi, J. A. Soto, *et al.*, "Application of texture analysis on parametric T1 and T2 maps for detection of hepatic fibrosis," *J Magn Reson Imaging,* Jun 1 2016.

[241] H. Satoh, M. Sano, K. Suwa, T. Saitoh, M. Nobuhara, M. Saotome, *et al.*, "Distribution of late gadolinium enhancement in various types of cardiomyopathies: Significance in differential diagnosis, clinical features and prognosis," *World J Cardiol,* vol. 6, pp. 585-601, Jul 26 2014.

[242] X. Duan, J. Li, Q. Zhang, Z. Zeng, Y. Luo, J. Jiang, *et al.*, "Prognostic value of late gadolinium enhancement in dilated cardiomyopathy patients: a meta-analysis," *Clin Radiol,* vol. 70, pp. 999-1008, Sep 2015.

[243] J. V. Venero, M. Doyle, M. Shah, V. K. Rathi, J. A. Yamrozik, R. B. Williams, *et al.*, "Mid wall fibrosis on CMR with late gadolinium enhancement may predict prognosis for LVAD and transplantation risk in patients with newly diagnosed dilated cardiomyopathy-preliminary observations from a high-volume transplant centre," *ESC Heart Fail,* vol. 2, pp. 150-159, Dec 2015.

[244] H. Chopra, D. Arangalage, C. Bouleti, S. Zarka, F. Fayard, S. Chillon, *et al.*, "Prognostic value of the infarct- and non-infarct like patterns and cardiovascular magnetic resonance parameters on long-term outcome of patients after acute myocarditis," *Int J Cardiol,* vol. 212, pp. 63-9, Jun 1 2016.

[245] E. Pozo, D. Viliani, N. Aguirre, P. Agudo-Quilez, M. J. Olivera, P. Caballero, *et al.*, "Early gadolinium enhancement in hypertrophic cardiomyopathy: a potential premature marker of myocardial damage," *Int J Cardiovasc Imaging*, vol. 32, pp. 1635-1643, Nov 2016.

[246] M. S. Maron, "Clinical utility of cardiovascular magnetic resonance in hypertrophic cardiomyopathy," *J Cardiovasc Magn Reson*, vol. 14, p. 13, Feb 01 2012.

[247] Z. Weng, J. Yao, R. H. Chan, J. He, X. Yang, Y. Zhou, *et al.*, "Prognostic Value of LGE-CMR in HCM: A Meta-Analysis," *JACC Cardiovasc Imaging*, vol. 9, pp. 1392-1402, Jul 19 2016.

[248] O. Bruder, A. Wagner, C. J. Jensen, S. Schneider, P. Ong, E. M. Kispert, *et al.*, "Myocardial scar visualized by cardiovascular magnetic resonance imaging predicts major adverse events in patients with hypertrophic cardiomyopathy," *Journal of the American College of Cardiology*, vol. 56, pp. 875-887, 2010.

[249] R. H. Chan, B. Maron, i. olivotto, G. Assenza, M. S. Hong, J. Lesser, *et al.*, "Prognostic Utility Of Contrast-Enhanced Cardiovascular Magnetic Resonance in Hypertrophic Cardiomyopathy: An International Multicenter Study," *Journal of the American College of Cardiology*, vol. 59, pp. E1570-E1570, 2012.

[250] M. S. Maron, "Contrast-enhanced CMR in HCM: what lies behind the bright light of LGE and why it now matters," *JACC Cardiovasc Imaging*, vol. 6, pp. 597-9, May 2013.

[251] M. Bizino, J. Amersfoort, Q. Tao, R. J. van der Geest, and H. J. Lamb, "Free-breathing 3D phase-sensitive inversion recovery late gadolinium enhancement at 3.0 Tesla: reliability and image quality in ischemic and non-ischemic cardiomyopathy in comparison with multiple breath-hold 3D imaging," *Journal of Cardiovascular Magnetic Resonance*, vol. 17, p. P97, 2015.

[252] P. Hammar, A. M. Nordenskjold, B. Lindahl, O. Duvernoy, H. Ahlstrom, L. Johansson, *et al.*, "Unrecognized myocardial infarctions assessed by cardiovascular magnetic resonance are associated with the severity of the stenosis in the supplying coronary artery," *J Cardiovasc Magn Reson*, vol. 17, p. 98, 2015.

[253] A. M. Nordenskjold, P. Hammar, H. Ahlstrom, T. Bjerner, O. Duvernoy, K. M. Eggers, *et al.*, "Unrecognized Myocardial Infarction Assessed by Cardiac Magnetic Resonance Imaging--Prognostic Implications," *PLoS One*, vol. 11, p. e0148803, 2016.

[254] E. B. Schelbert, J. J. Cao, S. Sigurdsson, T. Aspelund, P. Kellman, A. H. Aletras, *et al.*, "Prevalence and prognosis of unrecognized myocardial infarction determined by cardiac magnetic resonance in older adults," *JAMA*, vol. 308, pp. 890-6, Sep 5 2012.

[255] E. B. Levitan, M. M. Safford, M. L. Kilgore, E. Z. Soliman, S. P. Glasser, S. E. Judd, *et al.*, "Assessment tools for unrecognized myocardial infarction: a cross-sectional analysis of the REasons for Geographic and Racial Differences in Stroke population," *BMC Cardiovasc Disord*, vol. 13, p. 23, Mar 26 2013.

[256] P. C. Ursell, P. I. Gardner, A. Albala, J. J. Fenoglio, Jr., and A. L. Wit, "Structural and electrophysiological changes in the epicardial border zone of canine myocardial infarcts during infarct healing," *Circ Res*, vol. 56, pp. 436-51, Mar 1985.

[257] E. Golcuk, K. Yalin, T. Aksu, S. K. Tiryakioglu, A. K. Bilge, and K. Adalet, "Peri-Infarction Zone as a Risk Marker for Patients With Postmyocardial Infarction," *Am J Med Sci,* vol. 351, pp. 452-8, May 2016.

[258] I. Roifman, N. R. Ghugre, T. Vira, M. I. Zia, A. Zavodni, M. Pop, *et al.*, "Assessment of the longitudinal changes in infarct heterogeneity post myocardial infarction," *BMC Cardiovasc Disord,* vol. 16, p. 198, Oct 14 2016.

[259] J. C. Rubenstein, D. C. Lee, E. Wu, A. H. Kadish, R. Passman, D. Bello, *et al.*, "A comparison of cardiac magnetic resonance imaging peri-infarct border zone quantification strategies for the prediction of ventricular tachyarrhythmia inducibility," *Cardiol J,* vol. 20, pp. 68-77, 2013.

[260] A. Chaddad and C. Tanougast, "Extracted magnetic resonance texture features discriminate between phenotypes and are associated with overall survival in glioblastoma multiforme patients," *Med Biol Eng Comput,* vol. 54, pp. 1707-1718, Nov 2016.

[261] X. Chen, X. Wei, Z. Zhang, R. Yang, Y. Zhu, and X. Jiang, "Differentiation of true-progression from pseudoprogression in glioblastoma treated with radiation therapy and concomitant temozolomide by GLCM texture analysis of conventional MRI," *Clin Imaging,* vol. 39, pp. 775-80, Sep-Oct 2015.

[262] E. J. Sutton, J. H. Oh, B. Z. Dashevsky, H. Veeraraghavan, A. P. Apte, S. B. Thakur, *et al.*, "Breast cancer subtype intertumor heterogeneity: MRI-based features predict results of a genomic assay," *J Magn Reson Imaging,* vol. 42, pp. 1398-406, Nov 2015.

[263] T. Torheim, E. Malinen, K. Kvaal, H. Lyng, U. G. Indahl, E. K. Andersen, *et al.*, "Classification of dynamic contrast enhanced MR images of cervical cancers using texture analysis and support vector machines," *IEEE Trans Med Imaging,* vol. 33, pp. 1648-56, Aug 2014.

[264] T. C. Wang, Y. H. Huang, C. S. Huang, J. H. Chen, G. Y. Huang, Y. C. Chang, *et al.*, "Computer-aided diagnosis of breast DCE-MRI using pharmacokinetic model and 3-D morphology analysis," *Magn Reson Imaging,* vol. 32, pp. 197-205, Apr 2014.

[265] G. B. Joseph, T. Baum, J. Carballido-Gamio, L. Nardo, W. Virayavanich, H. Alizai, *et al.*, "Texture analysis of cartilage T2 maps: individuals with risk factors for OA have higher and more heterogeneous knee cartilage MR T2 compared to normal controls--data from the osteoarthritis initiative," *Arthritis Res Ther,* vol. 13, p. R153, 2011.

[266] M. S. de Oliveira, M. L. Balthazar, A. D'Abreu, C. L. Yasuda, B. P. Damasceno, F. Cendes, *et al.*, "MR imaging texture analysis of the corpus callosum and thalamus in amnestic mild cognitive impairment and mild Alzheimer disease," *AJNR Am J Neuroradiol,* vol. 32, pp. 60-6, Jan 2011.

[267] K. Engan, T. Eftestol, S. Orn, J. T. Kvaloy, and L. Woie, "Exploratory data analysis of image texture and statistical features on myocardium and infarction areas in cardiac magnetic resonance images," *Conf Proc IEEE Eng Med Biol Soc,* vol. 2010, pp. 5728-31, 2010.

[268] J. Zhang, L. Tong, L. Wang, and N. Li, "Texture analysis of multiple sclerosis: a comparative study," *Magn Reson Imaging,* vol. 26, pp. 1160-6, Oct 2008.

[269] L. Nanni, S. Brahnam, S. Ghidoni, E. Menegatti, and T. Barrier, "Different Approaches for Extracting Information from the Co-Occurrence Matrix," *PLoS ONE*, vol. 8, p. e83554, 2013.

[270] Z. P. Xu and W. B. Xu, *GPU in texture image processing*, 2006.

[271] Z. P. Xu and H. Y. Liu, *A fast algorithm of GLCM computation based on programmable graphics hardware*, 2007.

[272] N. Schwendener, C. Jackowski, A. Persson, M. J. Warntjes, F. Schuster, F. Riva, *et al.*, "Detection and differentiation of early acute and following age stages of myocardial infarction with quantitative post-mortem cardiac 1.5 T MR," *Forensic Science International*, 2016.